FAILURE BEHAVIOR OF COMPOSITE LAMINATES UNDER OUT-OF-PLANE LOADS

by

Murat KOÇ

B.S., Mechanical Engineering, Yıldız Technical University, 2009

Submitted to the Institute for Graduate Studies in
Science and Engineering in partial fulfillment of
the requirements for the degree of
Master of Science

Graduate Program in Mechanical Engineering
Boğaziçi University

2012

FAILURE BEHAVIOR OF COMPOSITE LAMINATES UNDER OUT-OF-PLANE LOADS

APPROVED BY:

Prof. Fazıl Önder Sönmez (Thesis Supervisor)	.....
Assoc. Prof. Nuri Ersoy (Thesis Supervisor)	.....
Prof. Günay Anlaş	.....
Assoc. Prof. Bülent Ekici	.....
Assist. Prof. Cahit Can Aydıner	.....

DATE OF APPROVAL:

ACKNOWLEDGEMENTS

I would like to express my gratitude to my thesis advisors Prof. Fazıl Önder Sönmez and Assoc. Prof. Nuri Ersoy for their invaluable patience, guidance and helpfulness throughout my thesis process.

I would also like to acknowledge Prof. Günay Anlaş, Assoc. Prof. Bülent Ekici and Assist. Prof. C. Can Aydıner for their very important guidance and suggestions.

Additionally, I would like to thank my friends. Especially Kenan Çınar for his great helps during experiments and encouragements. Then, Fatih Ertuğrul Öz and Niyazi Tanlak for all their supports.

Finally, there are no words to describe my indebtness to my family and Cansu Özyılmaz for all their love and encouragement.

ABSTRACT

FAILURE BEHAVIOR OF COMPOSITE LAMINATES UNDER OUT-OF-PLANE LOADS

In this study, failure behavior of fiber-reinforced composites under out-of-plane loads is investigated by means of four – point bending tests. Firstly, four – point bending tests are modeled analytically using the classical lamination theory (CLT). Considering unidirectional $[\theta_6]_s$ as well as balanced symmetric $[\theta_3/-\theta_3]_s$ composite laminates , the maximum allowable moment resultants as a function of fiber orientation angle, θ, are obtained using Tsai-Wu, maximum stress, maximum strain, Hashin, Tsai-Hill, Hoffman, quadric surfaces, modified quadric surfaces and Norris failure criteria. Secondly, the same tests are simulated using the finite element method (FEM) in ANSYS with layered 3-D solid elements. In order to apply the failure criteria like Tsai-Hill and obtain the maximum allowable moment resultants as a function of fiber orientation angle, θ, according to these failure criteria, ANSYS Parametric Design Language is used Convergence analysis is carried out to find a balance between computational cost and accuracy of results. Another analysis is conducted for optimal positioning of the loads so as to ensure that static failure modes dominate delamination failure mode. For this purpose, the failure index results of a delamination criterion are compared with the results of Tsai-Wu and maximum stress failure criteria for different loading positions. A test setup is then constructed according to the predicted optimal support positioning and experiments are conducted for both unidirectional and symmetric balanced laminates having fiber orientation angles ranging from 0° to 90° with 15° increments. The differences between the model predictions and experimental results are discussed.

ÖZET

DÜZLEM DIŞI YÜKE MARUZ KOMPOZİT PLAKALARIN KIRILMA DAVRANIŞI

Bu çalışmada, dört nokta eğme deneyleri yardımıyla, düzlem dışı yüke maruz kompozit plakaların kırılma davranışı araştırılmıştır. Öncelikle, dört nokta eğme deneyleri Klasik Katman Teorisi (KKT) yardımıyla simüle edilmiştir. Bu amaçla, tek yönlü $[\theta_6]_s$ olduğu kadar çok yönlü simetrik ve dengeli $[\theta_3/-\theta_3]_s$ kompozit plakalar dikkate alınmış ve Tsai-Wu, azami gerilme, azami gerinme, Hashin, Tsai-Hill, Hoffman, quadric surfaces, modified quadric surfaces ve Norris kırılma kriterlerinin izin verilebilir en yüksek moment resultant öngörüleri, elyaf açısı θ'nın fonksiyonu olarak elde edilmiştir. İkinci olarak, aynı deneyler Sonlu Elemanlar Metodu (SEM) yazılımı ANSYS v13.0 Mechanical APDL'de (ANSYS Parametric Design Language) Solid185, katmanlı 3-B yapısal katı elemanlarla tekrar edilmiştir. SEM analizleri esnasında hazır olarak gelmeyen kırılma kriterleri (Tsai-Hill, Hoffman, quadric surfaces, modified quadric surfaces, Norris) ANSYS'e eklenmiş ve izin verilebilir en yüksek moment resultant öngörüleri, elyaf açısı θ'nın fonksiyonu olarak elde edilmiştir. Hesaplama maliyeti ile sonuçların kesinliği arasındaki dengeyi bulmak için yakınsaklık analizi yapılmıştır. Bir başka analiz de, yükleri statik kırılma modlarının katman ayrışması kırılma moduna baskın geleceği şekilde yerleştirmek için yapılmıştır. Bu amaçla, bir kullanıcı tanımlı kırılma kriteri (USERFC) ANSYS'e eklenmiş ve bir kırılma kriterinin değişik yükleme konumlarıyla ilgili öngörüleri Tsai-Wu ve azami gerilme kriterlerinin öngörüleriyle karşılaştırılmıştır. Simülasyon ve deneyler muhtemel kırılma modunun katman ayrışması değil statik kırılma modunun olduğu en uygun yükleme koşullarında gerçekleştirilmiştir. Son olarak, deney düzeneği SEM analizinin öngördüğü en iyi yükleme pozisyonlarına göre üretilerek deneyler yapılmıştır. 0°'den 90°'ye kadar her 15°'lik elyaf açısı için hem tek yönlü hem de simetrik dengeli plakalar için birden fazla test yapılmış ve model öngörüleri ile deney sonuçları arasındaki farklar tartışılmıştır.

TABLE OF CONTENTS

LIST OF FIGURES

LIST OF TABLES

LIST OF SYMBOLS

A_{ij}	Extensional stiffnesses
B_{ij}	Bending-extension coupling stiffnesses
°C	Celsius
C_i	Characteristic parameters of Hoffman failure criterion
C_{ij}	Stiffness matrix
C_{ijkl}	Stiffness tensor
D_{ij}	Bending stiffnesses
E_i	Elastic modulus in direction i
F_i	Second order strength tensor
F_{ij}	Forth order strength tensor
G_{ij}	Shear modulus
N_{ij}	Force resultants
M_{ij}	Moment resultants
N_{ij}^T	Thermal force resultants
M_{ij}^T	Thermal moment resultants
M_{max}	Maximum allowable moment resultant
Q_{ij}	Reduced stiffness matrix
$\overline{Q}_{ij}$	Transformed reduced stiffness matrix
S_{12}	Shear strength in 1-2 plane
S_{IJ}	Compliance matrix
S_{ijkl}	Compliance tensor

S_ε	Shear strength in terms of strains in 1-2 plane
T	Transformation matrix
T_g	Glass transition temperature
u_i	Displacement in direction i
u^o	Midplane displacement in direction 1
v^o	Midplane displacement in direction 2
w^o	Midplane displacement in direction 3
X	Strength in direction 1
X_c	Compression strength in direction 1
X_t	Tensile strength in direction 1
X_{ε_c}	Compression strength in terms of strains in direction 1
X_{ε_t}	Tension strength in terms of strains in direction 1
Y	Strength in direction 2
Y_c	Compression strength in direction 2
Y_t	Tensile strength in direction 1
Y_{ε_c}	Compression strength in terms of strains in direction 2
Y_{ε_t}	Tension strength in terms of strains in direction 2
α_{ij}	Thermal extension coefficient
ε_I	Strains in Voigt notation
ε_{ij}	Strain matrix
$\varepsilon_{ij}^{\ o}$	Midplane strains
γ_{ij}	Engineering shear strain

κ_{ij}	Curvature terms
ν_{ij}	Poisson's ratios
σ_I	Stresses in Voigt notation
σ_{ij}	Stress matrix
ΔT	Temperature change

LIST OF ACCRONYMS/ABBREVIATIONS

2-D	Two dimensional
3-D	Three dimensional
APDL	ANSYS Parametric Design Language
CFRP	Carbon fibre reinforced plastic
CLT	Classical lamination theory
CMC	Ceramic matrix composites
Eq.	Equation
ESYS	Element coordinate system
FEM	Finite element method
GUI	Graphical user interface
MAX	Maximum
MIN	Minimum
MMC	Metallic matrix composites
mm	Millimetre
μm	Micrometer
PMC	Polymeric matrix composites
RAM	Random Access Memory
SOLID185	Layered 3-D structural solid element
UPF	User programmable feature
USERFC	User defined failure criterion
WWFE	Worldwide failure exercise

1. INTRODUCTION

Composite materials are widely used because of their high stiffness-to-weight and strength-to-weight ratios. Composites can be tailored to achieve desired characteristics by changing their laminate configurations in the design stage.

For the safe use of composite plates, one should use reliable failure theories during design stage that will correctly predict failure under given loading conditions for any chosen laminate configuration. There are quite a number of failure criteria proposed for predicting macroscale failure in composite structures in the literature [1-19]. Among them, one may cite Tsai-Wu, Tsai-Hill, the maximum stress, the maximum strain, Hoffman, Hashin, Norris, the quadric surfaces, and the modified quadric surfaces. Composite failure criteria are categorized in several ways: the ones with or without stress interaction, stress or strain based, failure mode dependent or independent, linear or quadratic, physically based, i.e. based on failure mechanisms, etc.

Reliability of a failure criterion depends on its success in correctly predicting failure for many different combinations of layup configuration, material, and loading condition, not just for some selected combinations. Validity and reliability of composite failure criteria are well studied for in-plane loads [20-28]. Among them, the most comprehensive study is known as the World Wide Failure Exercise (WWFE) [25-28]. In WWFE, the researchers who proposed a failure criterion were asked to predict the strength of some chosen composites for different layup configurations under various in-plane loading conditions. Following this, the failure criteria were categorized based on the correlation between theoretical and experimental results. WWFE showed that different failure criteria gave better results under different loading conditions and there was not a failure criterion valid for all conditions. However, similar studies are quite limited for out-of-plane loads, and the existing ones are not comprehensive; only some chosen configurations were studied under out-of-plane loads [29-32].

In many industrial applications, composite plates are subjected to not only in-plane loads but also out-of-plane loads. Recognizing that in-plane and out-of-plane responses of composite laminates are quite different, a criterion validated for in-plane loading cannot be

assumed to be also valid for out-of-plane loads. For this reason, there is a need to fully examine the validity of the failure criteria for out-of-plane loads. In this way, safety of a design can be ensured during a design process.

For a failure theory, not only the accuracy of the predictions for some selected configurations, but also the accuracy of the predicted trend of failure is important especially for design optimization studies. Comparison of Figures 1.1 and 1.2, and Figures 1.3 and 1.4 illustrates this point. Figures 1.1 and 1.2 show the change in the strength of unidirectional, $[\theta_{50}]$, and balanced symmetric laminates, $[\theta_{25}/\text{-}\theta_{25}]_s$, as a function of orientation angle, θ, under uniaxial tensile loading with respect to the maximum stress criterion and Tsai-Wu criterion, respectively. Figures 1.3 and 1.4, similarly, demonstrate the change in the strength of the laminates but under bending moment. Here, the safety factor is the ratio of the maximum allowable load to the applied load. The higher safety factor is above 1.0, the safer the design becomes. As the angle between fiber and loading directions decreases, plates are expected to be stronger and vice versa.

Figure 1.1 indicates that the maximum stress criterion predicts slight increase in the strength of unidirectional laminates under in-plane uniaxial loading as the fiber angle is varied from 0 to 7-8 degrees. In the same figure, the strength of balanced symmetric laminates drops suddenly around 27 degrees due to change in failure mode. Figure 1.2 illustrates that Tsai-Wu failure criterion predicts the maximum strength of $[\theta_{25}/\text{-}\theta_{25}]_s$ laminates to be around 15 degrees under uniaxial loading. Figure 1.3 indicates that according to the maximum stress criterion, strength is maximum around 12 degrees for $[\theta_{25}/\text{-}\theta_{25}]_s$ laminates. Besides, the figure shows that the strength of unidirectional laminates does not decrease as the fiber angle increases from 0 to 7-8 degrees. Figures from 1.1 to 1.4 prove that the failure trends predicted by the two of the most widely used failure criteria are inconsistent for uniaxial loading and bending moment for both unidirectional and balanced laminates. Although there are published studies that investigated the failure trend for in-plane loads, no study exists on the failure trend for out-of-plane loads. For this reason, the relative success of the failure theories in correctly predicting the trend for out-of-plane loads may not be decided.

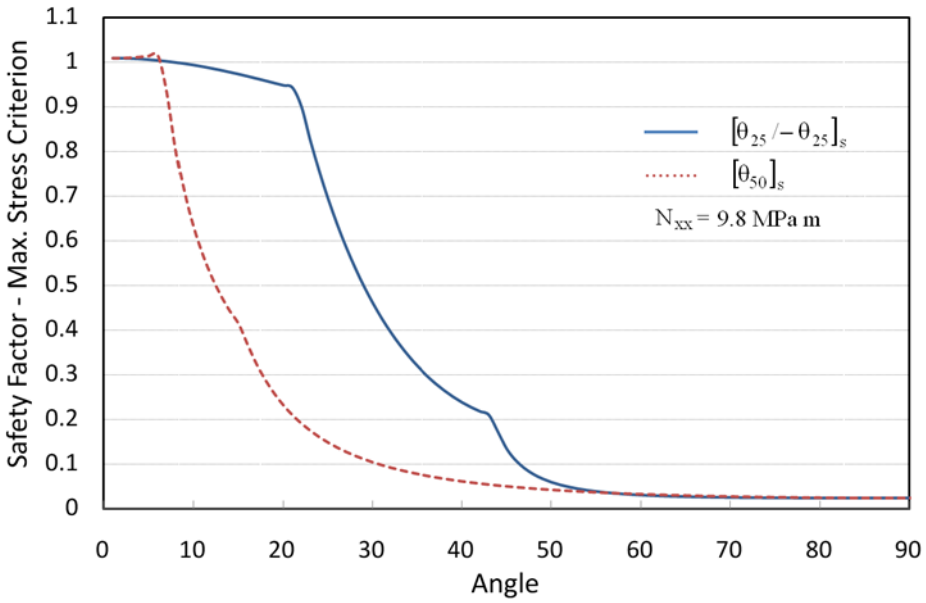

Figure 1.1. Safety factors calculated using the maximum stress criterion for a laminate subjected to uniaxial loading (only $N_{xx} \neq 0$) for a range of fiber orientation angles, θ [33].

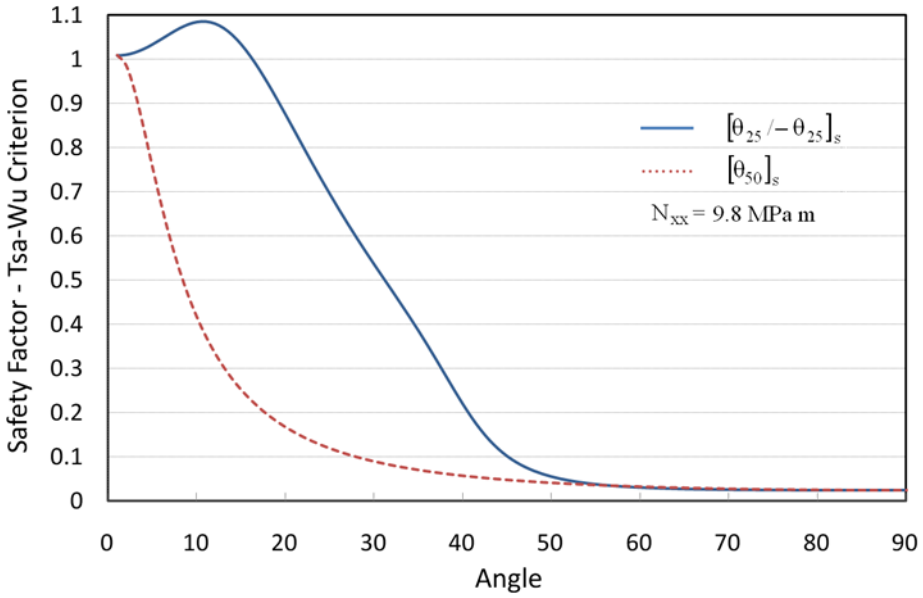

Figure 1.2. Safety factors calculated using the Tsai-Wu criterion for a laminate subjected to uniaxial loading (only $N_{xx} \neq 0$) for a range of fiber orientation angles, θ [33].

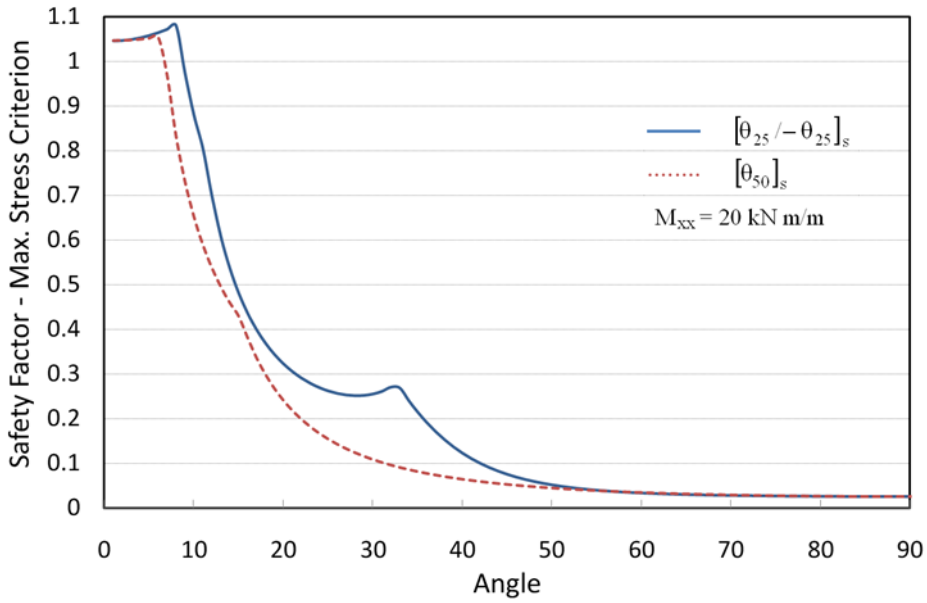

Figure 1.3. Safety factors calculated using the maximum stress criterion for a laminate subjected to one component of bending (only $M_{xx}\neq0$) for a range of fiber orientation angles, θ [33].

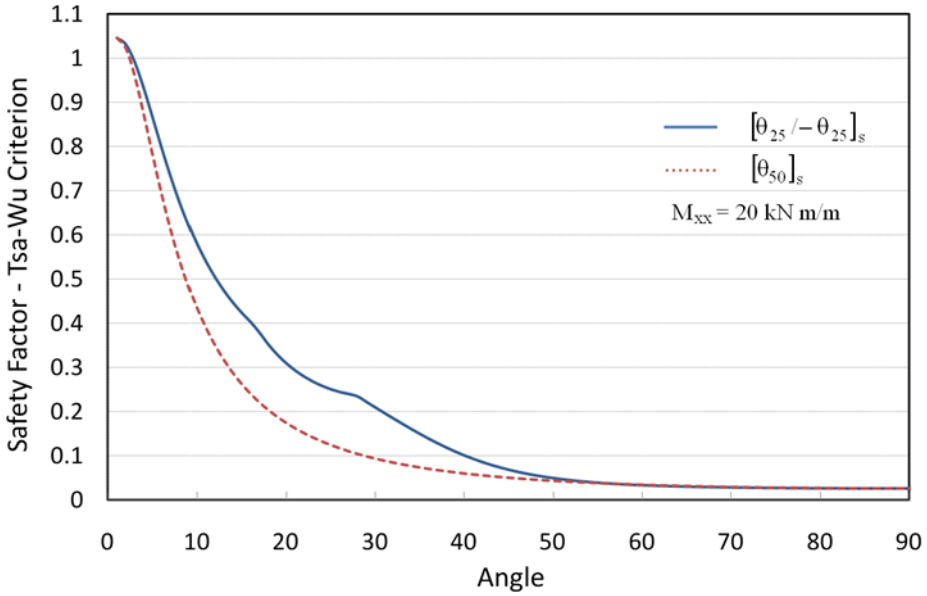

Figure 1.4. Safety factors calculated using the Tsai-Wu criterion for a laminate subjected to one component of bending (only $M_{xx}\neq0$) for a range of fiber orientation angles, θ [33].

In the rare studies in which the effect of out-of-plane loads on the failure behavior of composites was investigated, four-point bending tests [32] were not used as frequently as three-point bending tests [29-31]. The disadvantage of three-point bending test, which is

shown in Figure 1.5, is that a concentrated force exists at the most critical region of the plate. In that case, FE results highly depend on mesh density. Besides, not only bending moment but also transverse shear stress is induced; therefore, their separate effects cannot be differentiated. Considering that the critical region is small, strength highly depends on the local density of micro defects in this region. Different distributions of defects in different specimens will reduce the reliability of strength measurements. On the other hand, in four - point bending test specimens, pure bending moment develops between the loading locations.

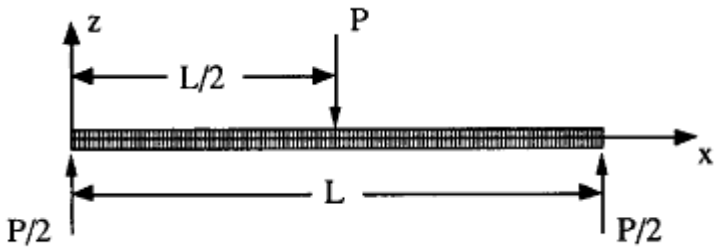

Figure 1.5. Load configuration for a beam in three-point bending [29].

Because of the difference between thermal expansion coefficients in the directions along the fiber and transverse to it, residual stresses develop after laminae with different fiber orientations are joined at a high temperature and cooled down. Microscopic residual stresses may occur in unidirectional laminated composites, but they are not as important when compared to macroscopic residual stresses in multidirectional laminates. Those macroscopic stresses may even cause matrix cracks during cooling process before the application of mechanical loads [41]. They may also lead to premature failure under loading. In the studies, in which failure of composites under out-of-plane loading was investigated, the effects of residual stresses were not taken into account.

In this study, the failure behavior of fiber-reinforced composites under out-of-plane loads was investigated. For this purpose, a four-point bending test setup was designed and constructed such that the static failure modes would be more critical than the delamination failure mode. Unidirectional $[\theta_6]_s$ and balanced symmetric $[\theta_3/-\theta_3]_s$ composite laminates were considered and the experiments were repeated three to six times to obtain their strength. The tests were simulated using both the classical lamination theory (CLT) and the

finite element method (FEM) and the maximum allowable moment resultants, M_{max}, as a function of fiber orientation angle, θ, were obtained using different failure criteria. For balanced symmetric laminates, residual stresses were considered, which in turn increased the reliability of analytical and numerical results. The values of M_{max} obtained numerically and analytically were then compared with the test results for $[\theta_6]_s$ and $[\theta_3/-\theta_3]_s$ layup sequences for fiber angles of 0°, 15°, 30°, 45°, 60°, 75°, and 90°. In addition, four unidirectional specimen with $[5_6]_s$ layup sequence were tested. In this way, not only the accuracy of the predictions was examined, but also the correctness of the predicted trend of failure was observed.

The original contributions of this study to the literature on this subject are as follows: First of all, this is a much more comprehensive study in that comparisons were not done for some selected configurations; but the predicted and actual failure trends were compared. Secondly, residual stresses were accounted for in failure assessments. Thirdly, a four-point bending test setup was designed such that the static failure modes dominated over delamination failure mode. Fourthly, a greater number of failure theories were considered.

2. THEORETICAL MODEL

2.1. Theory

Application of the failure theories requires the stress and strain states in the composite structure, which can be obtained via a structural analysis. Mechanics of composite materials may be investigated in micro and macro level. Micromechanical analysis of composites from its constituent properties is out of scope of this study. Only the macro behavior is analyzed.

A lamina is a basic building block of composite laminates. It is logical to deal with the mechanics of single lamina at the beginning and then progress to obtain stress-strain relations for laminates with the help of classical lamination theory (CLT). CLT makes a series of hypotheses which simplifies the problem from 3-D to 2-D.

$$\begin{bmatrix} \varepsilon_1 \\ \varepsilon_2 \\ \gamma_{12} \end{bmatrix} = \begin{bmatrix} S_{11} & S_{12} & 0 \\ S_{12} & S_{22} & 0 \\ 0 & 0 & S_{66} \end{bmatrix} \begin{bmatrix} \sigma_1 \\ \sigma_2 \\ \sigma_{12} \end{bmatrix} \tag{2.1}$$

$$\begin{bmatrix} \sigma_1 \\ \sigma_2 \\ \sigma_{12} \end{bmatrix} = \begin{bmatrix} Q_{11} & Q_{12} & 0 \\ Q_{12} & Q_{22} & 0 \\ 0 & 0 & Q_{66} \end{bmatrix} \begin{bmatrix} \varepsilon_1 \\ \varepsilon_2 \\ \gamma_{12} \end{bmatrix} \tag{2.2}$$

where Q_{ij} is the reduced stiffness matrix under plane stress. Constituents of Q_{ij} are demonstrated in terms of engineering constants in Equations 2.3 – 6.

$$Q_{11} = \frac{E_1}{1 - \nu_{12}\nu_{21}} \tag{2.3}$$

$$Q_{22} = \frac{E_2}{1 - \nu_{12}\nu_{21}} \tag{2.4}$$

$$Q_{12} = \frac{\nu_{12}E_2}{1-\nu_{12}\nu_{21}} = \frac{\nu_{21}E_1}{1-\nu_{12}\nu_{21}} \tag{2.5}$$

$$Q_{66} = G_{12} \tag{2.6}$$

For fiber reinforced composites, principal (native) and global coordinate systems merely coincides. Before proceeding stress-strain relations from lamina to laminate level, it is necessary to set forth transformations rules from native to global coordinate system. Figure 2.1 shows the positive rotation of principal axes from x-y axes. Here, θ is the positive angle from x- axis to 1- axis.

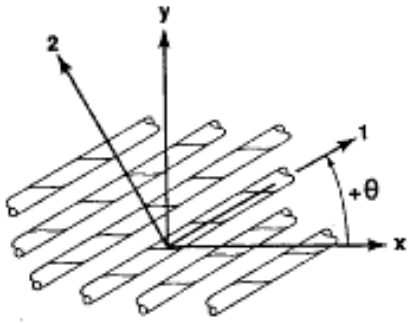

Figure 2.1. Positive rotation of principal material axes from x-y axes to 1-2 axes [35].

Stress and strain transformation rules for laminates given by Jones [35] are shown in Equations 2.7 – 2.8.

$$\begin{bmatrix}\sigma_x\\ \sigma_y\\ \sigma_{xy}\end{bmatrix} = \begin{bmatrix} cos^2\theta & sin^2\theta & -2\,cos\theta\,sin\theta \\ sin^2\theta & cos^2\theta & 2\,cos\theta\,sin\theta \\ cos\theta\,sin\theta & -cos\theta\,sin\theta & cos^2\theta - sin^2\theta \end{bmatrix} \begin{bmatrix}\sigma_1\\ \sigma_2\\ \sigma_{12}\end{bmatrix} \tag{2.7}$$

$$\begin{bmatrix}\varepsilon_x\\ \varepsilon_y\\ \frac{\gamma_{xy}}{2}\end{bmatrix} = \begin{bmatrix} cos^2\theta & sin^2\theta & -2\,cos\theta\,sin\theta \\ sin^2\theta & cos^2\theta & 2\,cos\theta\,sin\theta \\ cos\theta\,sin\theta & -cos\theta\,sin\theta & cos^2\theta - sin^2\theta \end{bmatrix} \begin{bmatrix}\varepsilon_1\\ \varepsilon_2\\ \frac{\gamma_{12}}{2}\end{bmatrix} \tag{2.8}$$

In Equations 2.7 – 8, the first term on the left hand side is the inverse of direction cosine matrix [T]. Thus, Equations 2.7 – 8 can be expresses as follows:

$$\begin{bmatrix}\sigma_x\\ \sigma_y\\ \sigma_{xy}\end{bmatrix} = [T]^{-1}\begin{bmatrix}\sigma_1\\ \sigma_2\\ \sigma_{12}\end{bmatrix} \tag{2.9}$$

$$\begin{bmatrix}\varepsilon_x\\ \varepsilon_y\\ \frac{\gamma_{xy}}{2}\end{bmatrix} = [T]^{-1}\begin{bmatrix}\varepsilon_1\\ \varepsilon_2\\ \frac{\gamma_{12}}{2}\end{bmatrix} \tag{2.10}$$

where -1 superscript denotes that $[T]^{-1}$ is inverse of [T]. Defining [R] matrix such that

$$R = \begin{bmatrix}1 & 0 & 0\\ 0 & 1 & 0\\ 0 & 0 & 2\end{bmatrix} \tag{2.11}$$

Stress - strain relations in global coordinates are

$$\begin{bmatrix}\sigma_x\\ \sigma_y\\ \sigma_{xy}\end{bmatrix} = [\bar{Q}]\begin{bmatrix}\varepsilon_x\\ \varepsilon_y\\ \gamma_{xy}\end{bmatrix} = \begin{bmatrix}\bar{Q}_{11} & \bar{Q}_{12} & \bar{Q}_{16}\\ \bar{Q}_{12} & \bar{Q}_{22} & \bar{Q}_{26}\\ \bar{Q}_{13} & \bar{Q}_{23} & \bar{Q}_{66}\end{bmatrix}\begin{bmatrix}\varepsilon_x\\ \varepsilon_y\\ \gamma_{xy}\end{bmatrix} \tag{2.12}$$

where

$$[\bar{Q}] = [T]^{-1}[\mathrm{Q}][\mathrm{R}][\mathrm{T}][R]^{-1} \tag{2.13}$$

$\bar{Q}_{\mathrm{ij}}$ is the transformed reduced stiffness matrix for laminae in which

$$\bar{Q}_{11} = Q_{11}cos^4\theta + 2(Q_{12} + 2Q_{66})sin^2\theta cos^2\theta + Q_{22}sin^4\theta \tag{2.14}$$

$$\bar{Q}_{12} = (Q_{11} + Q_{22} - 4Q_{66})sin^2\theta cos^2\theta + Q_{12}(sin^4\theta + cos^4\theta) \tag{2.15}$$

$$\bar{Q}_{22} = Q_{11}sin^4\theta + 2(Q_{12} + 2Q_{66})sin^2\theta cos^2\theta + Q_{22}cos^4\theta \tag{2.16}$$

$$\bar{Q}_{16} = (Q_{11} - Q_{12} - 2Q_{66})sin\theta cos^3\theta + (Q_{12} - Q_{22} + 2Q_{66})sin^3\theta cos\theta \quad (2.17)$$

$$\bar{Q}_{26} = (Q_{11} - Q_{12} - 2Q_{66})sin^3\theta cos\theta + (Q_{12} - Q_{22} + 2Q_{66})sin\theta cos^3\theta \quad (2.18)$$

$$\bar{Q}_{66} = (Q_{11} + Q_{22} - 2Q_{12} - 2Q_{66})sin^2\theta cos^2\theta + Q_{66}(sin^4\theta + cos^4\theta) \quad (2.19)$$

Hereafter, one can obtain stress-strain relations for laminates using CLT. CLT is an extension of Kirchoff plate and Kirchoff-Love shell theories and only applicable to thin laminates. The following are the assumptions of CLT given by Choo [53]:

(i) The laminae within the laminate are perfectly bonded together.

(ii) The layer of bonding agent is thin.

(iii) The laminate is thin.

(iv) No relative slippage occurs among the laminae. This implies that the displacements are continuous and unique across each lamina boundary (γ_{13}= γ_{23}=0).

(v) The normal strain ε_3 in the x_3 direction is negligible.

(vi) The interlaminate shear stresses are zero.

(vii) Straight lines originally perpendicular to the laminate midplane remain straight and perpendicular to the midplane in a deformed state.

(viii) Each lamina within laminate behaves elastically.

As it is shown in Figure 2.2, mechanical behavior of a lamina in a laminate may be different than a single lamina. Stress-strain relation for the kth layer of a multilayered laminate is as follows:

$$[\sigma]_k = [\bar{Q}]_k[\varepsilon] \quad (2.20)$$

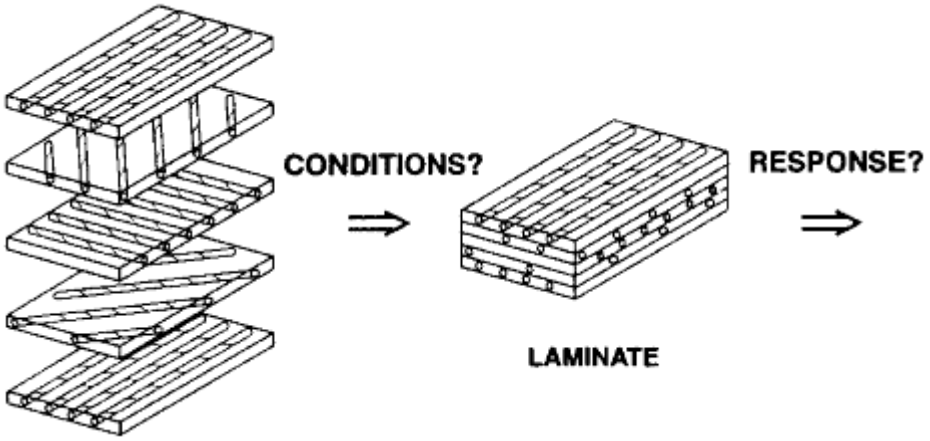

Figure 2.2. From lamina to laminate [35].

Displacements of a lamina in a multilayered laminate is different than a single lamina, so the strains. Displacements are not only dependent on fiber orientation angle but also the distance from the middle surface. Taking into account that straight lines originally perpendicular to the laminate middle plane remain straight and perpendicular to the midplane in a deformed state, deformations of a lamina in a laminate are given below:

$$u = u_o - z\frac{\partial w_o}{\partial x} \tag{2. 21}$$

$$v = v_o - z\frac{\partial w_o}{\partial y} \tag{2.22}$$

where z is the distance of lamina from the midplane and subscript “o” refers to midplane. Strains of a lamina in a laminate can be defined as the following:

$$\varepsilon_x = \frac{\partial u_o}{\partial x} - z\frac{\partial^2 w_o}{\partial x^2} \tag{2.23}$$

$$\varepsilon_y = \frac{\partial v_o}{\partial y} - z\frac{\partial^2 w_o}{\partial y^2} \tag{2.24}$$

$$\gamma_{xy} = \frac{\partial u_o}{\partial y} + \frac{\partial v_o}{\partial x} - 2z\frac{\partial^2 w_o}{\partial x \partial y} \tag{2.25}$$

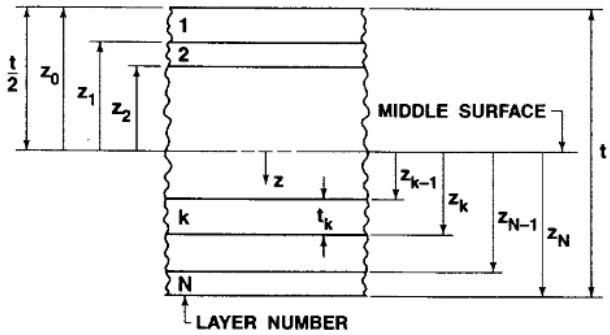

Figure 2.3. A laminate with N layers [35].

Midplane strains ε_{ij}^{o} and curvature terms κ_{ij} are defined as follows:

$$\begin{bmatrix} \varepsilon_x^o \\ \varepsilon_y^o \\ \gamma_{xy}^o \end{bmatrix} = -\begin{bmatrix} \dfrac{\partial u_o}{\partial x} \\ \dfrac{\partial v_o}{\partial y} \\ \dfrac{\partial u_o}{\partial y} + \dfrac{\partial v_o}{\partial x} \end{bmatrix} \tag{2.26}$$

$$\begin{bmatrix} \kappa_x \\ \kappa_y \\ \kappa_{xy} \end{bmatrix} = -\begin{bmatrix} \dfrac{\partial^2 w_o}{\partial x^2} \\ \dfrac{\partial^2 w_o}{\partial y^2} \\ 2\dfrac{\partial^2 w_o}{\partial x \partial y} \end{bmatrix} \tag{2.27}$$

Implementing Equations 2.26 – 27 into Equations 2.23 – 25, strains in the kth layer are defined below.

$$\begin{bmatrix} \varepsilon_x \\ \varepsilon_y \\ \varepsilon_{xy} \end{bmatrix} = \begin{bmatrix} \varepsilon_x^o \\ \varepsilon_y^o \\ \gamma_{xy}^o \end{bmatrix} + z\begin{bmatrix} \kappa_x \\ \kappa_y \\ \kappa_{xy} \end{bmatrix} \tag{2.28}$$

Stresses in the kth layer of a laminate are defined in terms of strains and curvatures in Equation 2.29.

$$\begin{bmatrix}\sigma_x\\ \sigma_y\\ \sigma_{xy}\end{bmatrix}_k = \begin{bmatrix}\bar{Q}_{11} & \bar{Q}_{12} & \bar{Q}_{16}\\ \bar{Q}_{12} & \bar{Q}_{22} & \bar{Q}_{26}\\ \bar{Q}_{13} & \bar{Q}_{23} & \bar{Q}_{66}\end{bmatrix}_k \left(\begin{bmatrix}\varepsilon_x^o\\ \varepsilon_y^o\\ \gamma_{xy}^o\end{bmatrix} + z \begin{bmatrix}\kappa_x\\ \kappa_y\\ \kappa_{xy}\end{bmatrix} \right) \tag{2.29}$$

Resultant in-plane loads and moments in a laminate are illustrated below:

$$\begin{bmatrix}N_x\\ N_y\\ N_{xy}\end{bmatrix} = \int_{-t/2}^{t/2} \begin{bmatrix}\sigma_x\\ \sigma_y\\ \sigma_{xy}\end{bmatrix} dz = \sum_{k=1}^{N} \int_{z_{k-1}}^{z_k} \begin{bmatrix}\sigma_x\\ \sigma_y\\ \sigma_{xy}\end{bmatrix}_k dz \tag{2.30}$$

$$\begin{bmatrix}M_x\\ M_y\\ M_{xy}\end{bmatrix} = \int_{-t/2}^{t/2} \begin{bmatrix}\sigma_x\\ \sigma_y\\ \sigma_{xy}\end{bmatrix} z\, dz = \sum_{k=1}^{N} \int_{z_{k-1}}^{z_k} \begin{bmatrix}\sigma_x\\ \sigma_y\\ \sigma_{xy}\end{bmatrix}_k z\, dz \tag{2.31}$$

Plugging Equation 2.29 into Equations 2.30 – 31, force and moment resultants, which are shown in Figure 2.4 and Figure 2.5, become

$$\begin{bmatrix}N_x\\ N_y\\ N_{xy}\end{bmatrix} = \sum_{k=1}^{N} \begin{bmatrix}\bar{Q}_{11} & \bar{Q}_{12} & \bar{Q}_{16}\\ \bar{Q}_{12} & \bar{Q}_{22} & \bar{Q}_{26}\\ \bar{Q}_{13} & \bar{Q}_{23} & \bar{Q}_{66}\end{bmatrix}_k \left(\int_{z_{k-1}}^{z_k} \begin{bmatrix}\varepsilon_x^o\\ \varepsilon_y^o\\ \gamma_{xy}^o\end{bmatrix} dz + \int_{z_{k-1}}^{z_k} \begin{bmatrix}\kappa_x\\ \kappa_y\\ \kappa_{xy}\end{bmatrix} z\, dz \right) \tag{2.32}$$

$$\begin{bmatrix}M_x\\ M_y\\ M_{xy}\end{bmatrix} = \sum_{k=1}^{N} \begin{bmatrix}\bar{Q}_{11} & \bar{Q}_{12} & \bar{Q}_{16}\\ \bar{Q}_{12} & \bar{Q}_{22} & \bar{Q}_{26}\\ \bar{Q}_{13} & \bar{Q}_{23} & \bar{Q}_{66}\end{bmatrix}_k \left(\int_{z_{k-1}}^{z_k} \begin{bmatrix}\varepsilon_x^o\\ \varepsilon_y^o\\ \gamma_{xy}^o\end{bmatrix} z\, dz + \int_{z_{k-1}}^{z_k} \begin{bmatrix}\kappa_x\\ \kappa_y\\ \kappa_{xy}\end{bmatrix} z^2\, dz \right) \tag{2.33}$$

or they can be expressed as

$$\begin{bmatrix}N_x\\ N_y\\ N_{xy}\end{bmatrix} = \begin{bmatrix}A_{11} & A_{12} & A_{16}\\ A_{12} & A_{22} & A_{26}\\ A_{13} & A_{23} & A_{66}\end{bmatrix} \begin{bmatrix}\varepsilon_x^o\\ \varepsilon_y^o\\ \gamma_{xy}^o\end{bmatrix} + \begin{bmatrix}B_{11} & B_{12} & B_{16}\\ B_{12} & B_{22} & B_{26}\\ B_{13} & B_{23} & B_{66}\end{bmatrix} \begin{bmatrix}\kappa_x\\ \kappa_y\\ \kappa_{xy}\end{bmatrix} \tag{2.34}$$

$$\begin{bmatrix}M_x\\ M_y\\ M_{xy}\end{bmatrix} = \begin{bmatrix}B_{11} & B_{12} & B_{16}\\ B_{12} & B_{22} & B_{26}\\ B_{13} & B_{23} & B_{66}\end{bmatrix} \begin{bmatrix}\varepsilon_x^o\\ \varepsilon_y^o\\ \gamma_{xy}^o\end{bmatrix} + \begin{bmatrix}D_{11} & D_{12} & D_{16}\\ D_{12} & D_{22} & D_{26}\\ D_{13} & D_{23} & D_{66}\end{bmatrix} \begin{bmatrix}\kappa_x\\ \kappa_y\\ \kappa_{xy}\end{bmatrix} \tag{2.35}$$

where

$$A_{ij} = \sum_{k=1}^{N} \left(\bar{Q}_{ij}\right)_k (z_k - z_{k-1}) \tag{2.36}$$

$$B_{ij} = \frac{1}{2} \sum_{k=1}^{N} \left(\bar{Q}_{ij}\right)_k (z_k^2 - z_{k-1}^2) \tag{2.37}$$

$$D_{ij} = \frac{1}{3} \sum_{k=1}^{N} \left(\bar{Q}_{ij}\right)_k (z_k^3 - z_{k-1}^3) \tag{2.38}$$

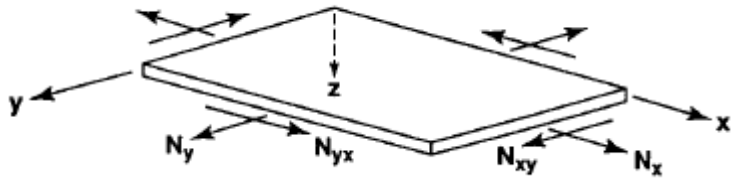

Figure 2.4. In plane force resultants on a flat laminate [35].

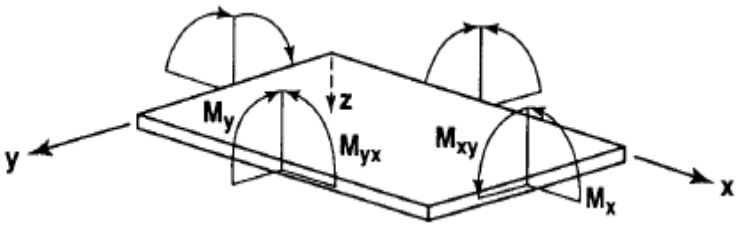

Figure 2.5. Moment resultants on a flat laminate [35].

2.1.1. Residual Stresses

If a laminate is multidirectional, thermal force and moment resultants should also be taken into account in failure analyses. Residual stresses in multidirectional plates are calculated according to the method given by Hyer [36] and added to the mechanical stresses.

Thermo-mechanical relationship between force and moment resultants and strains and curvatures in a laminate are as follows:

$$\begin{bmatrix} N_x + N_x^T \\ N_y + N_y^T \\ N_{xy} + N_{xy}^T \\ M_x + M_x^T \\ M_y + M_y^T \\ M_{xy} + M_{xy}^T \end{bmatrix} = \begin{bmatrix} A_{11} & A_{12} & A_{16} & B_{11} & B_{12} & B_{16} \\ A_{12} & A_{22} & A_{26} & B_{12} & B_{22} & B_{26} \\ A_{13} & A_{23} & A_{66} & B_{13} & B_{23} & B_{66} \\ B_{11} & B_{12} & B_{16} & D_{11} & D_{12} & D_{16} \\ B_{12} & B_{22} & B_{26} & D_{12} & D_{22} & D_{26} \\ B_{13} & B_{23} & B_{66} & D_{13} & D_{23} & D_{66} \end{bmatrix} \begin{bmatrix} \varepsilon_x^o \\ \varepsilon_y^o \\ \gamma_{xy}^o \\ \kappa_x \\ \kappa_y \\ \kappa_{xy} \end{bmatrix} \tag{2.39}$$

where superscript *T* refers to thermal force and moment resultants, which can be calculated by means of Equations 2.40 – 41.

$$\begin{bmatrix} N_x^T \\ N_y^T \\ N_{xy}^T \end{bmatrix} = \sum_{k=1}^{N} \begin{bmatrix} \bar{Q}_{11} & \bar{Q}_{12} & \bar{Q}_{16} \\ \bar{Q}_{12} & \bar{Q}_{22} & \bar{Q}_{26} \\ \bar{Q}_{13} & \bar{Q}_{23} & \bar{Q}_{66} \end{bmatrix}_k \begin{bmatrix} \alpha_x \\ \alpha_y \\ \alpha_{xy} \end{bmatrix}_k (z_k - z_{k-1})\, \Delta T \tag{2.40}$$

$$\begin{bmatrix} M_x^T \\ M_y^T \\ M_{xy}^T \end{bmatrix} = \sum_{k=1}^{N} \begin{bmatrix} \bar{Q}_{11} & \bar{Q}_{12} & \bar{Q}_{16} \\ \bar{Q}_{12} & \bar{Q}_{22} & \bar{Q}_{26} \\ \bar{Q}_{13} & \bar{Q}_{23} & \bar{Q}_{66} \end{bmatrix}_k \begin{bmatrix} \alpha_x \\ \alpha_y \\ \alpha_{xy} \end{bmatrix}_k (z_k^2 - z_{k-1}^2)\, \Delta T \tag{2.41}$$

where ΔT is the temperature difference between the cure temperature and the room temperature and α_x, α_y and α_{xy} are thermal expansion coefficients in global x- direction, y-direction and x-y plane, respectively. A laminate is stress free at cure temperature. Residual stresses occur when a multidirectional laminate cools down to room temperature because thermal expansion coefficients depend on fiber orientation angles of laminae. The relationship between thermal expansion coefficients in native and global coordinates are illustrated below:

$$\alpha_x = \alpha_1 cos^2\theta + \alpha_2 sin^2\theta \tag{2.42}$$

$$\alpha_y = \alpha_1 sin^2\theta + \alpha_2 cos^2\theta \tag{2.43}$$

$$\alpha_{xy} = 2(\alpha_1 - \alpha_2) cos\theta sin\theta \tag{2.44}$$

2.2. Stress – Moment Resultant Relationship

The thickness of the plate is small as compared to its width and length (less than one-twentieth) which turns the problem into a plane stress problem. Classical Lamination Theory (CLT) is utilized to relate loading to the resulting stress state. Bending-extension coupling matrix [B] reduces to zero thanks to symmetry conditions. Considering that only M_{xx} is applied to the laminate, stresses in layer k are as follows:

$$\begin{bmatrix} \varepsilon_x^o \\ \varepsilon_y^o \\ \gamma_{xy}^o \\ \kappa_x \\ \kappa_y \\ \kappa_{xy} \end{bmatrix} = \begin{bmatrix} A_{11} & A_{12} & A_{16} & 0 & 0 & 0 \\ A_{12} & A_{22} & A_{26} & 0 & 0 & 0 \\ A_{13} & A_{23} & A_{66} & 0 & 0 & 0 \\ 0 & 0 & 0 & D_{11} & D_{12} & D_{16} \\ 0 & 0 & 0 & D_{12} & D_{22} & D_{26} \\ 0 & 0 & 0 & D_{13} & D_{23} & D_{66} \end{bmatrix}^{-1} \begin{bmatrix} N_x^T \\ N_y^T \\ N_{xy}^T \\ M_{max} + M_x^T \\ M_y^T \\ M_{xy}^T \end{bmatrix} \tag{2.45}$$

where M_{max} is the maximum allowable moment resultant, which makes the failure index of the laminate for the respective failure criterion equal to 1.0. Force and moment resultants as a result of residual stresses are calculated using Equations 2.40 – 41 and added to the mechanical resultants. Implementing Equation 2.45 into Equation 2.29, stresses in the kth layer become:

$$\begin{bmatrix} \sigma_x \\ \sigma_y \\ \sigma_{xy} \end{bmatrix}_k = z \begin{bmatrix} \overline{Q}_{11} & \overline{Q}_{12} & \overline{Q}_{16} \\ \overline{Q}_{12} & \overline{Q}_{22} & \overline{Q}_{26} \\ \overline{Q}_{13} & \overline{Q}_{23} & \overline{Q}_{66} \end{bmatrix}_k \left(\begin{bmatrix} A_{11} & A_{12} & A_{16} \\ A_{12} & A_{22} & A_{26} \\ A_{13} & A_{23} & A_{66} \end{bmatrix}^{-1} \begin{bmatrix} N_x^T \\ N_y^T \\ N_{xy}^T \end{bmatrix} + \begin{bmatrix} D_{11} & D_{12} & D_{13} \\ D_{12} & D_{22} & D_{23} \\ D_{13} & D_{23} & D_{33} \end{bmatrix}_k^{-1} \begin{bmatrix} M_{max} + M_x^T \\ M_y^T \\ M_{xy}^T \end{bmatrix} \right) \tag{2.46}$$

Stresses in Equation 2.46 are in global coordinates. These stresses are transformed into native coordinates by means of transformation matrix [T]. Then, the maximum allowable moment is obtained for each lamina by implementing the failure criteria using the stresses in the principal material directions. The minimum value is then assigned to M_{max}.

$$\begin{bmatrix}\sigma_1\\ \sigma_2\\ \sigma_{12}\end{bmatrix}_k = \mathrm{z}\,[\mathrm{T}]\begin{bmatrix}\overline{\mathrm{Q}}_{11} & \overline{\mathrm{Q}}_{12} & \overline{\mathrm{Q}}_{16}\\ \overline{\mathrm{Q}}_{12} & \overline{\mathrm{Q}}_{22} & \overline{\mathrm{Q}}_{26}\\ \overline{\mathrm{Q}}_{13} & \overline{\mathrm{Q}}_{23} & \overline{\mathrm{Q}}_{66}\end{bmatrix}_{\mathrm{k}}\left(\begin{bmatrix}A_{11} & A_{12} & A_{16}\\ A_{12} & A_{22} & A_{26}\\ A_{13} & A_{23} & A_{66}\end{bmatrix}^{-1}\begin{bmatrix}N_x^T\\ N_y^T\\ N_{xy}^T\end{bmatrix} + \begin{bmatrix}\mathrm{D}_{11} & \mathrm{D}_{12} & \mathrm{D}_{13}\\ \mathrm{D}_{12} & \mathrm{D}_{22} & \mathrm{D}_{23}\\ \mathrm{D}_{13} & \mathrm{D}_{23} & \mathrm{D}_{33}\end{bmatrix}_{\mathrm{k}}^{-1}\begin{bmatrix}\mathrm{M}_{\max}+\mathrm{M}_{\mathrm{x}}^{\mathrm{T}}\\ \mathrm{M}_{\mathrm{y}}^{\mathrm{T}}\\ \mathrm{M}_{\mathrm{xy}}^{\mathrm{T}}\end{bmatrix}\right) \quad (2.47)$$

2.3.Failure Criteria

In this study, some of the most widely recognized criteria in each category are studied and their predictions are compared by simulating four - point bending test, where the middle regions of the laminate are subjected to pure bending moment. Among the chosen failure criteria, Tsai-Wu, Norris, quadric surfaces and modified quadric surfaces are both nonlinear and stress based; they account for stress interaction and failure mode independent; Maximum Stress is stress based, linear and failure mode dependent; Maximum Strain is strain based, linear and failure mode dependent; Hashin is physically based, nonlinear, failure mode dependent and it accounts for stress interaction.

2.3.1. Tsai-Wu Failure Criterion

Tsai-Wu failure criterion is well accepted among researchers and design engineers for the failure analysis of fiber reinforced laminated composites. It is a non-linear, stress based criterion. The criterion accounts for stress interaction; however, does not account for failure mode. According to this criterion [35], the onset of failure is estimated by the following equation:

$$F_i\sigma_i + F_{ij}\sigma_{ij} \geq 1 \quad i,j=1\ldots6 \quad (2.48)$$

wherein F_i and F_{ij} are second and forth rank strength tensors, respectively. Under plane stress conditions, Equation 2.48 reduces to the following:

$$F_1\sigma_1 + F_2\sigma_2 + F_6\sigma_6 + F_{11}\sigma_1^2 + F_{22}\sigma_2^2 + F_{66}\sigma_6^2 + 2F_{12}\sigma_1\sigma_2 \geq 1 \qquad (2.49)$$

Plugging F_i and F_{ij} into Equation 2.49 in extended form, failure under plane stress is estimated by the following equation:

$$\left(\frac{1}{X_t} + \frac{1}{X_c}\right)\sigma_1 + \left(\frac{1}{Y_t} + \frac{1}{Y_c}\right)\sigma_2 - \frac{\sigma_1^2}{X_t X_c} - \frac{\sigma_2^2}{Y_t Y_c} + \frac{\sigma_{12}^2}{{S_{12}}^2} - \frac{\sigma_1\sigma_2}{\sqrt{X_t Y_t X_c Y_c}} \geq 1 \qquad (2.50)$$

In Equation 2.50, X and Y denote strengths in 1-direction and 2-direction and S_{12} refers to shear strength in 1-2 plane, respectively. Subscripts "t" and "c", on the other hand, refers to tensile and compression strengths.

One can obtain the maximum bending moment, M_{max}, that can be applied to the plate without causing failure in a lamina by substituting the stress components in that lamina in the principal material coordinates, σ_1, σ_2, and σ_{12}, given in Equation 2.47 into Equation 2.50. The maximum moment that can be applied to the laminated plate is the minimum of M_{max} calculated for the laminae.

2.3.2. Maximum Stress Failure Criterion

Maximum stress is a linear, stress based, failure mode dependent criterion without stress interaction. According to this criterion [35], safety of a composite plate under plane stress is ensured if the following conditions are satisfied:

$$X_c < \sigma_1 < X_t \qquad (2.51)$$

$$Y_c < \sigma_2 < Y_t \qquad (2.52)$$

$$|\sigma_{12}| < S_{12} \tag{2.53}$$

M_{max} is found for a lamina by substituting the stress components in the principal material coordinates, σ_1, σ_2, and σ_{12}, given in Equation. 2.47 into Equations 2.51 – 53 and solving for M_{max} for the equality cases and choosing the minimum value.

2.3.3. Maximum Strain Failure Criterion

Maximum strain criterion is a strain based criterion as opposed to maximum stress and Tsai-Wu failure criteria. It is also linear and failure mode dependent; yet, does not account for interaction between strains.

$$X_{\varepsilon_c} < \varepsilon_1 < X_{\varepsilon_c} \tag{2.54}$$

$$Y_{\varepsilon_c} < \varepsilon_2 < Y_{\varepsilon_t} \tag{2.55}$$

$$|\varepsilon_{12}| < S_{\varepsilon} \tag{2.56}$$

where $X_{\varepsilon_t}$and X_{ε_c} are the maximum tensile and compression strains in the 1-direction, Y_{ε_t} and Y_{ε_c} are the maximum tensile and compression strains in the 2-direction and S_{ε} is the maximum shear strain in the 1-2 plane, respectively. M_{max} is found for a lamina by substituting the strain components in the principal material coordinates, ε_1, ε_2, and, ε_{12}, into Equations 2.54 – 56 for the equality cases. Principal strains are found by means of the transformation matrix as follows:

$$\begin{bmatrix} \varepsilon_1 \\ \varepsilon_2 \\ \varepsilon_{12} \end{bmatrix} = [T] \begin{bmatrix} \varepsilon_x \\ \varepsilon_y \\ \varepsilon_{xy} \end{bmatrix} \tag{2.57}$$

2.3.4. Hashin Failure Criterion

Hashin [9] proposed a physically based failure criterion that determined the failure modes of fiber – reinforced laminates. The criterion is also nonlinear and accounts for stress interaction. According to the criterion, failure occurs under plane stress condition, if one of the following conditions occurs:

Tensile Fiber Mode ($\sigma_{11}>0$):

$$\frac{\sigma_1^2}{{X_t}^2}+\frac{\sigma_{12}^2}{{S_{12}}^2}\geq 1 \tag{2.58}$$

Compressive Fiber Mode ($\sigma_{11}<0$):

$$\sigma_1 \geq -X_c \tag{2.59}$$

Tensile Matrix Mode ($\sigma_{22}>0$):

$$\frac{\sigma_2^2}{{Y_t}^2}+\frac{\sigma_{12}^2}{{S_{12}}^2}\geq 1 \tag{2.60}$$

Compressive Matrix Mode ($\sigma_{22}<0$):

$$\left(\frac{\sigma_2}{2S_{23}}\right)^2+\left[\left(\frac{X_c}{2S_{23}}\right)^2-1\right]\frac{\sigma_2}{X_c}+\left(\frac{\sigma_{12}}{S_{12}}\right)^2\geq 1 \tag{2.61}$$

where S_{23} is the maximum allowable shear stress in 2-3 plane.

2.3.5. Tsai-Hill Failure Criterion

Hill [3] proposed a stress based, quadratic, failure mode independent criterion which accounts for stress interaction. According to the criterion failure occurs if the Equation 2.62 is satisfied:

$$(G+H)\sigma_1^2 + (F+H)\sigma_2^2 + (F+G)\sigma_3^2 - 2H\sigma_1\sigma_2 - 2G\sigma_1\sigma_3 - 2F\sigma_2\sigma_3 + 2L\sigma_{23}^2 + 2M\sigma_{13}^2 + 2N\sigma_{12}^2 \geq 1 \quad (2.62)$$

where F, G, H, L, M and N are characteristic parameters. Considering that the material is transversely isotropic, Equation 2.62 becomes under plane stress condition as follows:

$$\left(\frac{\sigma_1}{X}\right)^2 - \frac{\sigma_1\sigma_2}{X^2} + \left(\frac{\sigma_2}{Y}\right)^2 + \left(\frac{\sigma_{12}}{S}\right)^2 \geq 1 \quad (2.63)$$

wherein X and Y are either tensile or compression strengths depending on the sign of respective stresses.

2.3.6. Hoffman Failure Criterion

Hoffman [5] introduced a new failure criterion by adding linear terms to Hill's criterion. Just like Tsai-Hill failure criterion, Hoffman criterion is a stress based, quadratic, failure mode independent criterion which accounts for stress interaction. Hoffman claims that failure occurs if the equation below is satisfied:

$$C_1(\sigma_2-\sigma_3)^2 + C_2(\sigma_1-\sigma_3)^2 + C_3(\sigma_1-\sigma_2)^2 + C_4\sigma_1 + C_5\sigma_2 + C_6\sigma_3 + C_7\sigma_{23}^2 + C_8\sigma_{13}^2 + C_9\sigma_{12}^2 \geq 1 \quad (2.64)$$

wherein C_1, C_2, C_3, C_4, C_5, C_6, C_7, C_8 and C_9 are characteristic parameters. Considering plane stress condition and transverse isotropy, Hoffman failure criterion simplifies to the following:

$$-\frac{\sigma_1^2}{X_t X_c}+\frac{\sigma_1\sigma_2}{X_t X_c}-\frac{\sigma_2^2}{Y_t Y_c}+\frac{X_c+X_t}{X_c X_t}\sigma_1+\frac{Y_c+Y_t}{Y_c Y_t}\sigma_2+\frac{\sigma_{12}^2}{S_{12}^2}\geq 1 \qquad (2.65)$$

In Equation 2.65, compressive strengths are negative values.

2.3.7. Quadric Surfaces Criterion

Quadric surfaces criterion is a stress based, non-linear, failure mode independent failure criterion with stress interaction. The generalized form of the quadric surfaces failure function, f, can be stated as below [14]:

$$f = A_{ii}\sigma_i^2 + A_{jj}\sigma_j^2 + A_{ij}\sigma_{ij}^2 + B_{ij}\sigma_i\sigma_j + C_{ij}\sigma_i\sigma_{ij} + D_{ij}\sigma_j\sigma_{ij} + F_i\sigma_i + F_j\sigma_j + F_{ij}\sigma_{ij} \geq 1 \qquad (2.66)$$

for i, j=1,2,3, where, A_{ii}, A_{jj}, A_{ij}, B_{ij}, C_{ij}, D_{ij}, F_i, F_j, F_{ij} are characteristic parameters and the repeated index is not summed. Quadric surfaces criterion claims that failure occurs under plane stress condition in a composite plate if the equation below is satisfied:

$$\frac{a}{X^2}\sigma_1^2+\frac{a}{Y^2}\sigma_2^2+\frac{a}{S^2}\sigma_{12}^2+\frac{b}{XY}\sigma_1\sigma_2+\frac{b}{XS}\sigma_1\sigma_{12}+\frac{b}{YS}\sigma_2\sigma_{12}+\frac{c}{X}\sigma_1+\frac{c}{Y}\sigma_2+\frac{c}{S}\sigma_{12}\geq 1 \qquad (2.67)$$

wherein, a=0.98, b=0.49 and c=0.002 .

2.3.8. Modified Quadric Surfaces Criterion

The modified quadric surfaces failure criterion for the composite materials is a modification of quadric surfaces criterion. Just like that one, the modified quadric surfaces criterion is also a stress based, non-linear, failure mode independent failure criterion with stress interaction. The difference between them is that coefficients of in-plane and shear

coupling terms are assumed to be zero in the latter one. The generalized form of the modified quadric surfaces failure function, f, is given below [15]:

$$f = A_{ii}\sigma_i^2 + A_{jj}\sigma_j^2 + A_{ij}\sigma_{ij}^2 + B_{ij}\sigma_i\sigma_j + F_i\sigma_i + F_j\sigma_j + F_{ij}\sigma_{ij} \geq 1 \tag{2.68}$$

for i, j=1,2,3, where, A_{ii}, A_{jj}, A_{ij}, B_{ij}, F_i, F_j, F_{ij} are characteristic parameters and the repeated index is not summed.. According to the modified quadric surfaces criterion failure occurs if the Equation 2.69 is satisfied:

$$\frac{a}{X^2}\sigma_1^2 + \frac{a}{Y^2}\sigma_2^2 + \frac{a}{S^2}\sigma_{12}^2 + \frac{b}{XY}\sigma_1\sigma_2 + \frac{c}{X}\sigma_1 + \frac{c}{Y}\sigma_2 + \frac{c}{S}\sigma_{12} \geq 1 \tag{2.69}$$

wherein, a=0.98, b=0.49 and c=0.002.

2.3.9. Norris Criterion

Norris proposed a failure theory for orthotropic materials based on the Henky-von Mises energy theory. It is a non-linear, stress-based criterion. The criterion accounts for stress interaction; however, it does not account for failure mode. According to Norris, the onset of failure occurs if at least one of the following equations is satisfied [4]:

$$\frac{\sigma_1^2}{X^2} + \frac{\sigma_2^2}{Y^2} - \frac{\sigma_1\sigma_2}{XY} + \frac{\sigma_{12}^2}{S^2} \geq 1 \tag{2.70}$$

$$\frac{\sigma_1^2}{X^2} \geq 1 \tag{2.71}$$

$$\frac{\sigma_2^2}{Y^2} \geq 1 \tag{2.72}$$

3. FINITE ELEMENT MODELING

Finite element analysis of the plate was performed using finite element software Ansys v13 with SOLID185 layered 3-D structural solid elements. SOLID185 is used for 3-D modeling of solid structures. SOLID185 is defined by eight nodes having three degrees of freedom at each node: translations in the nodal x, y, and z directions 37.

Finite element analysis of the problem was completed in three steps. Firstly, a finite element modeling of the problem was developed. Secondly, a convergence analysis was carried out to find a balance between the computational cost and the accuracy of results. Thirdly, an analysis was conducted for optimal positioning of the loads so as to ensure that the static failure modes dominate delamination failure mode. For this purpose, the results of a delamination criterion [9] were compared with the results of Tsai-Wu and maximum stress failure criteria for different load positions. Then, simulations were conducted using the optimal loading condition in which the most likely failure mode was static failure, not delamination. Lastly, all of the criteria were implemented into ANSYS and M_{max} predictions were obtained as a function of fiber orientation angle.

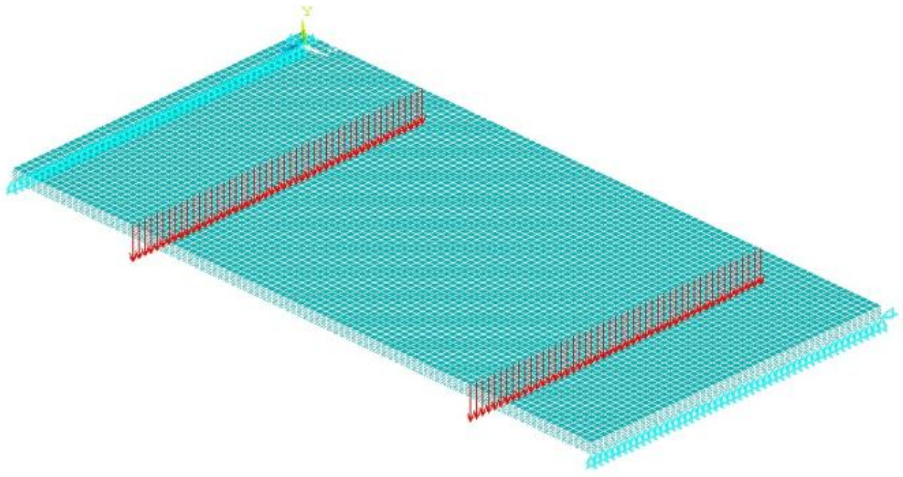

Figure 3.1. Finite element model of the problem showing force and displacement boundary conditions.

3.1. FEM Modeling of the Problem

The problem was modeled using ANSYS Parametric Design Language (APDL). In this way, the maximum allowable moment resultants, M_{max}, were computed for fiber orientation angles, θ, from 0° to 90° with 1° increments; thus M_{max} was obtained as a function of θ.

In ANSYS, a problem is modeled in three steps: preprocessing, solution and postprocessing. In the preprocessing phase, 3-D model of the plate is built and meshed. In the solution phase, displacement and force boundary conditions are applied and the problem is solved. The nodes which coincide with bottom supports are held in the z direction. In addition to this, the node at x = y = z = 0 is held at all directions and the node at x = L, y = z = 0 is held in y direction to avoid free body motion. Following this, force is applied on the nodes which are located at the position of the top supports. Then ΔT (temperature difference between the cure temperature and the room temperature) is applied to calculate thermal loads. Those thermal loads are added to the mechanical loads and the problem is solved. In the postprocessing stage, stresses of each node in the native coordinate system are determined and failure analysis is carried out by means of the respective criterion. Tsai-Wu, maximum stress, maximum strain and Hashin failure criteria come as default in ANSYS; however, Tsai-Hill, Hoffman, quadric surfaces, modified quadric surfaces and Norris criteria are implemented to the software using the parametric design language. Results of the nodes with stress concentration effect are excluded. If maximum failure index is not equal to one, all forces are removed and the solution phase is repeated by changing the magnitude of the force depending on the magnitude of the maximum failure index of the respective criterion. If the maximum failure index is not equal to 1.0, the magnitude of the force is proportionally decreased or increased. The iterations are continued until the magnitude of the force, *P*, is found that causes the maximum failure index to be equal to 1.0. The maximum allowable moment resultant is calculated by multiplying P with *b*, (the distance between top and bottom supports) and dividing by 48 mm (the width of the plate). All of these steps are repeated for each fiber orientation angle. The algorithm of the FEM solution of the problem is given in Figure 3.2.

The computational cost of FEM solution of the problem is very high. All necessary parameters and commands are written into a text file and read by ANSYS in batch mode. The aim of using ANSYS in batch mode is to decrease computational cost by avoiding graphical display. In every loop, ANSYS records the model features and results first in the memory; and then in the hard disk, when the memory capacity is exceeded. However, the speed of hard disks is slow as compared to RAMs. This is called “bottle neck”. Considering that a system is as fast as its slowest component, one should avoid using hard disks as much as possible during FEM analyses. To avoid this, geometry and results of the problem are not written into the memory. Instead, only the necessary parameters and the results are written to a text file using *VWRITE command [37].

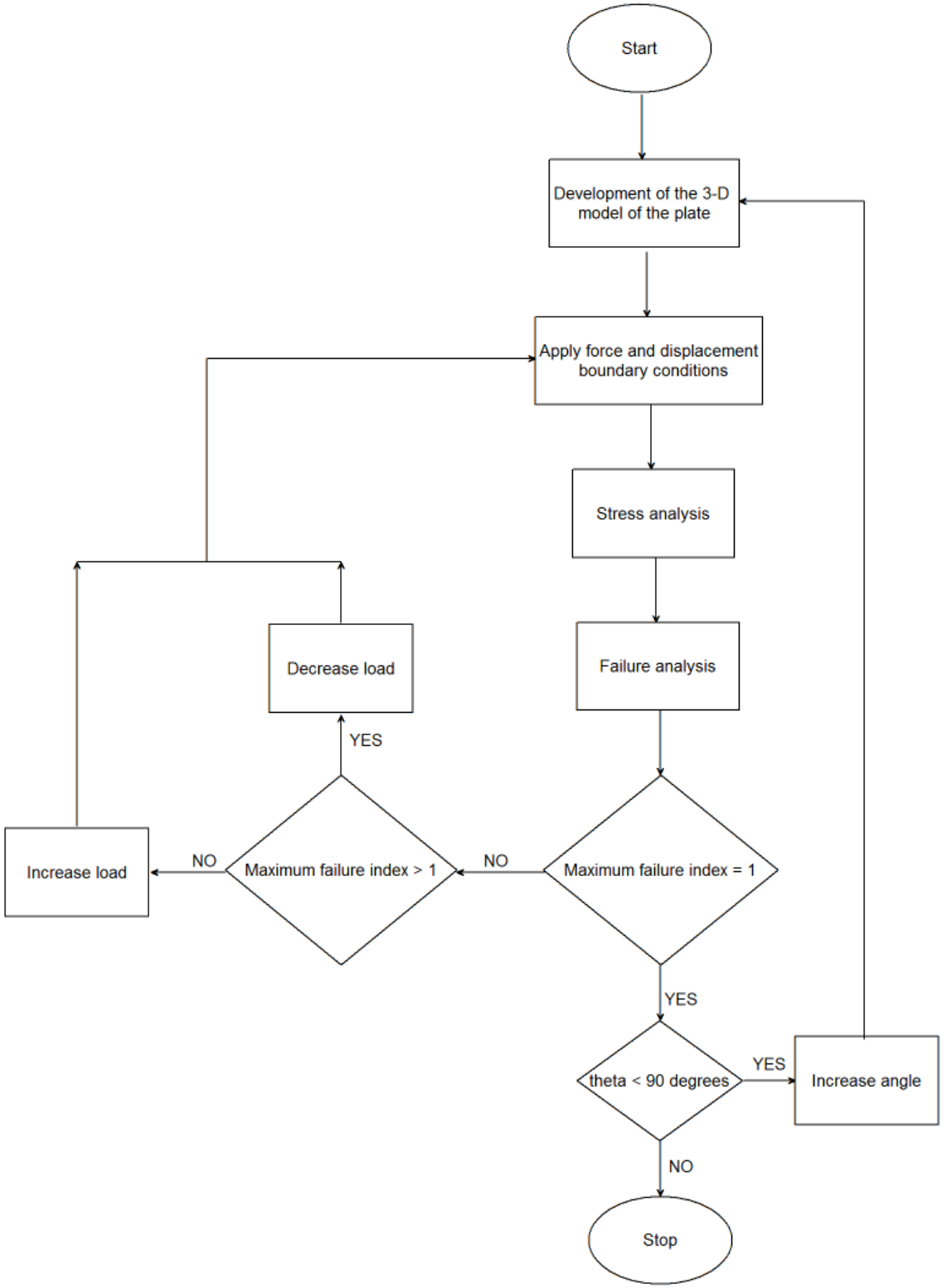

Figure 3.2. Flow chart of the FEM analyses.

3.2. Convergence Analysis

The accuracy of the results of a finite element analysis depends on mesh density. Finer meshes, in general, increase the accuracy of the results. However, in some cases, e.g. models containing sharp edges or regions at which a concentrated force exists, higher mesh density results in higher stress levels. Besides that, computational cost may increase remarkably. Optimum mesh density should be determined before FEM analyses are carried out.

Convergence analysis was performed for the middle regions where pure bending moment develops. Tension and compression stresses occur due to bending moment below and above the mid-plane, respectively. The stress increases linearly with the z coordinate; thus, the maximum stress is obtained at the top and bottom surfaces between top supports. Therefore, the maximum failure index at the top and the bottom was considered in the convergence analysis.

Finite element models developed for a 12-layered $48 \times 96 \times 2.208$ [mm^3] composite plate was with different element sizes by dividing the length, width, and thickness with different divisions. The maximum failure index was computed using Tsai-Wu, maximum stress and a Hashin-type delamination [42] criteria for each case. The delamination criterion was implemented into ANSYS using the user programmable features of ANSYS [37].

Table 3.1 illustrates the failure index variation for a unidirectional $[0]_{12}$ laminate under 2000 N load.

Table 3.1. Failure index variation for a unidirectional $[0]_{12}$ laminate under 2000 N load.

	Element edge size	Delamination maximum failure index	Tsai-Wu maximum failure index	Maximum stress maximum failure index
2 elements through the thickness	8x8 mm	0.0549	0.8140	0.6977
	6x6 mm	0.0647	0.7994	0.6988
	4x4 mm	0.0646	0.680	0.6754
	3x3 mm	0.0682	0.6730	0.6756
	2x2 mm	0.0691	0.6754	0.6693
	1x1 mm	0.0680	0.6649	0.6640
	0.5x0.5 mm	0.0783	0.661	0.6605
4 elements through the thickness	8x8 mm	0.0898	0.8204	0.6984
	6x6 mm	0.1069	0.8260	0.6999
	4x4 mm	0.1055	0.6807	0.6728
	3x3 mm	0.1125	0.6761	0.6726
	2x2 mm	0.1170	0.6799	0.6690
	1x1 mm	0.1182	0.6649	0.6638
	0.5x0.5 mm	0.1150	0.6613	0.6607
6 elements through the thickness	8x8 mm	0.0995	0.8291	0.6984
	6x6 mm	0.1171	0.8354	0.7000
	4x4 mm	0.1159	0.6808	0.6721
	3x3 mm	0.1235	0.6779	0.67165
	2x2 mm	0.1281	0.6820	0.6696
	1x1 mm	0.1284	0.6650	0.6639
	0.5x0.5 mm	0.1245	0.6611	0.6608
8 elements through the thickness	8x8 mm	0.1029	0.8334	0.6984
	6x6 mm	0.1209	0.8402	0.7000
	4x4 mm	0.1200	0.6808	0.6719
	3x3 mm	0.1259	0.6792	0.6712
	2x2 mm	0.1321	0.6837	0.6701
	1x1 mm	0.1321	0.6652	0.6639
	0.5x0.5 mm	0.1280	0.6610	0.6608
10 elements through the thickness	8x8 mm	0.1045	0.8360	0.6983
	6x6 mm	0.1226	0.8431	0.7000
	4x4 mm	0.1277	0.6808	0.6718
	3x3 mm	0.1327	0.6802	0.6710
	2x2 mm	0.1340	0.6851	0.6705
	1X1 mm	0.1338	0.6652	0.6639
	0.5X0.5 mm	0.1296	0.6610	0.6608
12 elements through the thickness	8x8 mm	0.1054	0.8377	0.6983
	6x6 mm	0.1236	0.8450	0.6999
	4x4 mm	0.1225	0.6807	0.6717
	3x3 mm	0.1288	0.6811	0.6710
	2x2 mm	0.1350	0.6863	0.6707
	1x1 mm	0.1347	0.6652	0.6640
	0.5x0.5 mm	0.1305	0.6610	0.6608

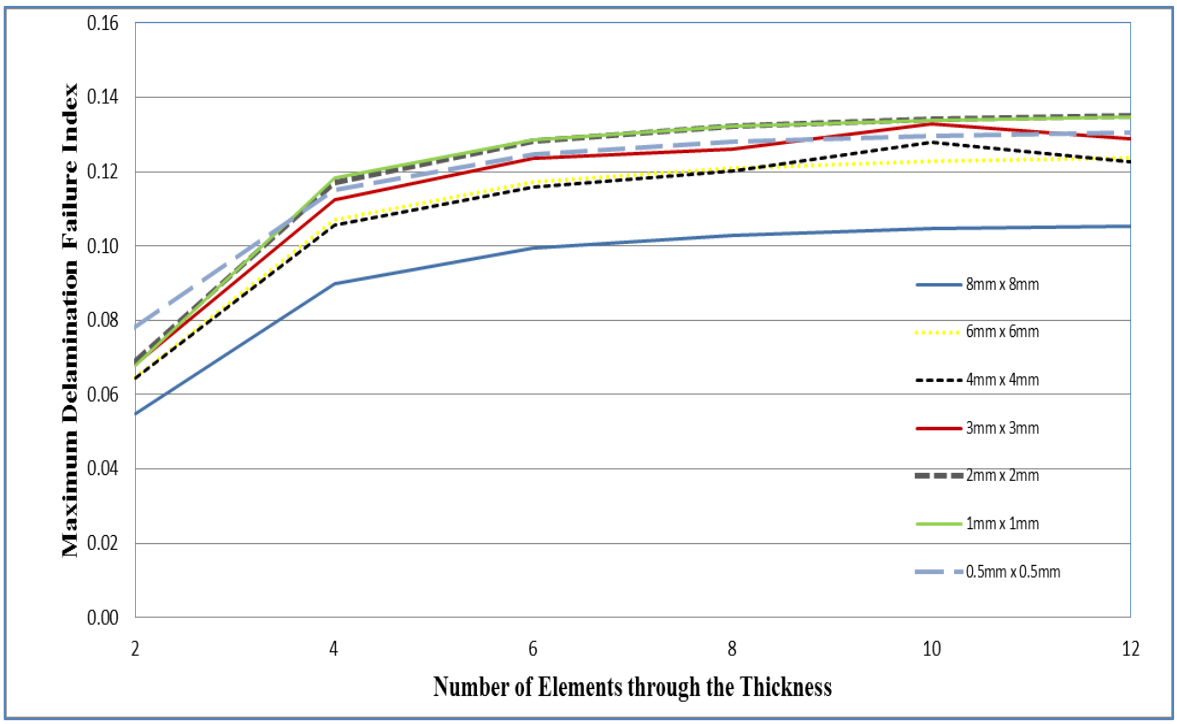

Figure 3.3. Delamination criterion's maximum failure index variation as a function of number of elements through the thickness.

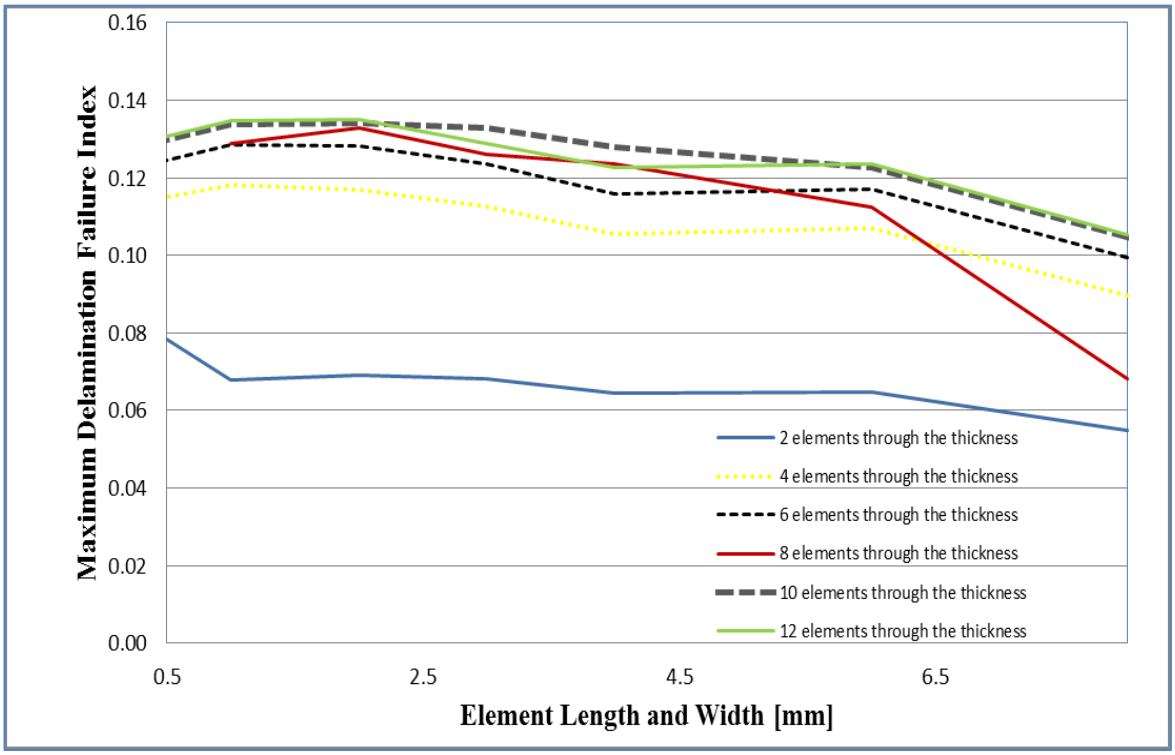

Figure 3.4. Delamination criterion's maximum failure index variation as a function of element edge size.

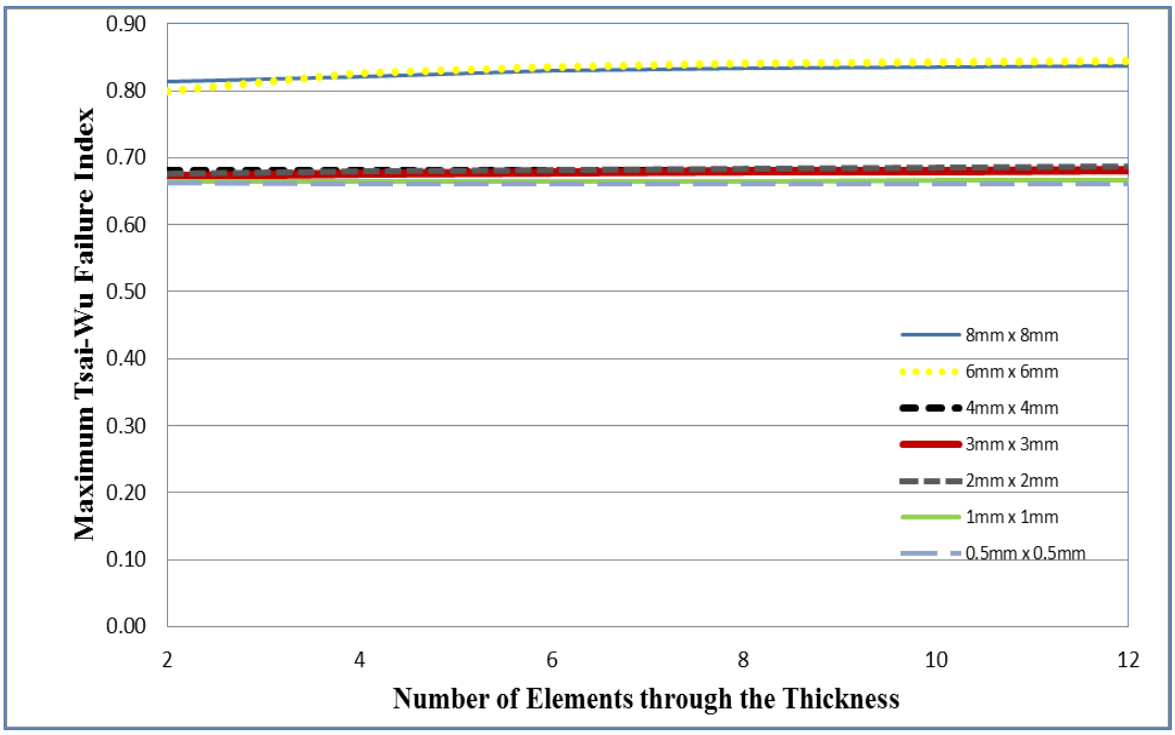

Figure 3.5. Tsai-Wu criterion's maximum failure index variation as a function of number of elements through the thickness.

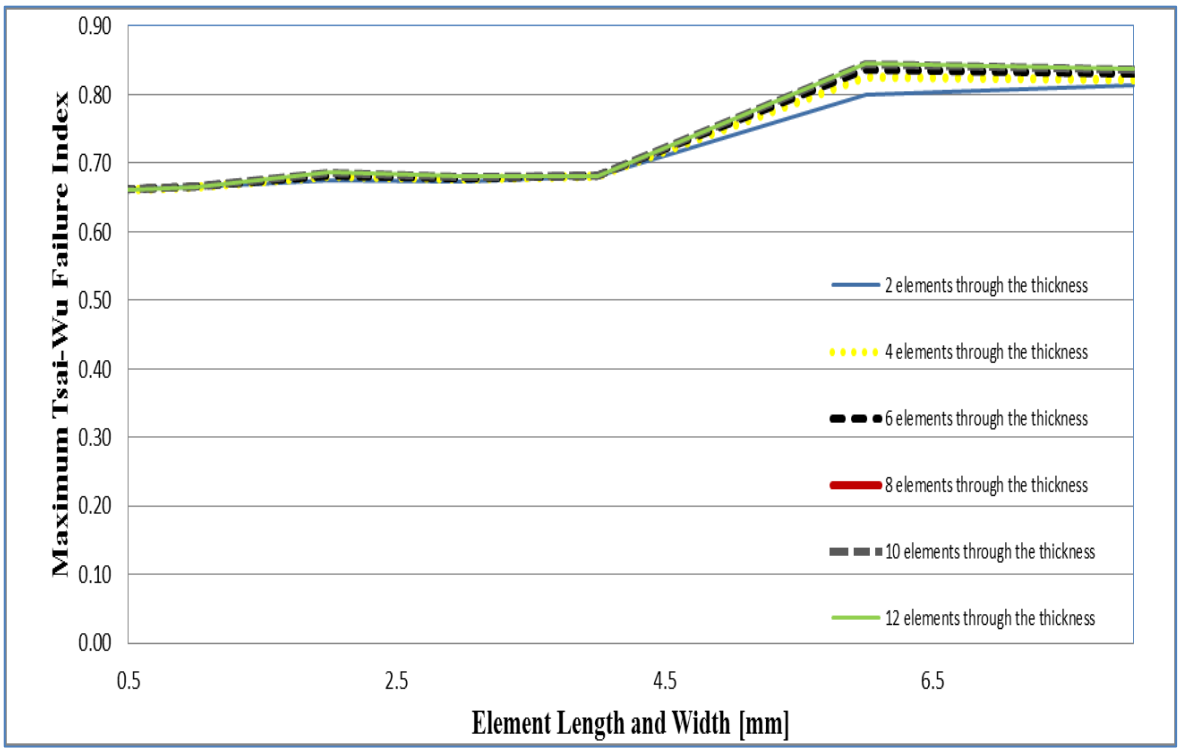

Figure 3.6. Tsai-Wu criterion's maximum failure index variation as a function of element edge size.

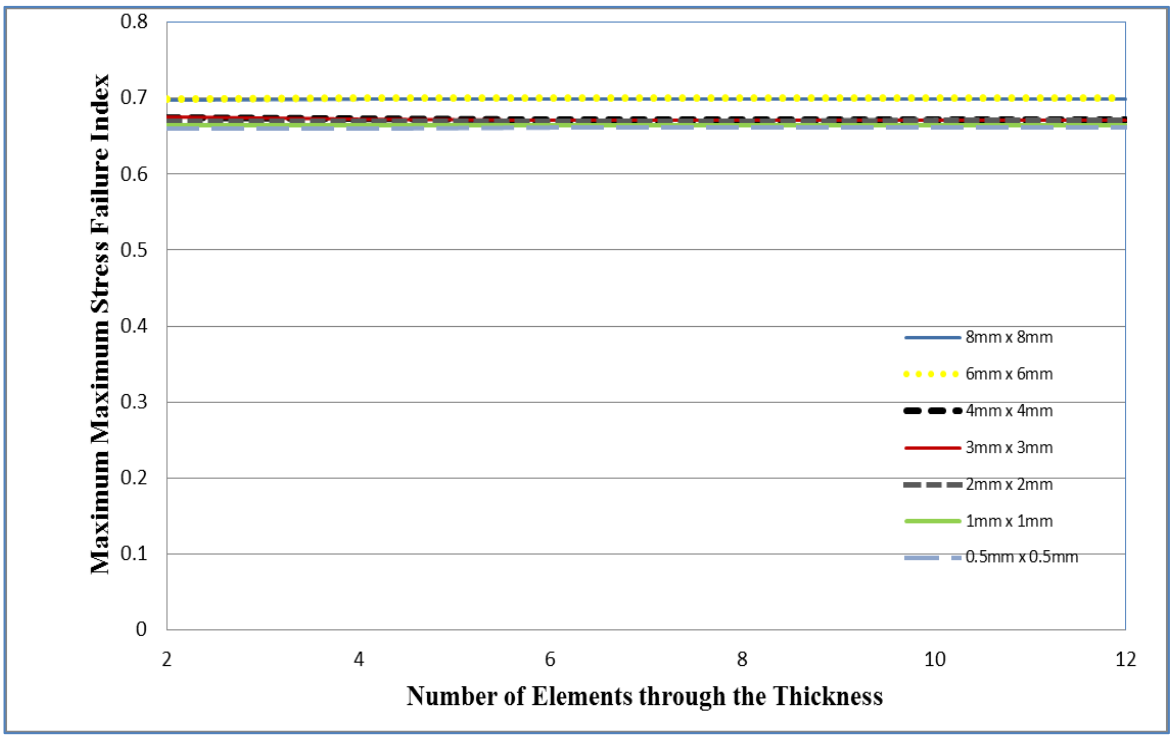

Figure 3.7. Maximum stress criterion's maximum failure index variation as a function of number of elements through the thickness.

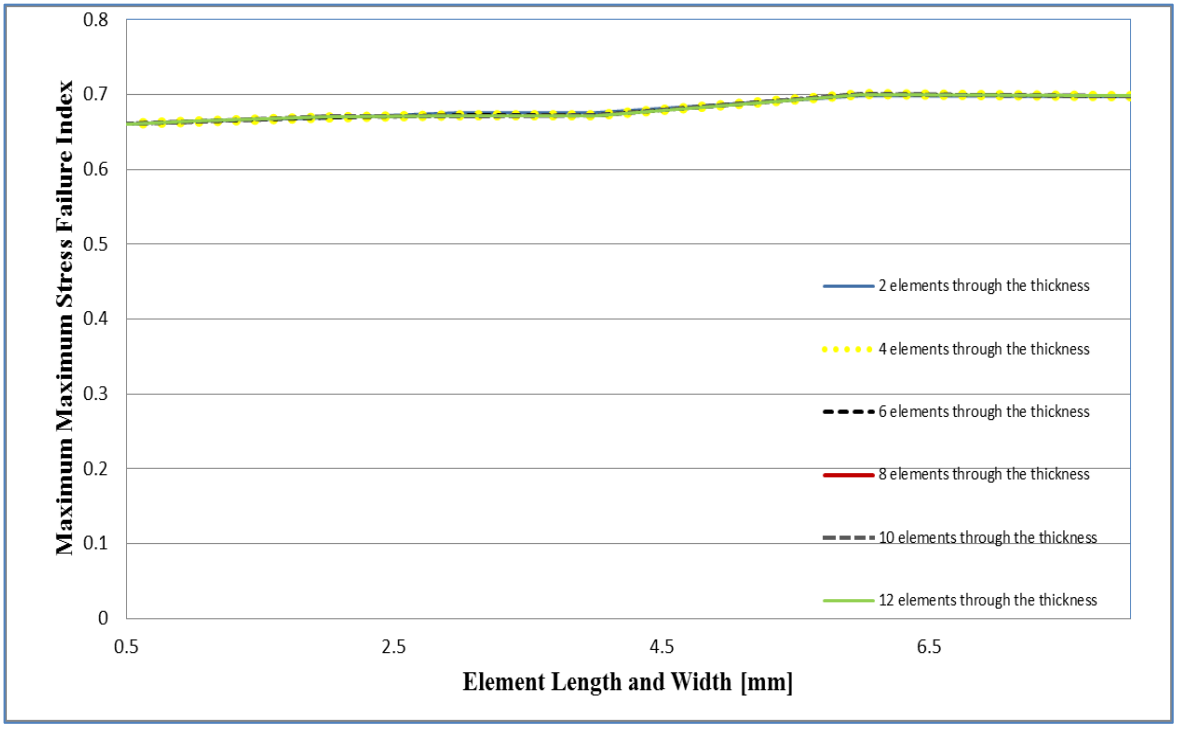

Figure 3.8. Maximum stress criterion's maximum failure index variation as a function of element edge size.

3.3. Test Setup Design

In this part of the study, the optimum support positions are sought to avoid delamination. While the bottom supports are fixed in the z direction at the two edges of the plate as shown in Figure 3.9, the top supports are allowed to move from the edges towards the center. The distance between the top supports and the nearest edges is changed from 14 to 32 millimeters with 2-millimeter increments for every 15° of fiber orientation angle, θ, from 0° to 90°. Moreover, cross-ply laminates with $[0_3/90_3]_s$ and $[90_3/0_3]_s$ layup sequences are also analyzed. Because of the geometric features of the setup, the support positions are selected in the range between 14 and 32 millimeters. The supports are pins with 10 millimeters diameters. Therefore, the distance between top and bottom supports must be greater than 10 millimeters in order to prevent clash of the upper and lower supports after fracture of the specimens. 4 millimeters are added because of security concerns. 32 millimeters (one third of the plate length), on the other hand, is chosen to keep the critical region, which is subjected to pure bending moment, large enough. As the top supports get closer to the center of the plate, the difference between three-point and four-point bending tests decreases.

The onset of delamination failure is predicted according the model proposed by [42]. The criterion is formulated as follows:

Delamination in Tension ($\sigma_{33}>0$):

$$\frac{\sigma_3^2}{{Z_t}^2}+\frac{\sigma_{13}^2}{{S_{13}}^2}+\frac{\sigma_{23}^2}{{S_{23}}^2}\geq 1 \tag{3.1}$$

Delamination in Compression ($\sigma_{33}<0$):

$$\frac{\sigma_3^2}{{Z_c}^2}+\frac{\sigma_{13}^2}{{S_{13}}^2}+\frac{\sigma_{23}^2}{{S_{23}}^2}\geq 1 \tag{3.2}$$

where Z denotes strength in the 3-direction and S_{13} and S_{23} refer to out-of-plane shear strengths.

In each step, the applied forces were normalized by dividing with the maximum failure index to obtain standardized graphics. The analyses were repeated for both unidirectional and multidirectional laminates and optimum support positions were obtained. Figures 3.10-23 demonstrate the relationship between support position and delamination and static failure modes.

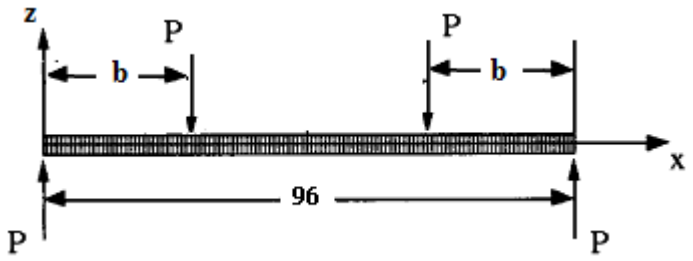

Figure 3.9. Four-point bending test setup.

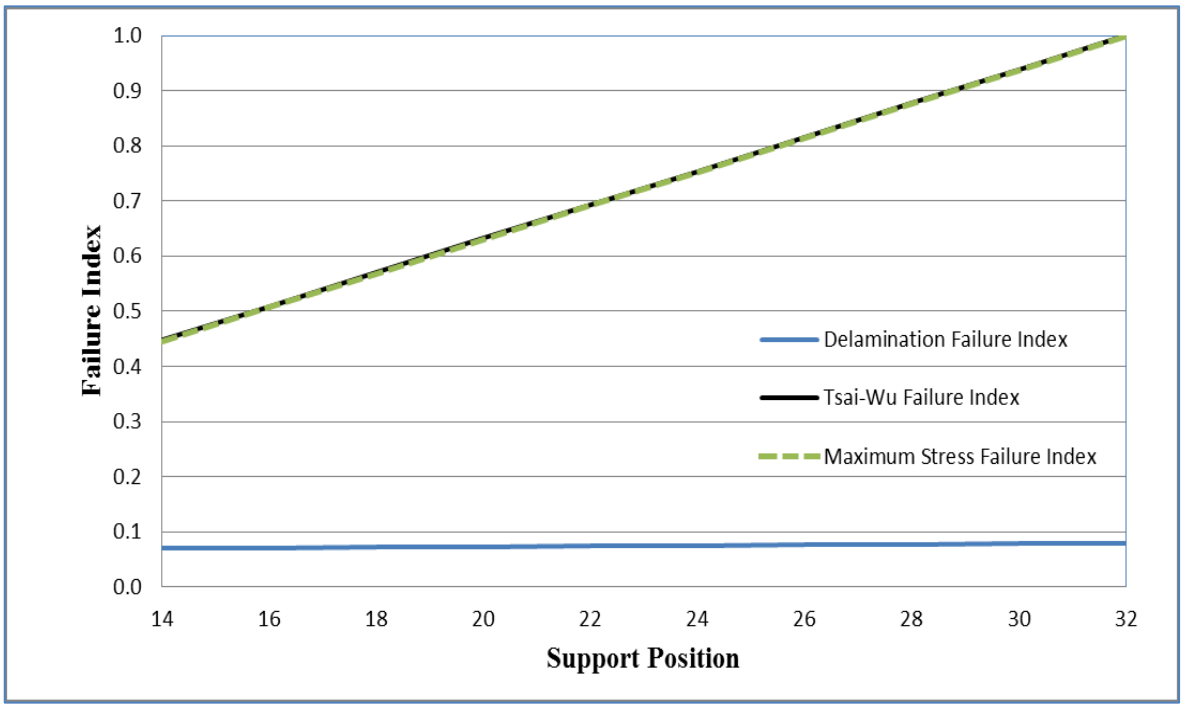

Figure 3.10. Change in the failure indices for $[0_6]_s$ plate as a function of support positions.

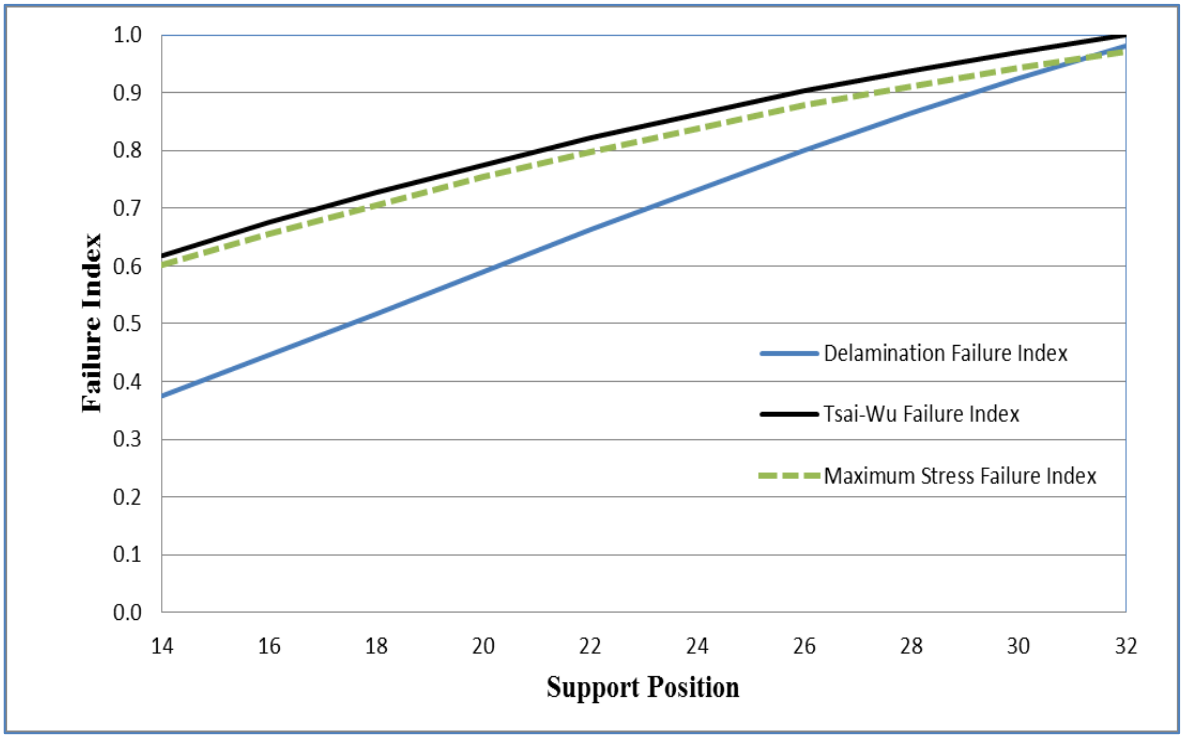

Figure 3.11. Change in the failure indices for $[15_6]_s$ plate as a function of support positions.

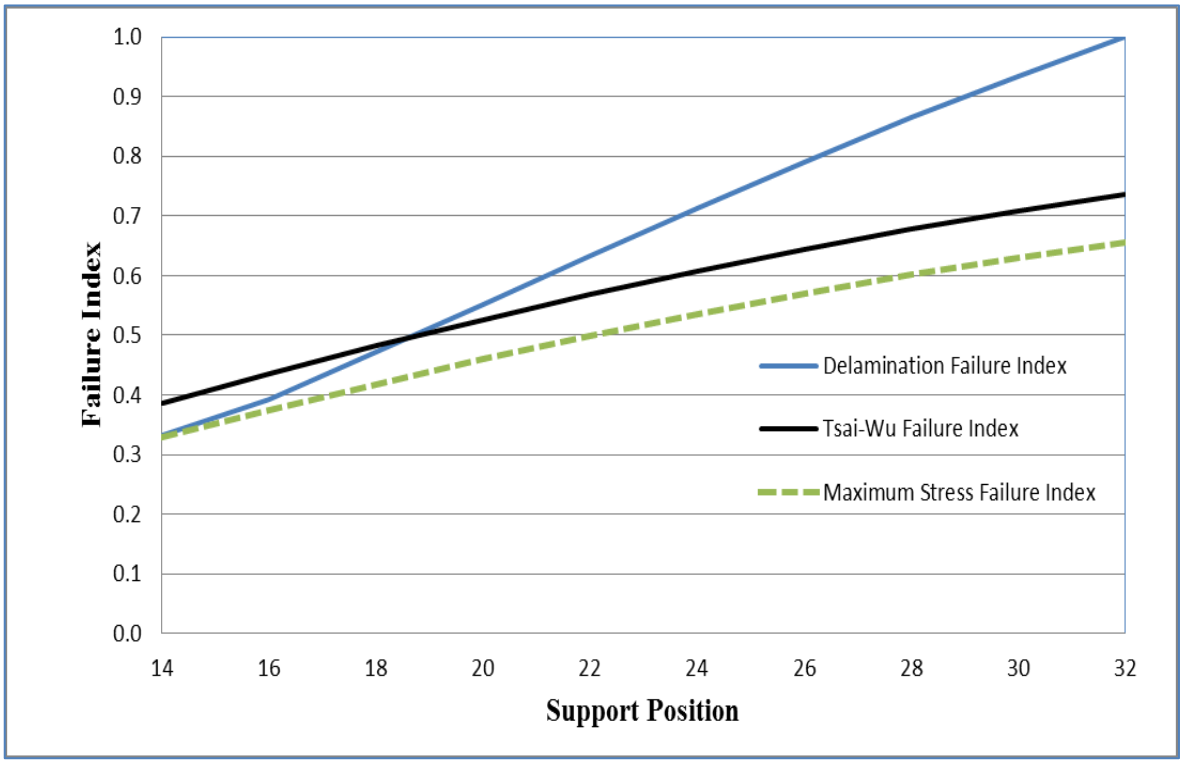

Figure 3.12. Change in the failure indices for $[30_6]_s$ plate as a function of support positions.

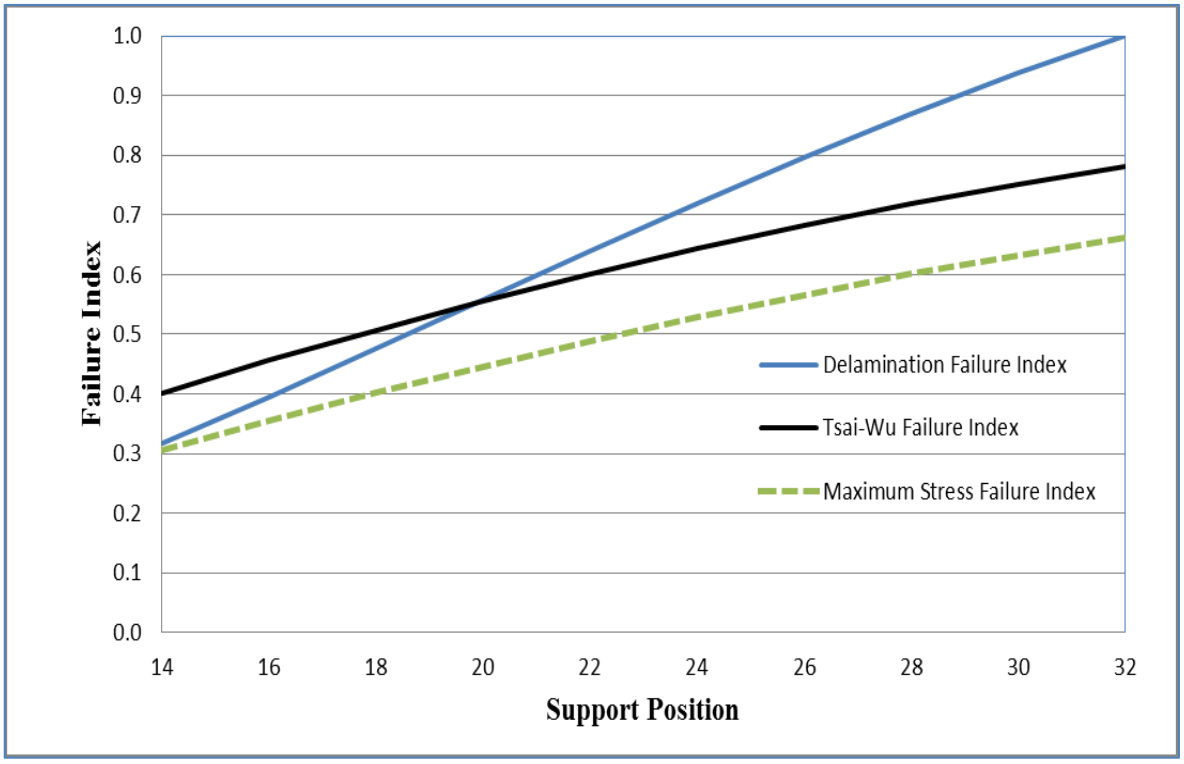

Figure 3.13. Change in the failure indices for $[45_6]_s$ plate as a function of support positions.

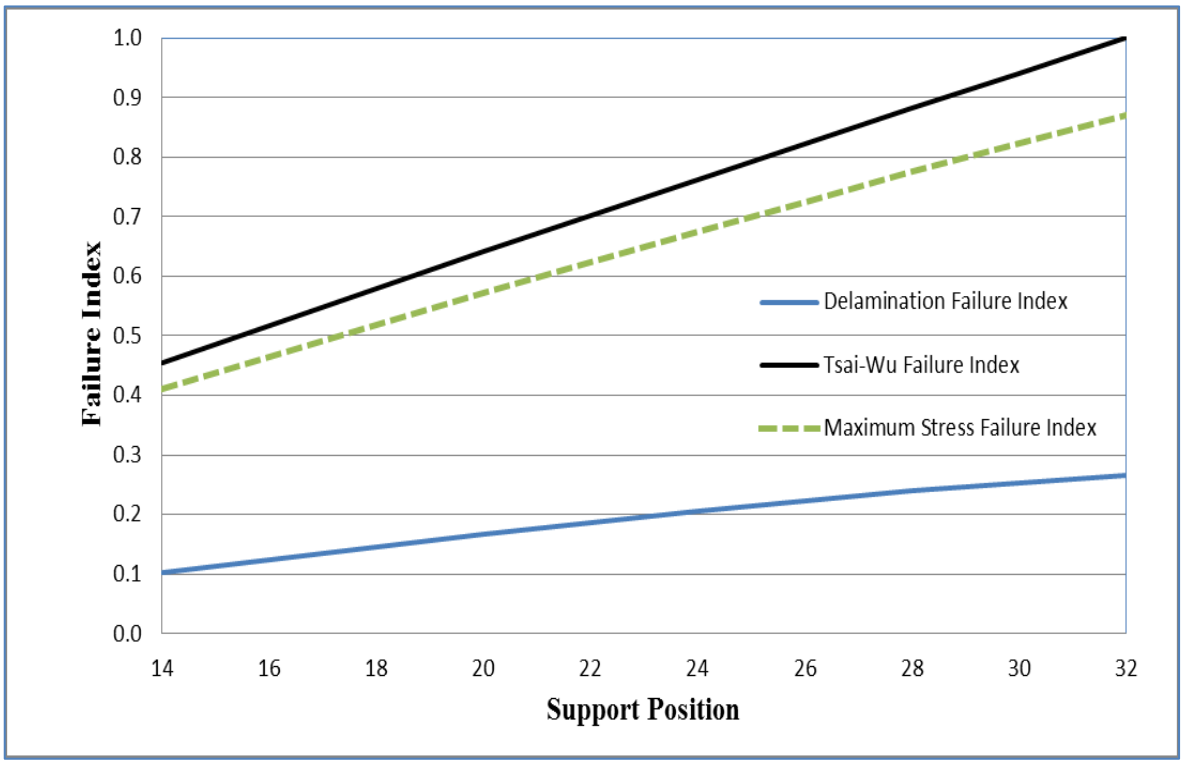

Figure 3.14. Change in the failure indices for $[60_6]_s$ plate as a function of support positions.

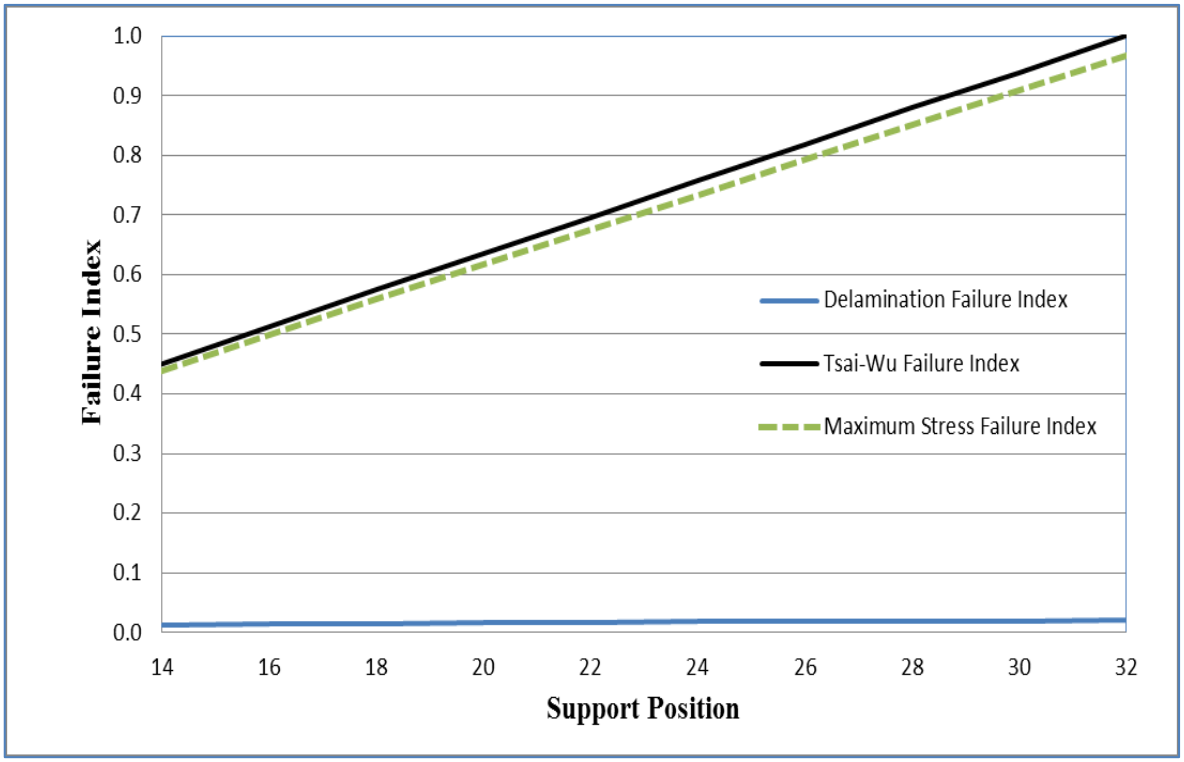

Figure 3.15. Change in the failure indices for $[75_6]_s$ plate as a function of support positions.

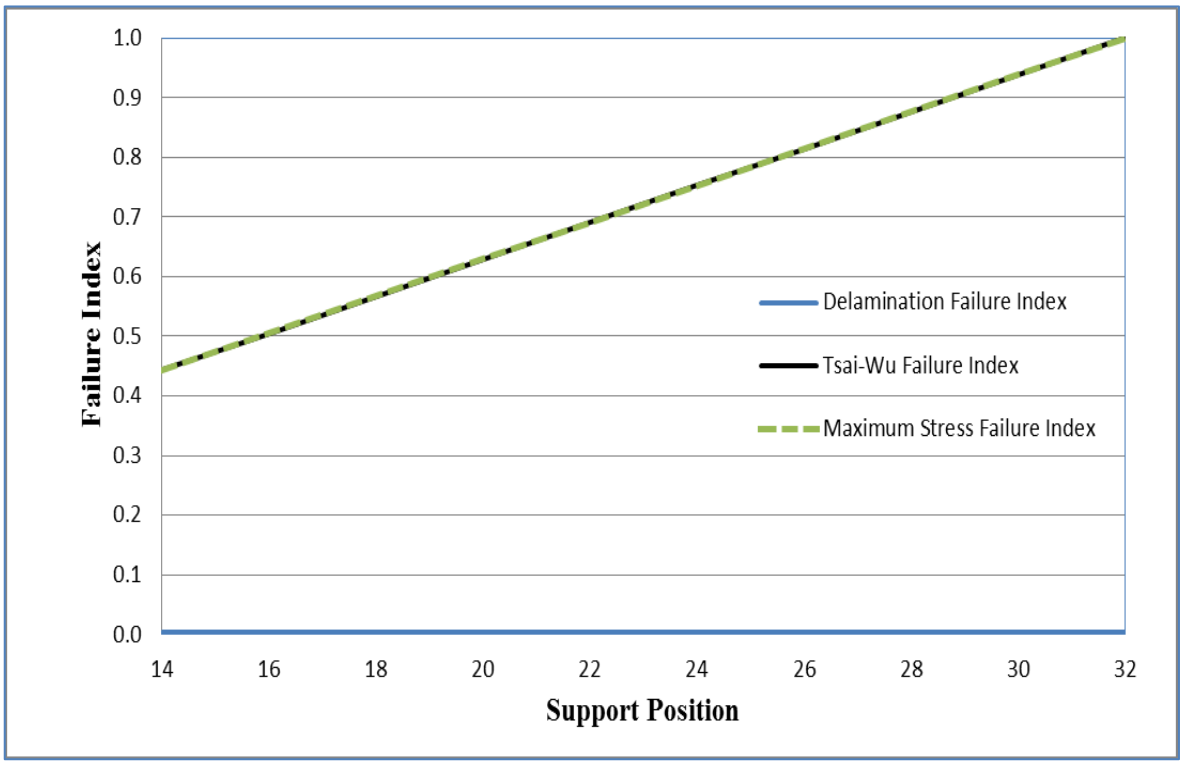

Figure 3.16. Change in the failure indices for $[90_6]_s$ plate as a function of support positions.

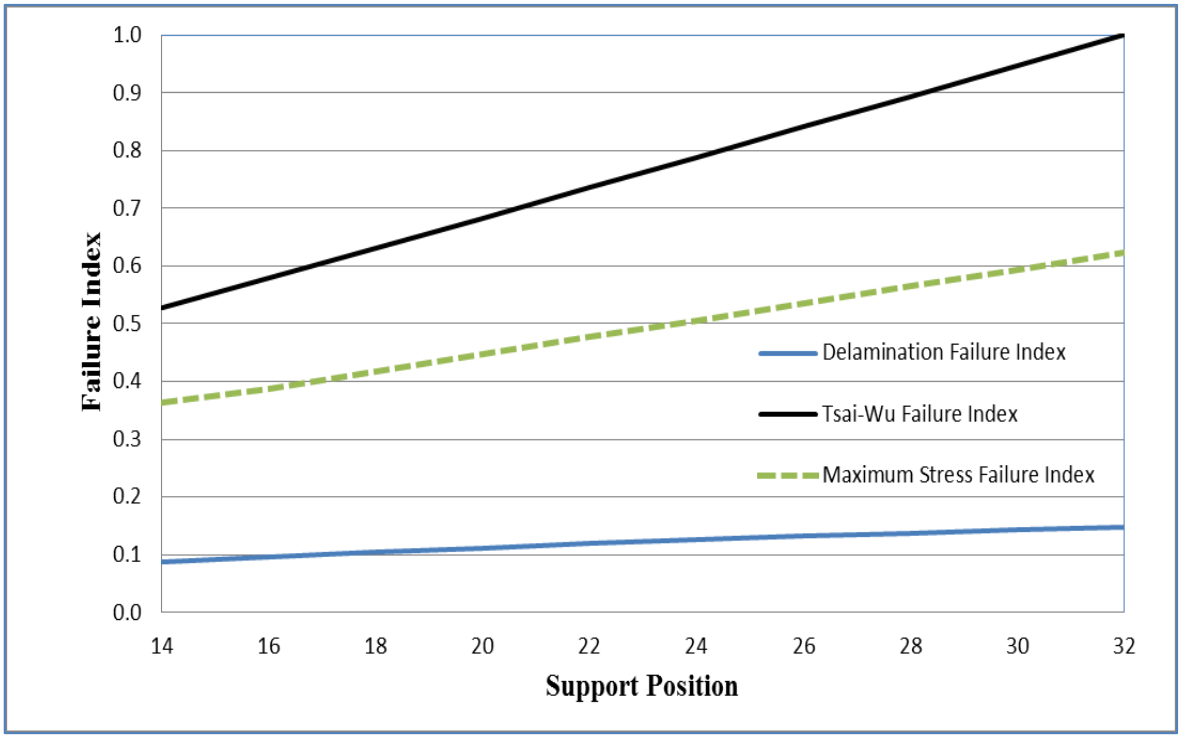

Figure 3.17. Change in the failure indices for $[15_3/\text{-}15_3]_s$ plate as a function of support positions.

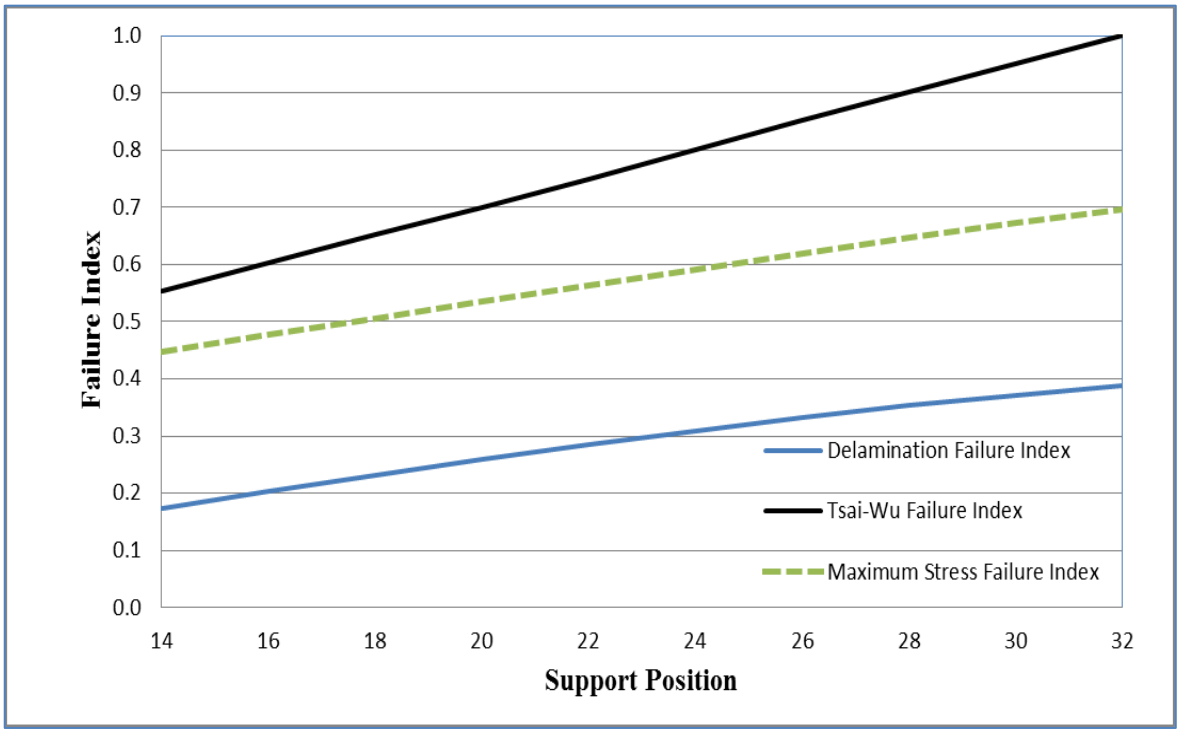

Figure 3.18. Change in the failure indices for $[30_3/\text{-}30_3]_s$ plate as a function of support positions.

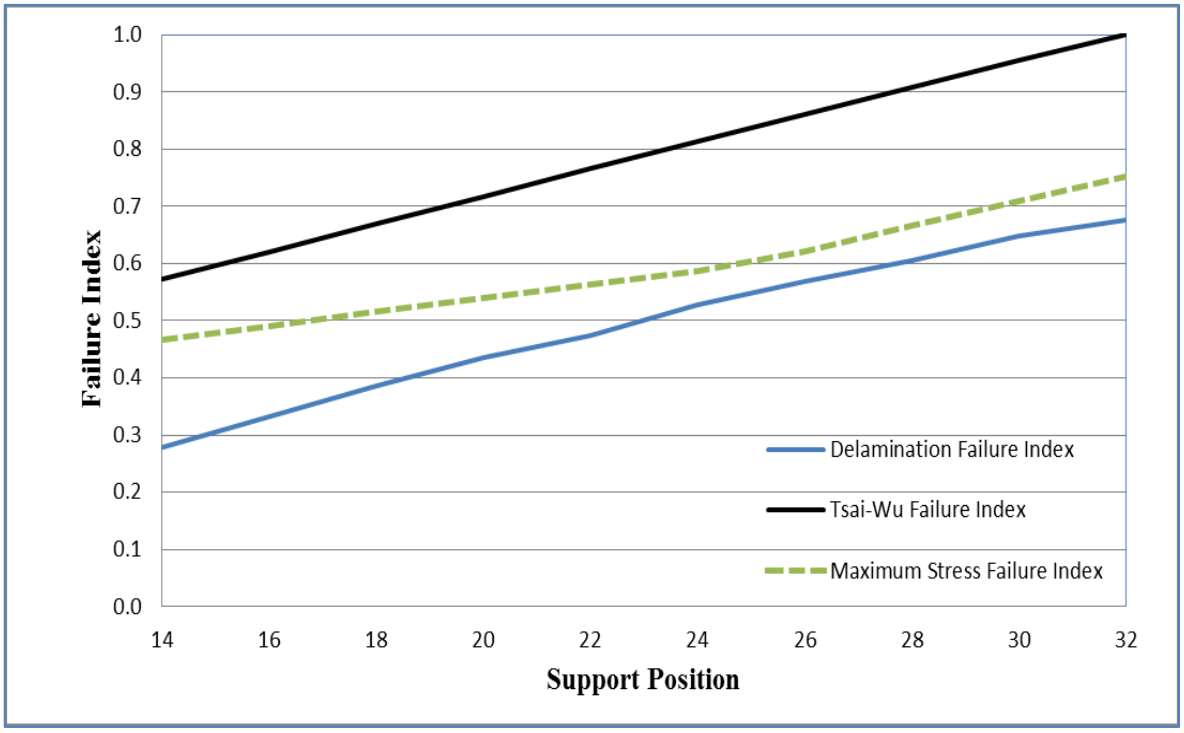

Figure 3.19. Change in the failure indices for $[45_3/-45_3]_s$ plate as a function of support positions.

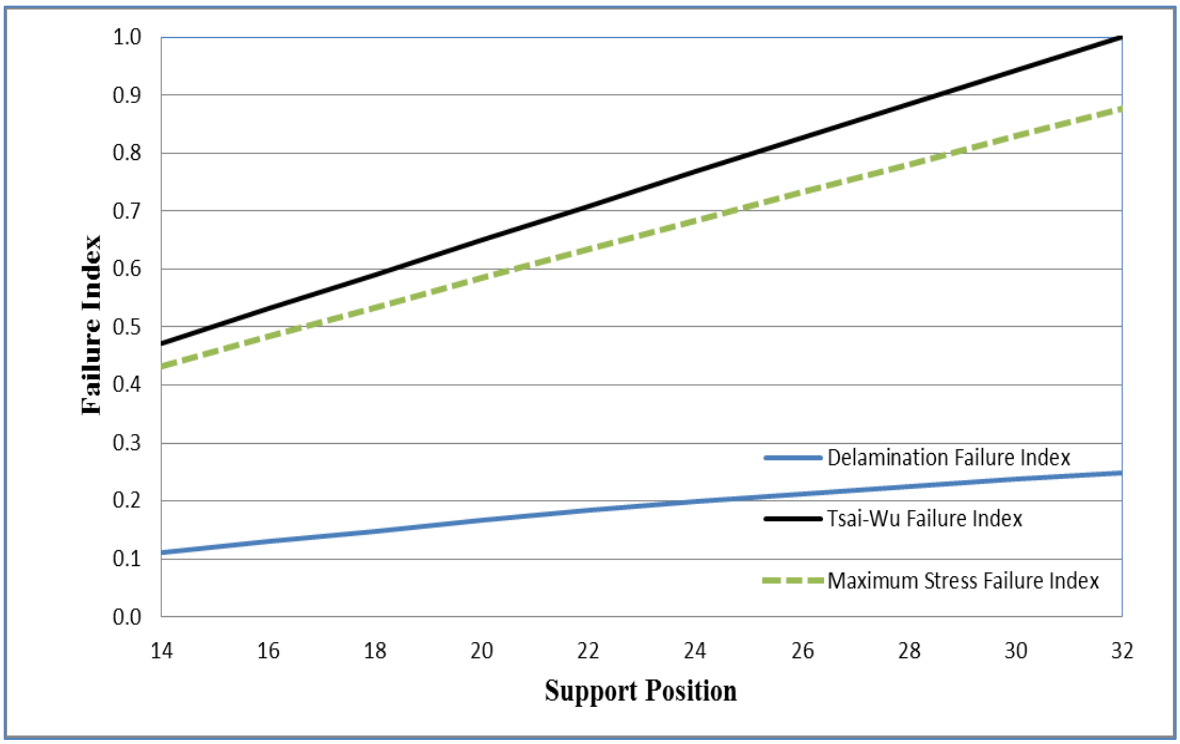

Figure 3.20. Change in the failure indices for $[60_3/-60_3]_s$ plate as a function of support positions.

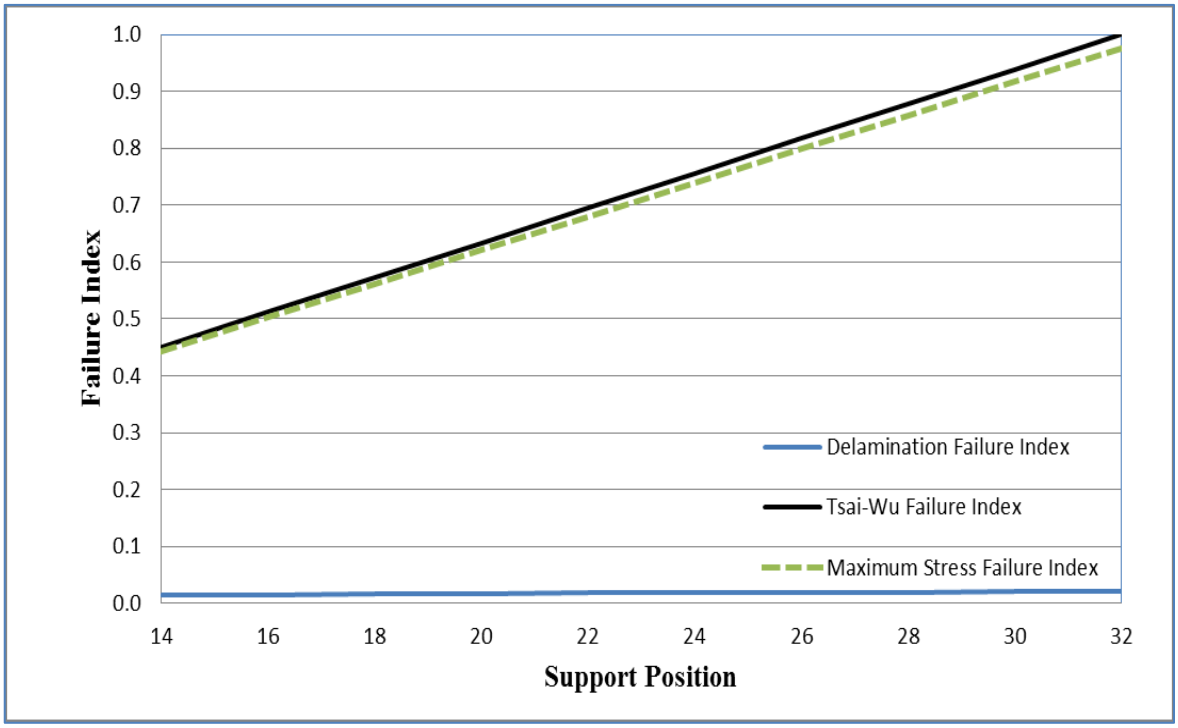

Figure 3.21. Change in the failure indices for $[75_3/-75_3]_s$ plate as a function of support positions.

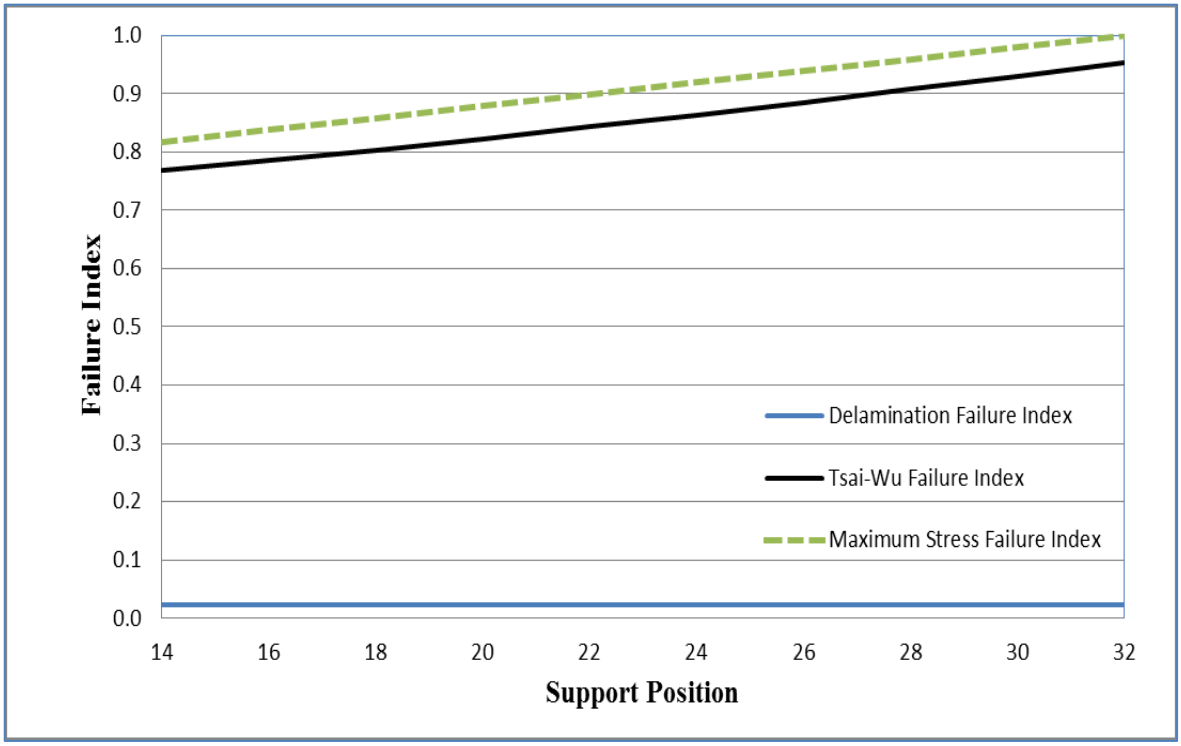

Figure 3.22. Change in the failure indices for $[0_3/90_3]_s$ plate as a function of support positions.

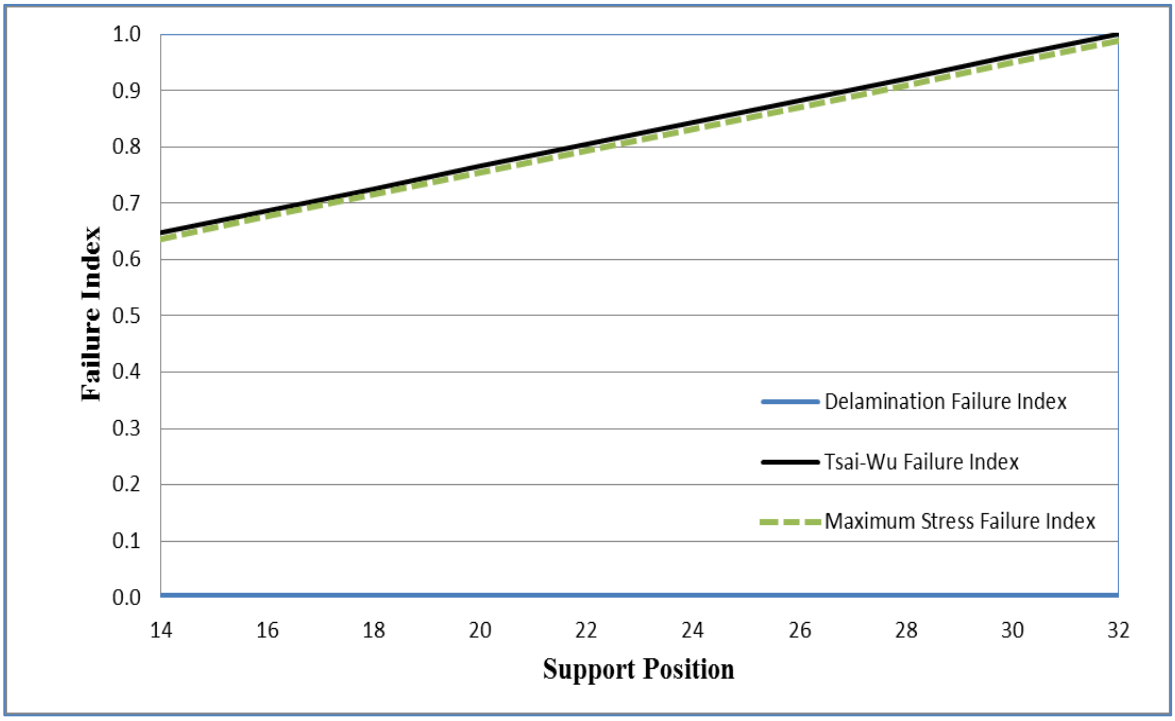

Figure 3.23. Change in the failure indices for $[90_3/0_3]_s$ plate as a function of support positions.

Figures 3.10 – 3.23 demonstrate that delamination is not the dominant failure mode for symmetrically balanced and cross-ply laminates. However, there is a risk of delamination for unidirectional plates with fiber angles between 30° – 45°. According to the maximum stress criterion, delamination is unavoidable for unidirectional laminates with 30° and 45° fiber orientation angles. On the other hand, Tsai-Wu criterion predicts that delamination can be avoided if the distance between the top supports and the nearest edges is less than or equal to 20 millimeters. The magnitude of moment is dependent on not only force but also the distance between the supports. Hence, if supports are placed too close, the maximum capacity of the test machine might be exceed. Accordingly, the top supports are placed at L_1=20 mm and L_2=76 mm in the FEM analyses and the experiments.

4. EXPERIMENTS

Experimental studies are conducted in two stages: Manufacturing of composite plates and four-point bending tests.

4.1. Manufacturing of Composite Plates

The plates were manufactured by stacking individual AS4/8552 unidirectional prepregs, a carbon-fiber-reinforced epoxy, in a 118 mm × 190 mm mold, which is shown in Figure 4.1, with desired stacking sequence and cured in accordance with the manufacturer's catalogue. A typical prepreg's thickness is 0.184 mm and fiber volume fraction (FVF) is 57.42%. [50]. Three specimens with 48 mm x 96 mm x 2.21 mm dimensions were cut from each plate.

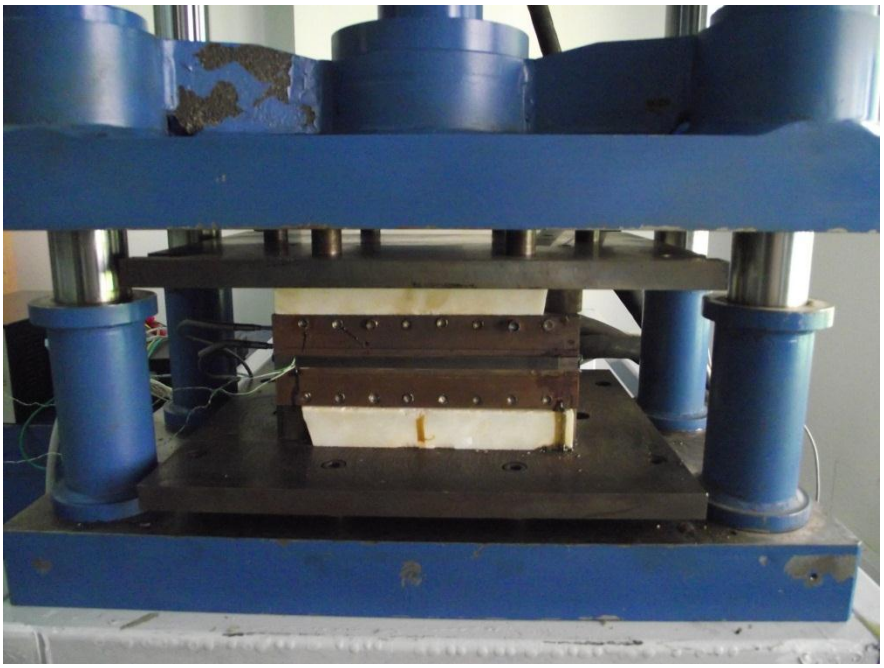

Figure 4.1. Mold and hydraulic pressure.

Thermoset composites are processed at high-temperatures; this process is generally called as "Cure Cycle". Cure cycle can be defined as a time period in which the temperature of the part follows a predefined profile over time during processing. Curing is a complex series of chemical reactions that takes place in thermosetting composites. Sometimes it is named as polymerization or cross-linking. Initially a thermosetting resin is

solid at room temperature. When exposed to heat and pressure, curing reaction initiates. During the curing of a thermosetting resin, molecular chains form a three-dimensional cross-linked network. This builds up the stiffness and strength of the material [43]. A typical cure cycle is shown in Figure 4.2. As it is illustrated in the figure, there are three main steps in the cure cycle: Increasing the temperature to a set point at a specific rate (180^o C), holding the temperature until the part cures to a reasonable extent and then cooling the part to room temperature. An earlier dwell (120 ^{o}C) is applied when thermosetting composites are considered. First dwell is for the consolidation of the laminate and the second dwell is for the curing of the matrix [43]. Temperature is increased by 2 ^{o}C/min. The dotted line in Figure 4.2 demonstrates the magnitude of pressure. According to product data sheet of the AS4/8552 required pressure is P_c = 0.7 *MPa* = 7 *Bar*. Considering that the dimensions of the mold are 190 mm x 118 mm, magnitude of the pressure applied by pump is determined as follows:

$$A_s = 190\ x\ 118\ = 22420\ mm^2 \tag{4.1}$$

$$F_{req} = P_c x A_s = 0.7\ x\ 22420 = 15694\ N \tag{4.2}$$

$$A_{piston} = \frac{\pi}{4}\ x\ 100^2 = 7853.94\ mm^2 \tag{4.3}$$

where A_s is the area of the mold, A_{piston} is the area of the hydraulic pressure and F_{req} is the force to apply required pressure. What is seen from the indicator of pump is:

$$P_{pump} = \frac{F_{req}}{A_{piston}} = 1.998\ MPa = 19.98\ Bar \tag{4.4}$$

wherein, P_{pump} is the pressure of pump. Hence $P_{pump} \geq 20$ MPa.

A temperature control unit, which is shown in Figure 4.3, is used to control the cure cycle process.

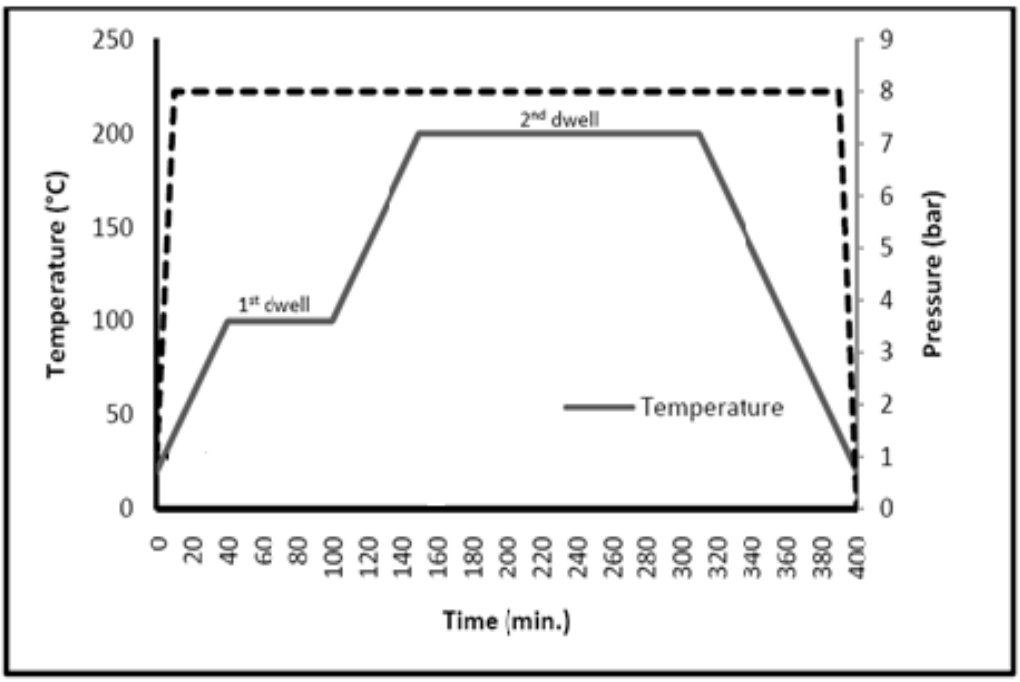

Figure 4.2. A typical cure cycle.

Figure 4.3. Temperature control unit.

4.2.Four-Point Bending Tests

The test setup, which is designed with the help of FEM analyses, is manufactured from forged steel at Bogazici University machine workshop. The supports are made of carbon steel. The test machine is an electric controlled Zwick/Roell with 10 kN maximum loading capacity [44].

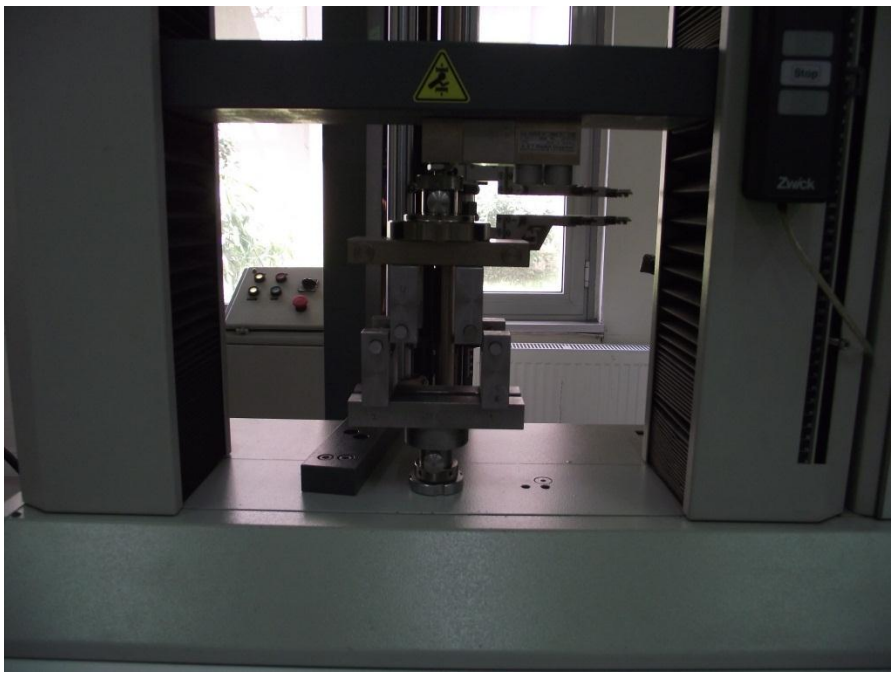

Figure 4.4. Test setup.

In the literature, there are no standard specifications for four-point bending testing of composite materials. Both force and displacement controlled tests are possible with the test machine. In general, force controlled tests cause sudden failure while displacement controlled tests cause progressive failure in case of unidirectional and symmetric balanced laminates. This is because, in displacement control, the magnitude of the applied force is decreased when the strength of the sample decreases as a result of ply failure. One may think that force controlled tests might be more suitable; however, for plates with small fiber angle, θ, force control may cause supports to crush because the magnitude of load is very high. Hence, displacement controlled tests were conducted for all samples to provide similar loading conditions. To avoid dynamic loading effects, the plates are loaded quasi-statically with 1 mm displacement per minute (1 mm/min) downwards.

For each 15° of fiber orientation angle, θ, from 0° to 90°, multiple samples were tested. Some of the chosen failure criteria predict a slight increase in strength as the fiber angle is varied from 0 to 3 - 5 degrees. $[5_6]_s$ plates are tested to observe the correlation between experimental results and predictions. The samples were cut off from at least two different plates by means of a power saw to prevent consistent error due to a

manufacturing defect in a given sample. Figures 4.5 – 4.8 show the technical drawings of the parts of the text fixture. Dimensions are in millimeters in Figures 4.5 – 4.8.

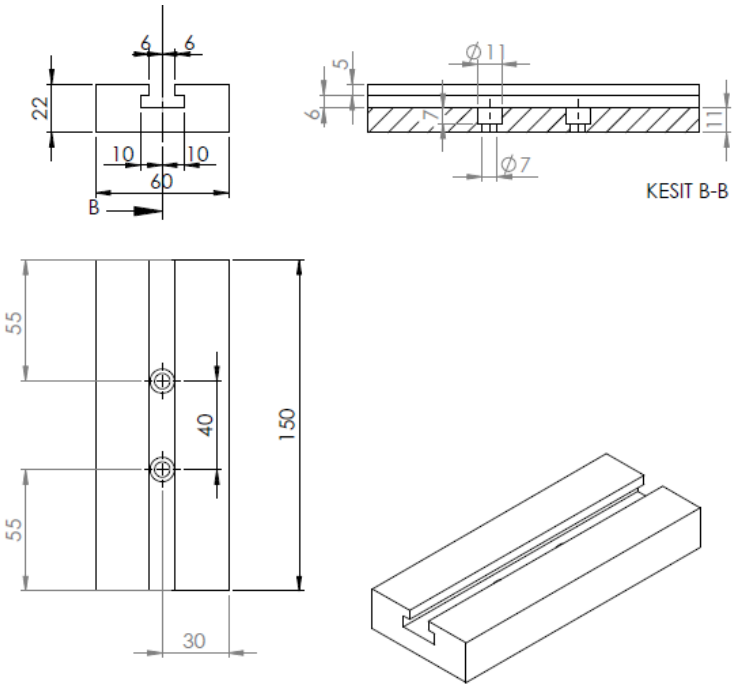

Figure 4.5. Technical drawing of the parts of test fixture.

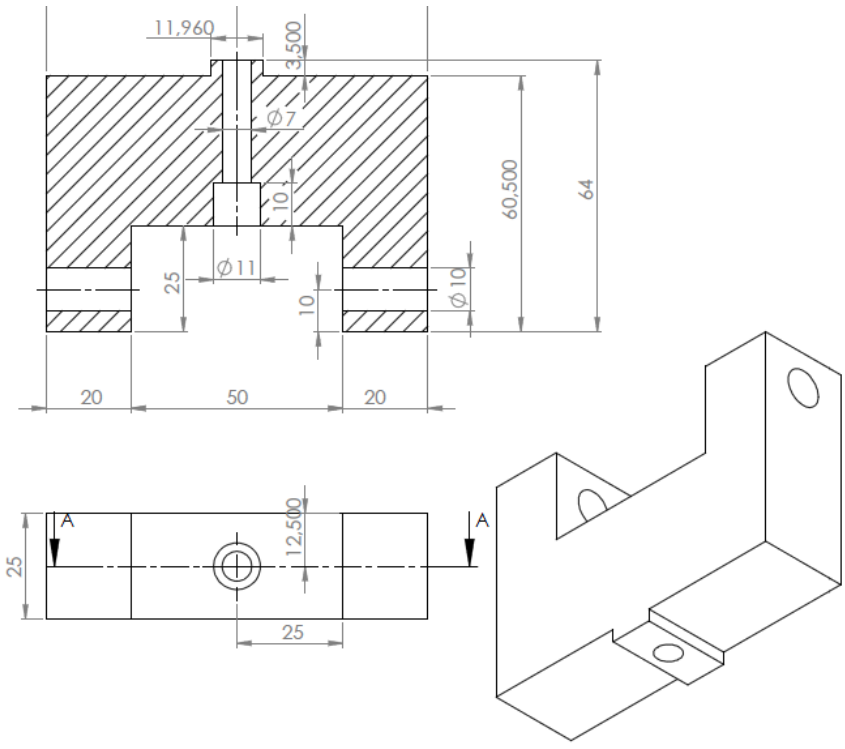

Figure 4.6. Technical drawing of the parts of test fixture.

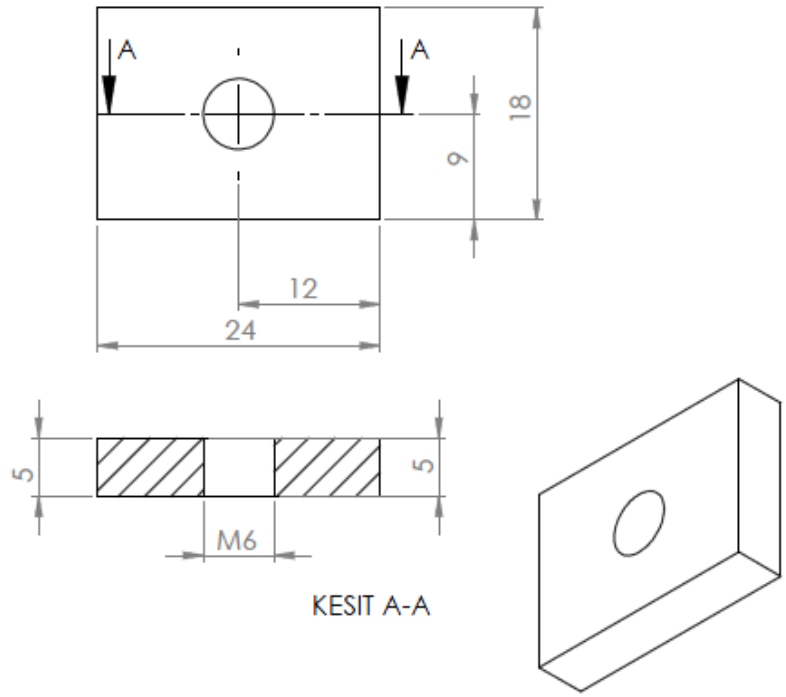

Figure 4.7. Technical drawing of the parts of test fixture.

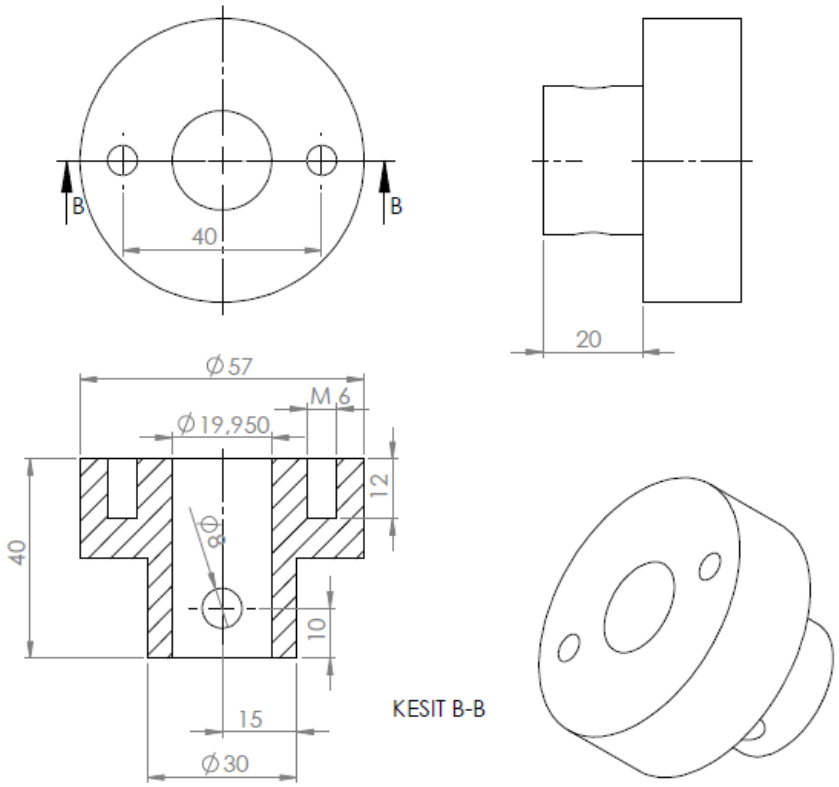

Figure 4.8. Technical drawing of the parts of test fixture.

5. RESULTS AND DISCUSSION

5.1. Mechanical Properties of AS4/8552

Mechanical properties of AS4/8552 are not clearly stated in the catalogue provided by Hexcel [50]. Some of the mechanical properties including transverse compression strength shear moduli and out-of-plane Poisson's ratios are not given. There is a statistical report [45] that states mechanical properties of the material; however, values are not consistent with the ones given by Hexcel. It can be seen from Table 5.1 that there are noticeable differences between catalogue values and statistical report. Furthermore, both catalogue and report values show that mechanical properties of the material changes under tension and compression stresses.

Assuming different mechanical properties under tension and compression complicates calculations significantly. Four-point bending causes different type of stresses below and above neutral axis (compression and tension, respectively). However, different mechanical moduli under tension and compression disrupt symmetry conditions even if laminate has symmetric stacking sequences. Coupling terms and B matrix do not disappear for any stacking sequences. Table 5.1 illustrates that error for averaged values are tiny. Considering computational cost of using different moduli under tension and compression, averaged values are to be used in CLT and FEM calculations.

Table 5.1. Mechanical properties of AS4/8552.

		MEAN VALUE	STANDART DEVIATION	MAX.	MIN.	Average	Error (%)
E_{1t}	STATISTICAL REPORT	131.6 GPa	4 Gpa	142.7 GPa	126 GPa	131.69 GPa	2.55
	CATALOGUE	135.14 GPa	-	-	-		
E_{1c}	STATISTICAL REPORT	116 GPa	2.9 GPa	119GPa	105.4 GPa		
	CATALOGUE	128.24 GPa	-	-	-		
E_{2t}	STATISTICAL REPORT	9.24 GPa	0.21 GPa	9.58 GPa	8.89GPa	9.72 GPa	1.42
	CATALOGUE	9.58 GPa	-	-	-		
E_{2c}	STATISTICAL REPORT	9.86 GPa	0.276 GPa	10.34 GPa	9.45 GPa		
	CATALOGUE	-	-	-	-		
v_{12t}	STATISTICAL REPORT	0.302	-	-	-	0.319	4.8
	CATALOGUE	-	-	-	-		
v_{12c}	STATISTICAL REPORT	0.335	-	-	-		
	CATALOGUE	-	-	-	-		
v_{21c}	STATISTICAL REPORT	0.029	-	-	-		
	CATALOGUE	-	-	-	-		
α_1	STATISTICAL REPORT	-	-	-	-		
	CATALOGUE	0.1265×10^{-6}	-	-	-		
α_2	STATISTICAL REPORT	-	-	-	-		
	CATALOGUE	37.12×10^{-6}	-	-	-		

Table 5.2. Strength properties of AS4/8552.

		MEAN VALUE	STANDART DEVIATION	MAX.	MIN
Xt	STATISTICAL REPORT	1928 MPa	87 MPa	2116 MPa	1758 MPa
	CATALOGUE	2137.38 MPa	-	-	-
Xc	STATISTICAL REPORT	1484 MPa	59 MPa	1671 MPa	1408 MPa
	CATALOGUE	1530.64 MPa	-	-	-
Yt	STATISTICAL REPORT	63.9 MPa	6.1 MPa	70.74 MPa	50.3 MPa
	CATALOGUE	80.67 MPa	-	-	-
Yc	STATISTICAL REPORT	267.9 MPa	6.27 MPa	280 MPa	256.6 MPa
	CATALOGUE	-	-	-	-
$X_{\varepsilon t}$	STATISTICAL REPORT	-	-	-	-
	CATALOGUE	0.0155	-	-	-
$X_{\varepsilon c}$	STATISTICAL REPORT	-	-	-	-
	CATALOGUE	-0.012	-	-	-
$Y_{\varepsilon t}$	STATISTICAL REPORT	-	-	-	-
	CATALOGUE	0.00833	-	-	-
$Y_{\varepsilon c}$	STATISTICAL REPORT	-	-	-	-
	CATALOGUE	-0.028	-	-	-
S_{12}	STATISTICAL REPORT	-	-	-	-
	CATALOGUE	0.019	-	-	-
S_{23}	STATISTICAL REPORT	-	-	-	-
	CATALOGUE	0.031	-	-	-

5.2. Comparison of Theoretical, FEM and Experimental Results

5.2.1. Unidirectional Laminates

In Figures 5.1 – 5.11, analytical and finite element M_{max} predictions as a function of orientation angle, θ, obtained using the chosen failure criterion for unidirectional off-axis $[\theta_6]_s$ specimens are compared with the experimental results. The error bars show the minimum, maximum and average values of M_{max} obtained by the experiments. Figures 5.12 – 5.17, on the other hand illustrate force – displacement diagrams. Experimental results for unidirectional laminates are given in Table 5.3, as well.

Figures 5.1 – 5.6 demonstrate the analytical and finite element model predictions of Tsai-Wu, Tsai-Hill, Hoffman, the quadric surfaces, the modified quadric surfaces and Norris criteria for UD laminates, respectively. All of these criteria are quadratic and they do not account for failure mode. Both finite element and analytical predictions of these criteria for UD laminates change smoothly as the fiber angle changes from 0° to 90° degrees. As seen in these figures, finite element and analytical predictions of each criterion mostly coincide between 30° - 35° and 90°; where the dominant failure mode is matrix failure; however, there are relatively large discrepancies in the range between 0° and 30° - 35°, in which the dominant failure mode is fiber failure.

Figures 5.7 – 5.9, on the other hand, show the analytical and finite element model predictions of the maximum stress, the maximum strain and Hashin criteria. Even though Hashin criterion is nonlinear as opposed to maximum stress and maximum strain criteria, they all account for failure modes. According to these figures, the analytical model predicts a slight increase in strength as the fiber angle is varied from 0 to 3 - 4 degrees. The FEM model does not predict increase in strength; however the trend of failure for small fiber orientation angles is not smooth due to abrupt changes in the dominant failure mode. Analytical and finite element predictions are very close between 30° - 35° and 90°. Between 0° and 30°, predictions coincide with each other and experimental results only around 5°.

As indicated in Figures 5.1 – 5.9, finite element model M_{max} predictions of all the criteria for $[0_6]_s$ laminates are higher than the analytical ones. This difference arises from the fact that CLT neglects the out-of-plane Poisson effect. If the Poisson's ratios are set to zero during calculations, FEM and analytical model predictions coincide for $[\theta_6]_s$ laminates.

Figures 5.10 – 5.11 give the predictions of all the failure criteria for UD laminates, $[\theta_6]_s$, based on the analytical and finite element models and the experimental results. In both cases the predictions of the all criteria coincide well with the experimental results at 5°, 45°, 60°, 75° and 90°; yet, they do not correlate well for 0°, 15° and 30°. Considering the figures, it can be seen that the finite element model predictions are closer to each other compared to analytical model predictions.

As seen in Figures 5.12 – 5.19 and Table 5.3, the first ply failure loads are taken into account instead of the maximum allowable loads. In the fiber dominant region, the maximum allowable moment is not always equal to the first ply failure moment.

Consider $[0_6]_s$ laminates, for which the predictions of the failure criteria do not correlate well with the experimental results. Figure 5.12 gives the force – displacement diagram for $[0_6]_s$ laminates. As seen in the figure, the force – displacement relation becomes nonlinear between 6000 – 7000 N. In addition to this, $[0_6]_s$ laminates always fail below the symmetry plane, in which they are subjected to tensile stress. Considering that the compressive strength is less than the tensile strength, this result is unexpected. Cracking and buckling might occur in this region in the micro level without noticeable effect on the macro behavior. Failure behavior of $[15_6]_s$ laminates under four-point bending, as it is shown in Figure 5.14, is very complex. They do not fail at once. Some of the samples can even carry higher loads after the first ply failure; which is not observed for UD laminates. Advanced techniques, such as acoustic emission, are required to observe the failure strength of laminates with 0° - 30° fiber orientation angles.

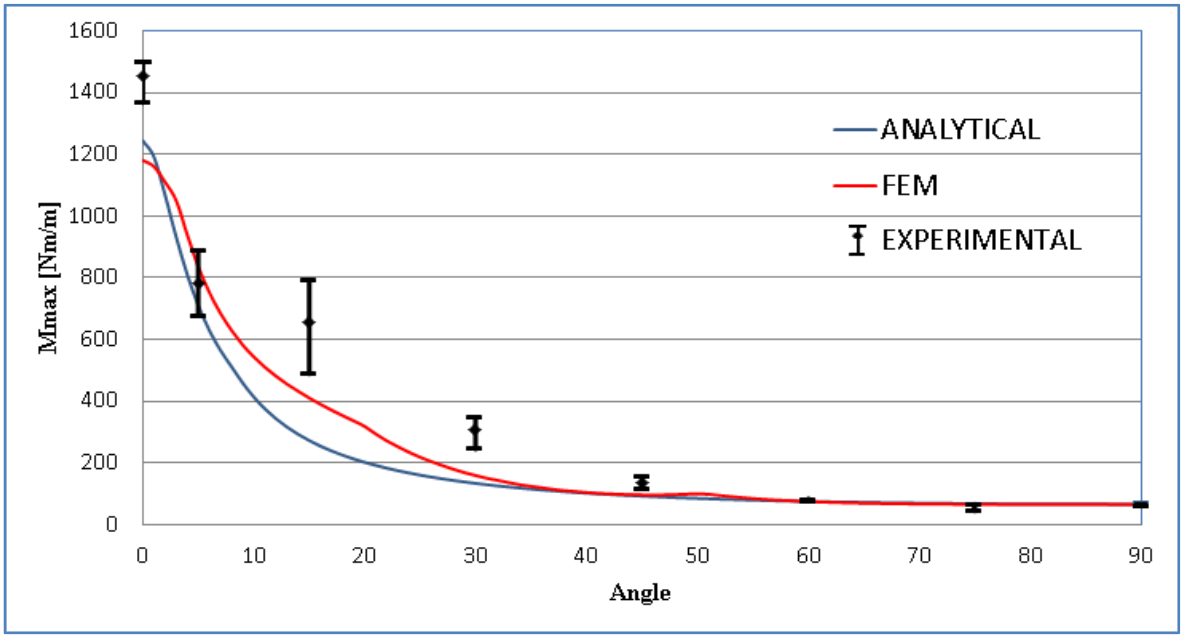

Figure 5.1. Comparison of the analytical and finite element M_{max} predictions obtained using Tsai-Wu criterion for unidirectional off-axis $[\theta_6]_s$ specimens with the experimental results.

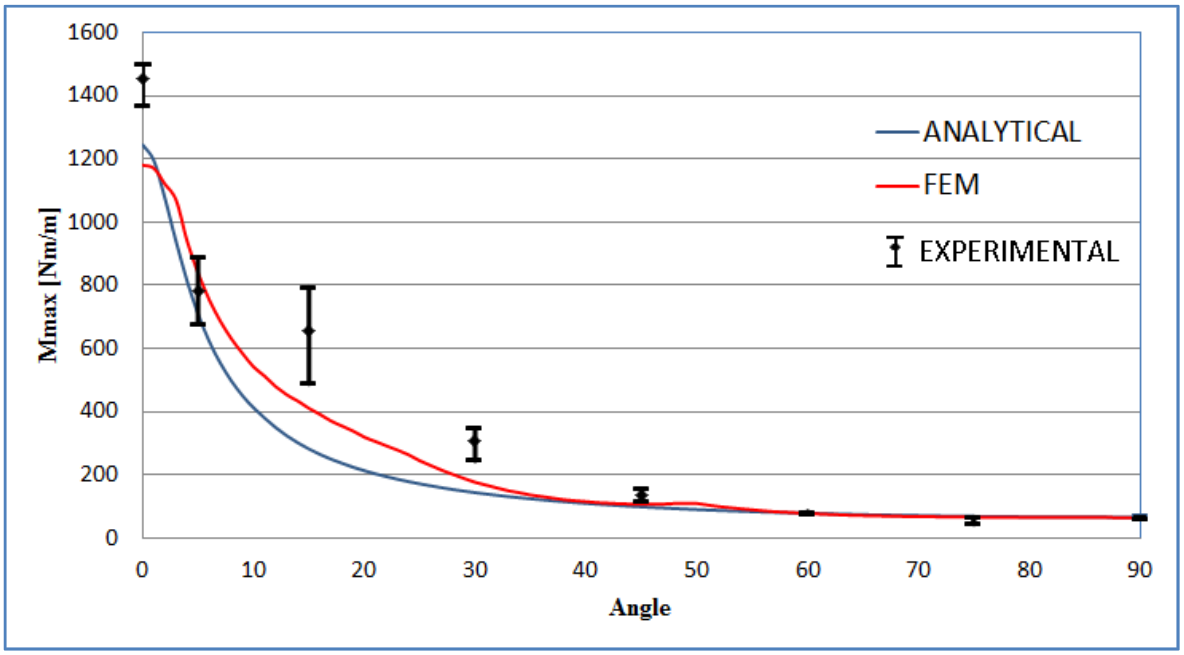

Figure 5.2. Comparison of the analytical and finite element M_{max} predictions obtained using Tsai-Hill criterion for unidirectional off-axis $[\theta_6]_s$ specimens with the experimental results.

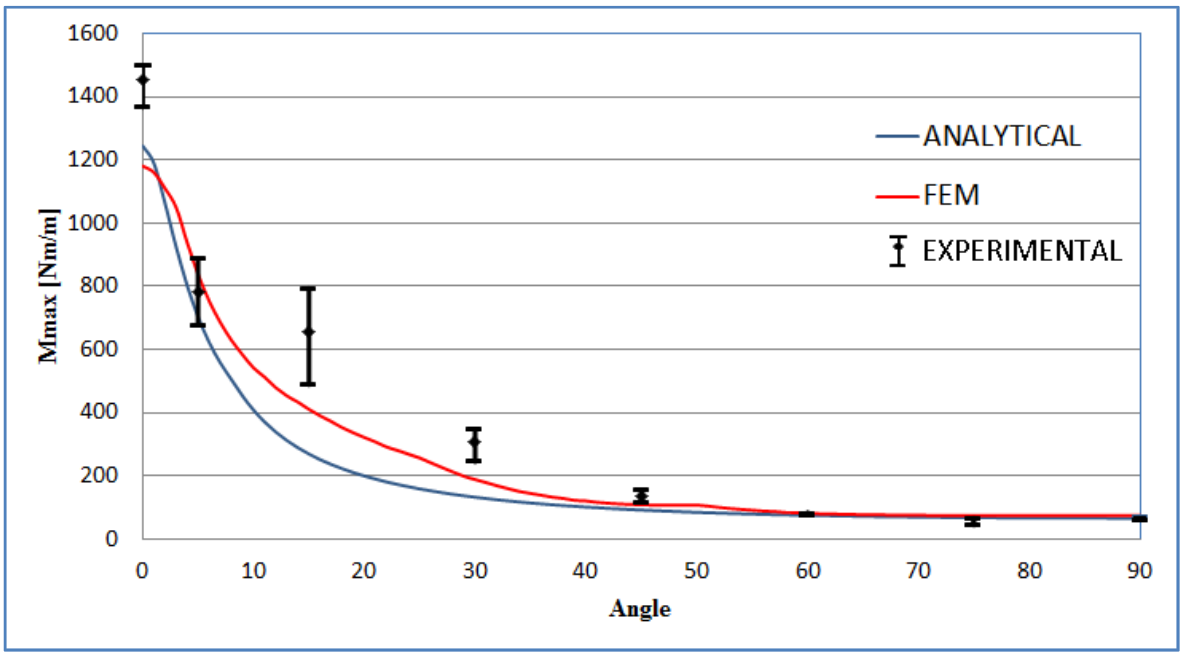

Figure 5.3. Comparison of the analytical and finite element M_{max} predictions obtained using Hoffman criterion for unidirectional off-axis $[\theta_6]_s$ specimens with the experimental results.

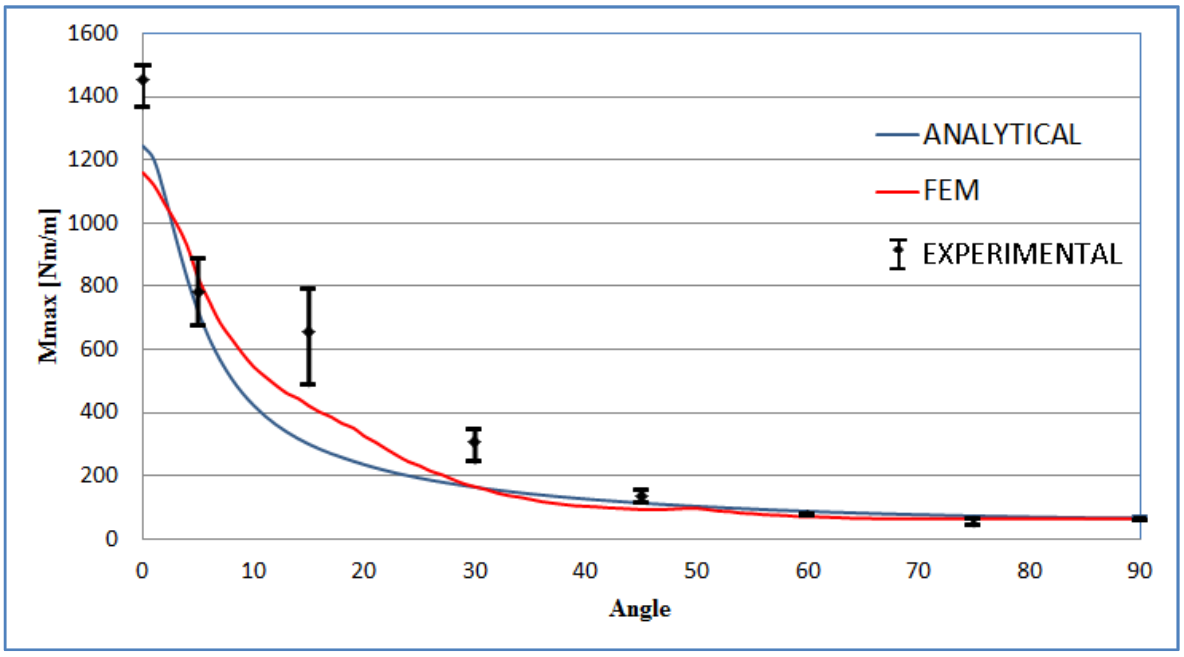

Figure 5.4. Comparison of the analytical and finite element M_{max} predictions obtained using quadric surfaces criterion for unidirectional off-axis $[\theta_6]_s$ specimens with the experimental results.

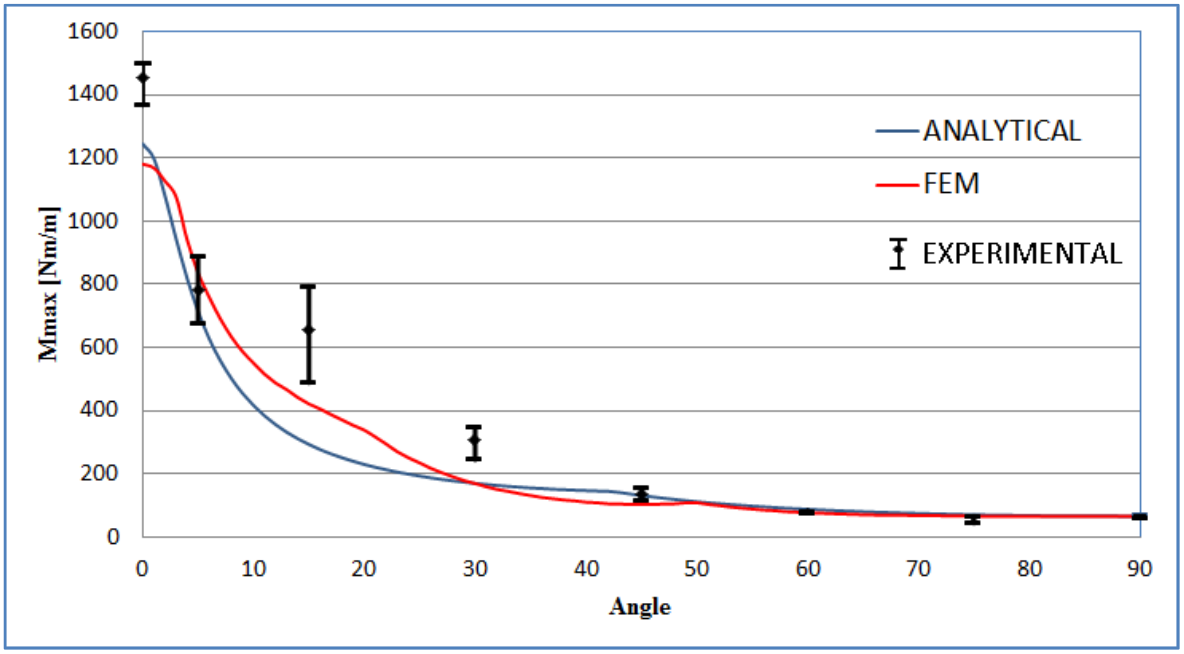

Figure 5.5. Comparison of the analytical and finite element M_{max} predictions obtained using modified quadric surfaces criterion for unidirectional off-axis $[\theta_6]_s$ specimens with the experimental results.

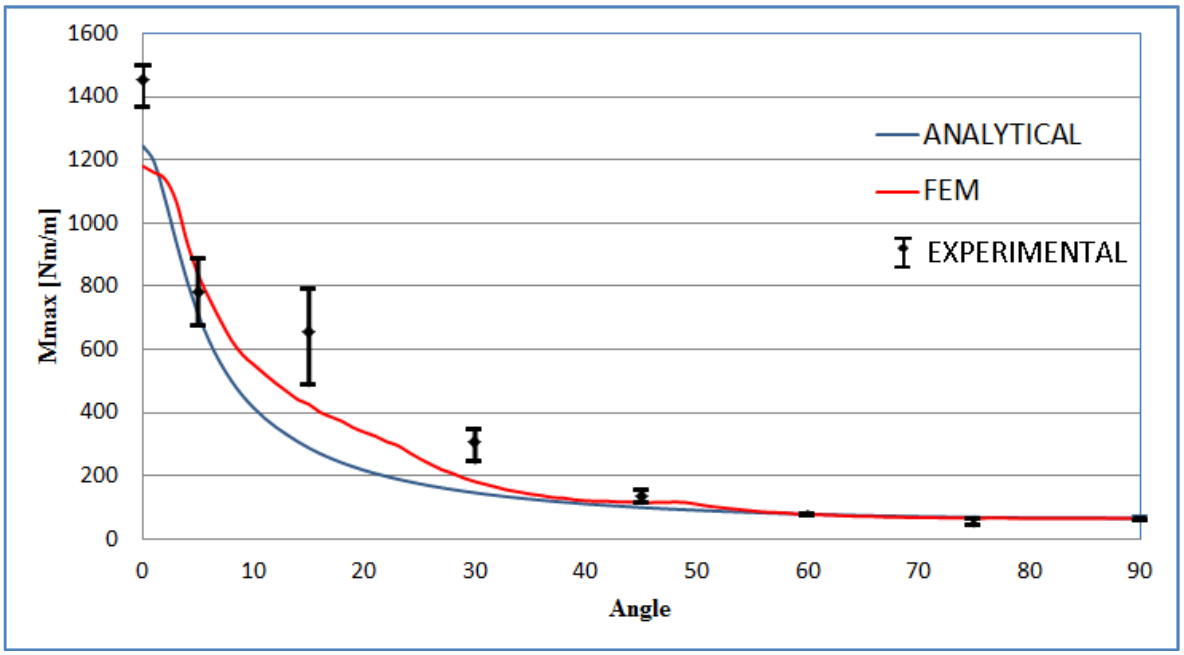

Figure 5.6. Comparison of the analytical and finite element M_{max} predictions obtained using Norris criterion for unidirectional off-axis $[\theta_6]_s$ specimens with the experimental results.

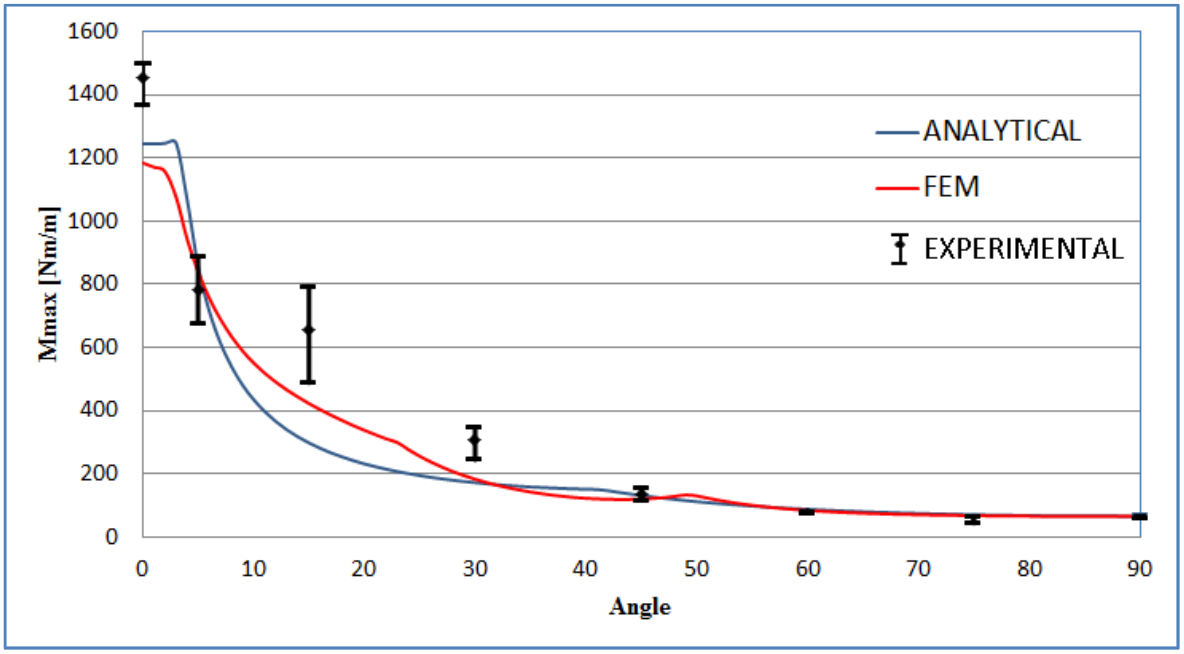

Figure 5.7. Comparison of the analytical and finite element M_{max} predictions obtained using the maximum stress criterion for unidirectional off-axis $[\theta_6]_s$ specimens with the experimental results.

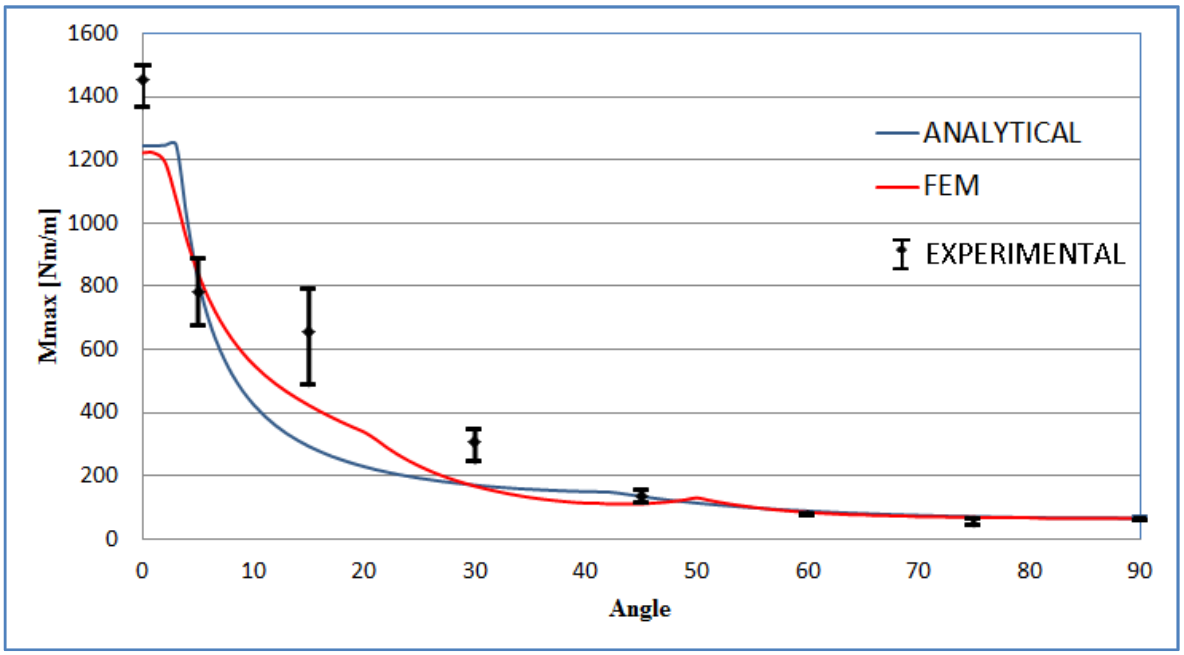

Figure 5.8. Comparison of the analytical and finite element M_{max} predictions obtained using the maximum strain criterion for unidirectional off-axis $[\theta_6]_s$ specimens with the experimental results.

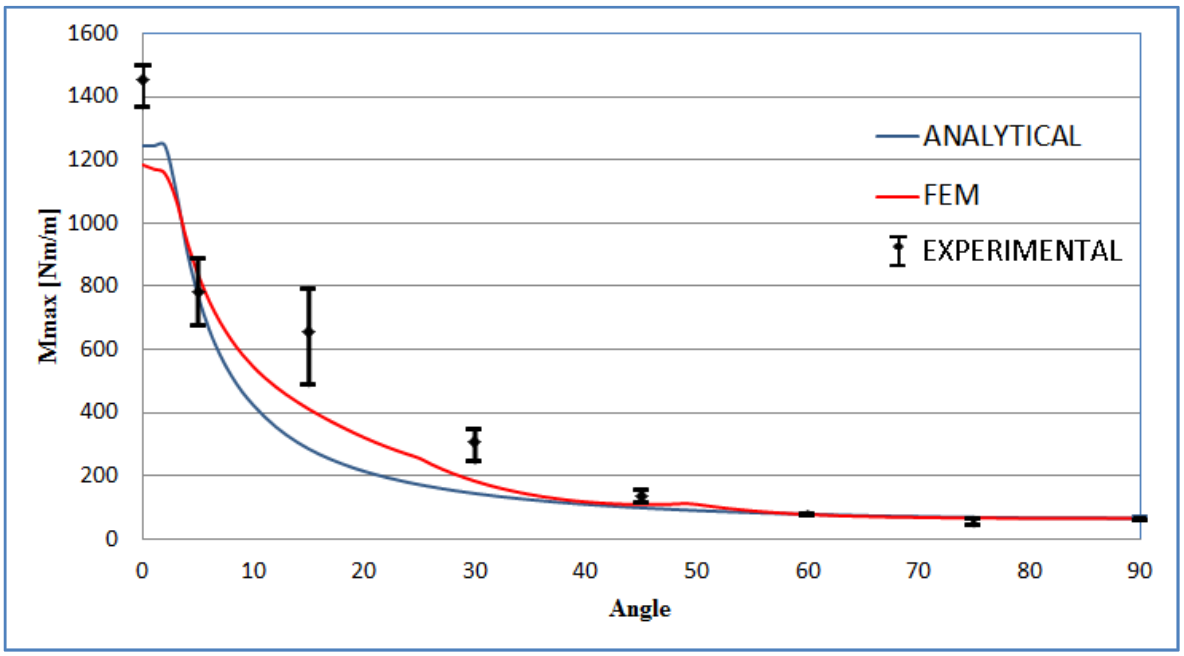

Figure 5.9. Comparison of the analytical and finite element M_{max} predictions obtained using Hashin criterion for unidirectional off-axis $[\theta_6]_s$ specimens with the experimental results.

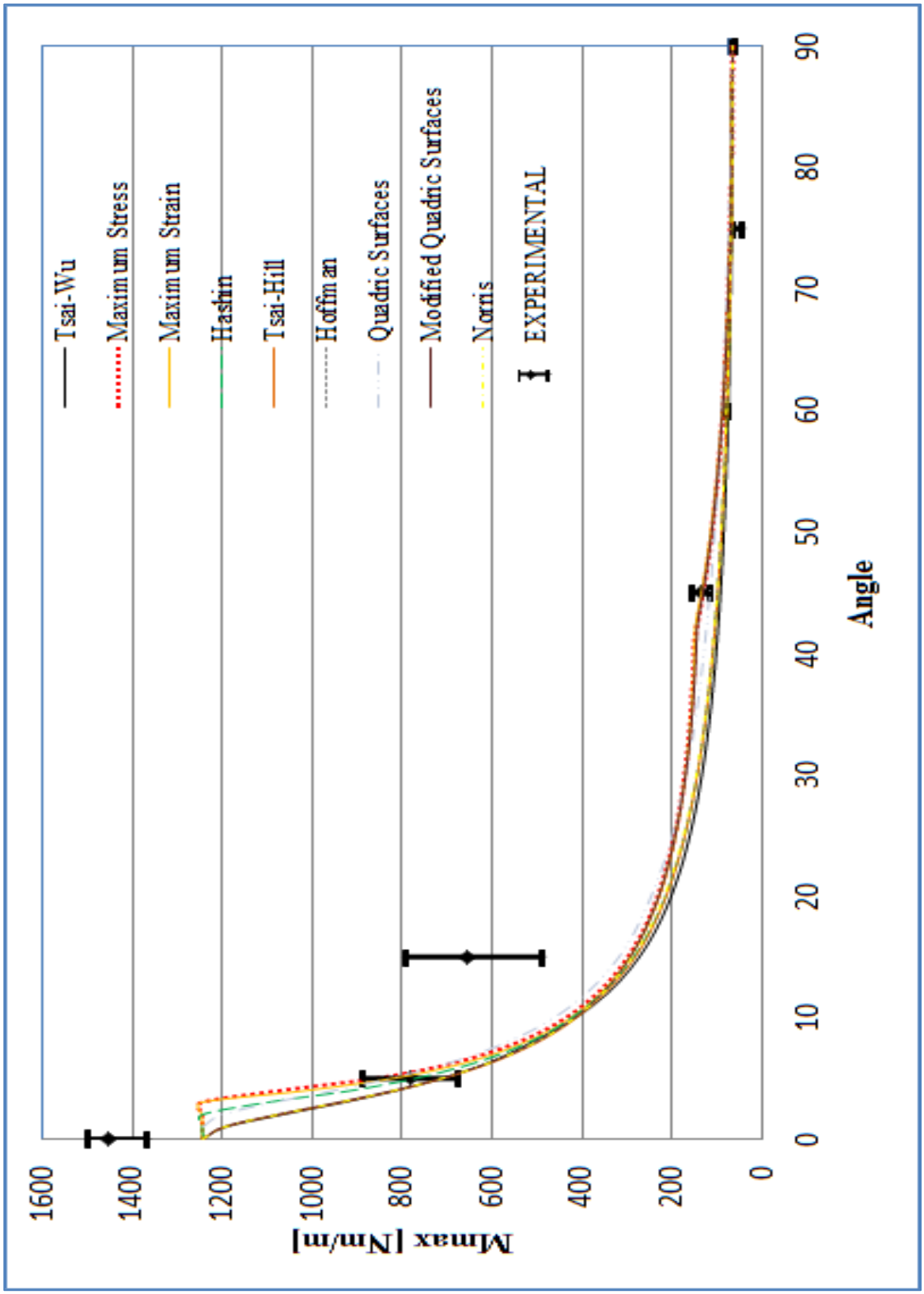

Figure 5.10: M_{max} predictions of the failure criteria for unidirectional $[\theta_6]_s$ laminates based on the analytical model.

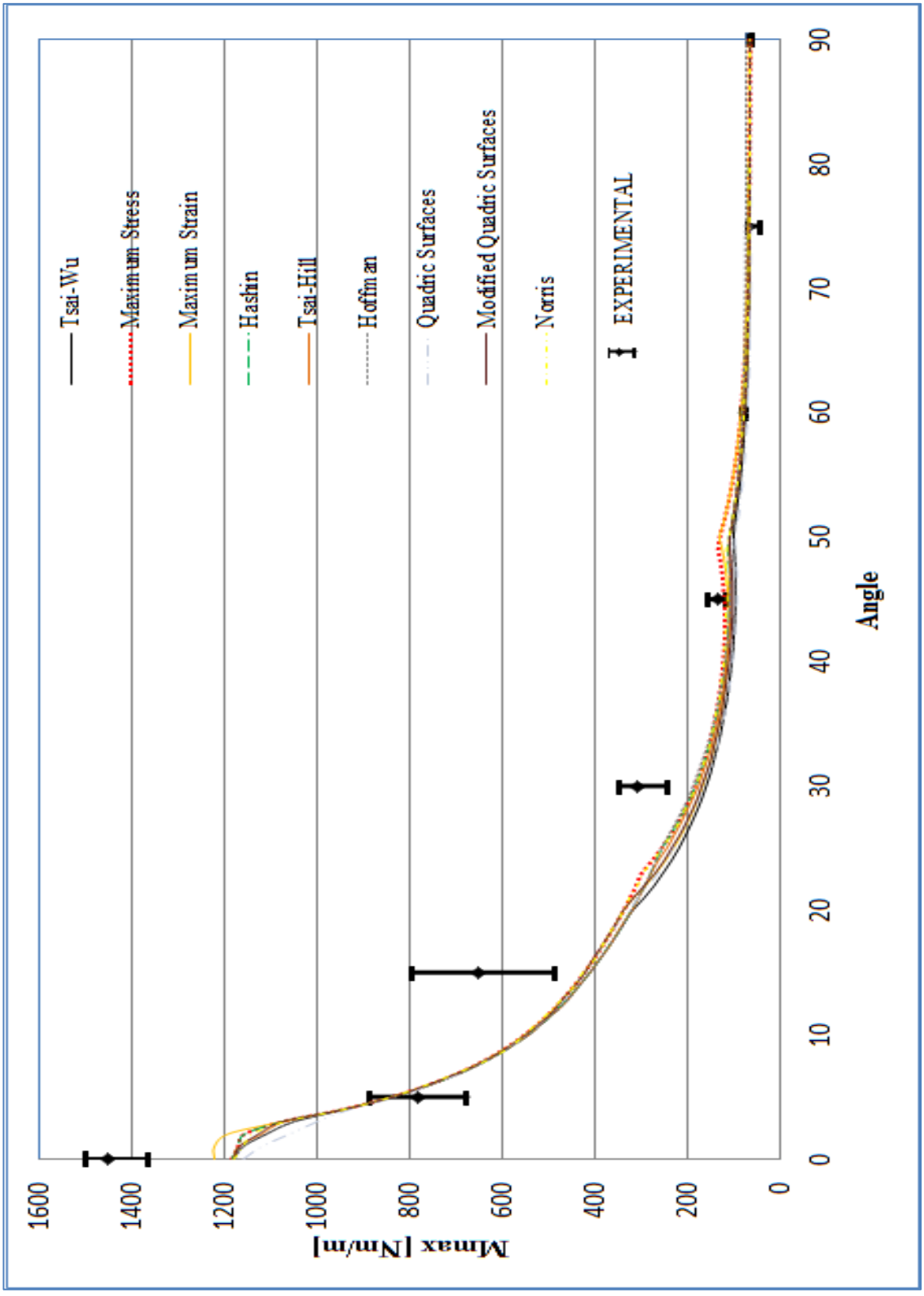

Figure 5.11. M_{max} predictions of the failure criteria for unidirectional $[\theta_6]_s$ laminates based on the FE model.

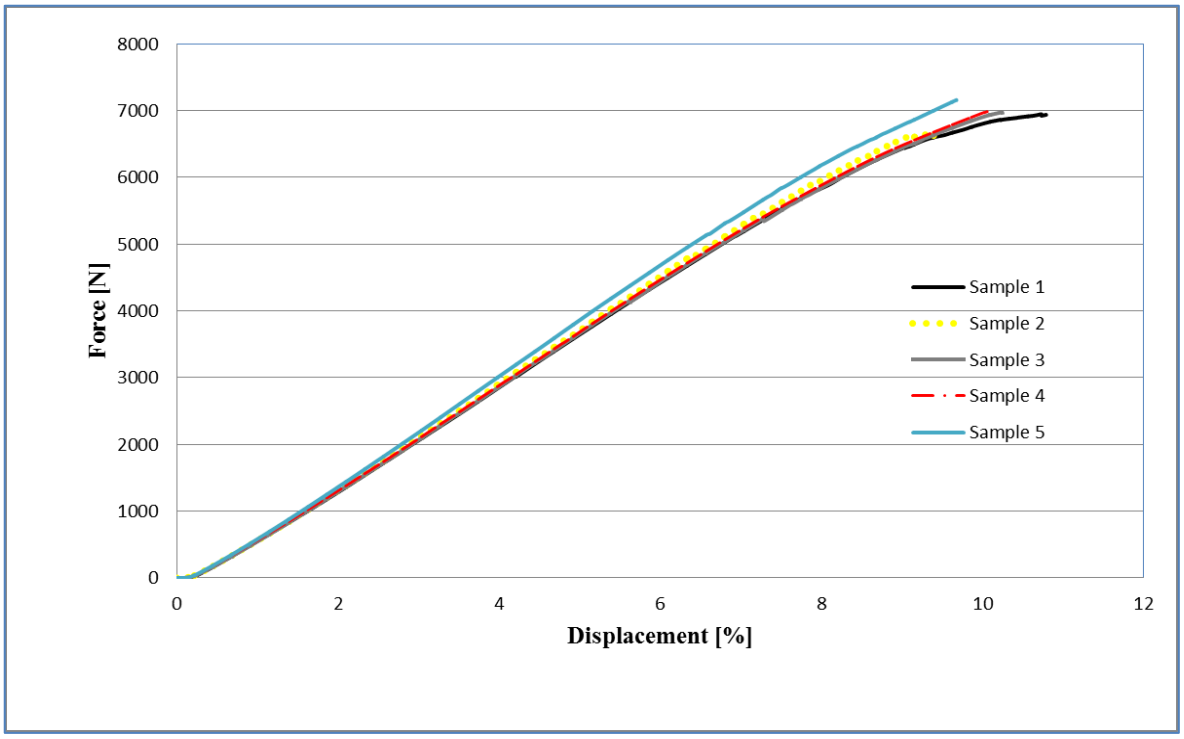

Figure 5.12. Force – displacement diagram for $[0_6]_s$ specimens.

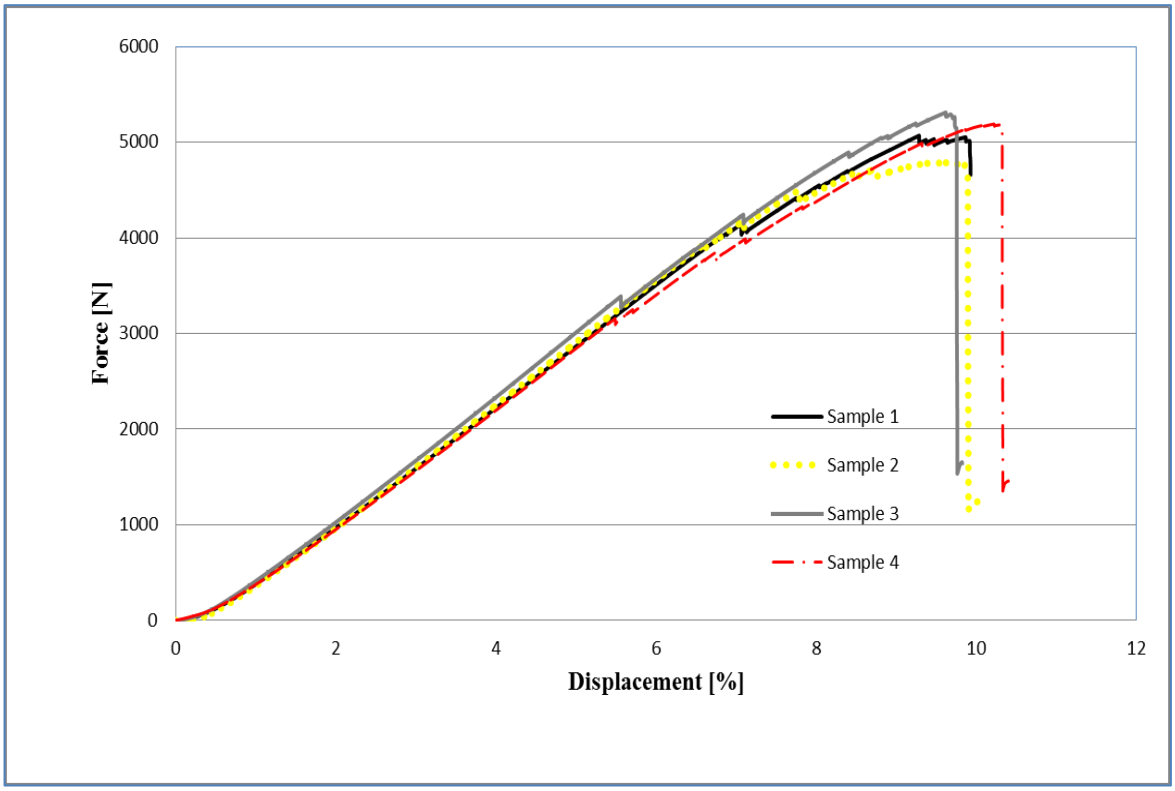

Figure 5.13. Force – displacement diagram for $[5_6]_s$ specimens.

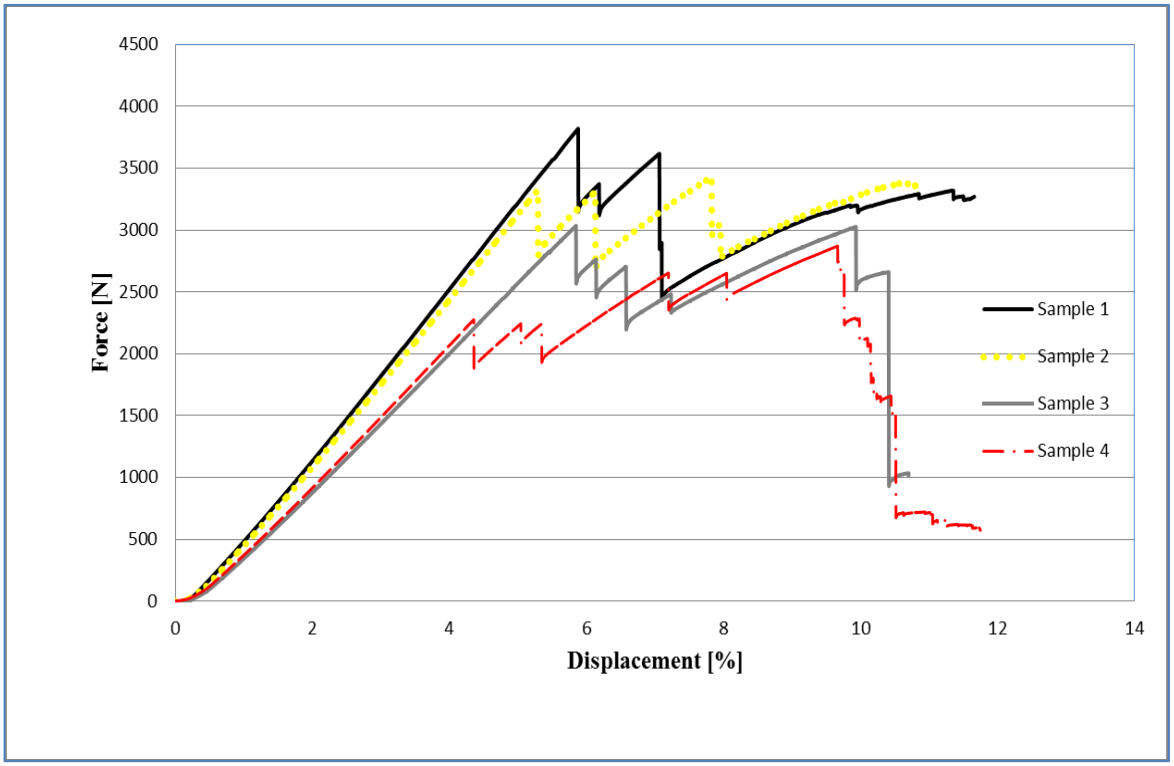

Figure 5.14. Force – displacement diagram for $[15_6]_s$ specimens.

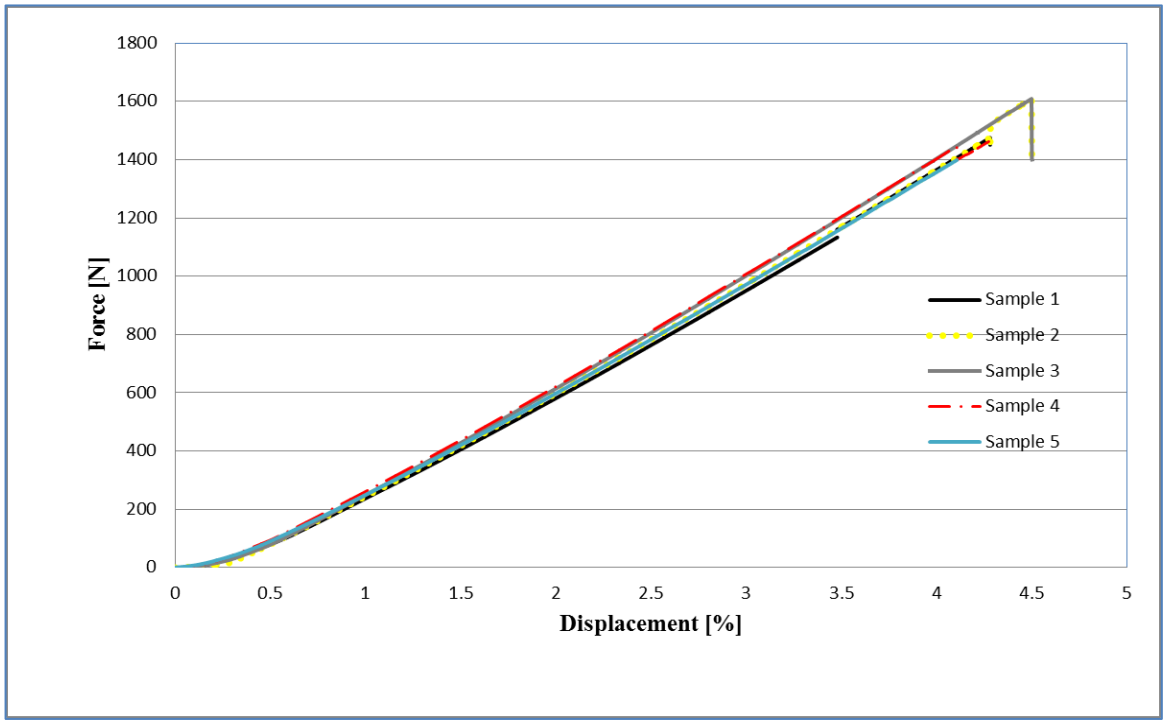

Figure 5.15. Force – displacement diagram for $[30_6]_s$ specimens.

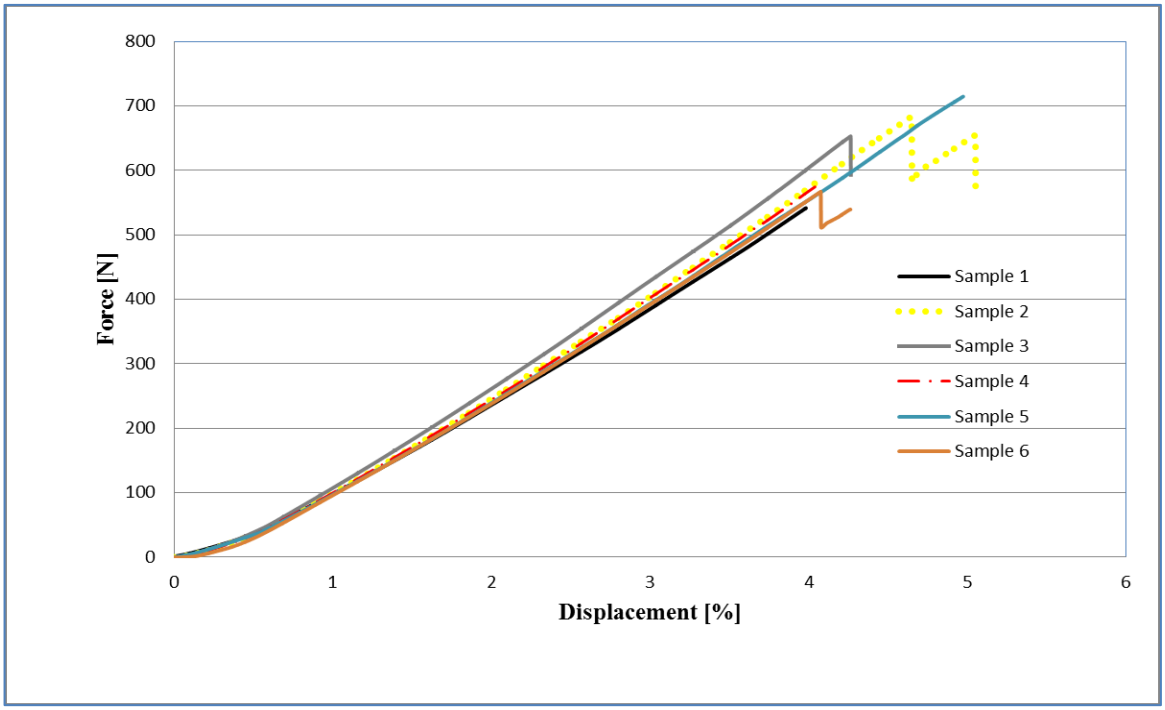

Figure 5.16. Force – displacement diagram for $[45_6]_s$ specimens.

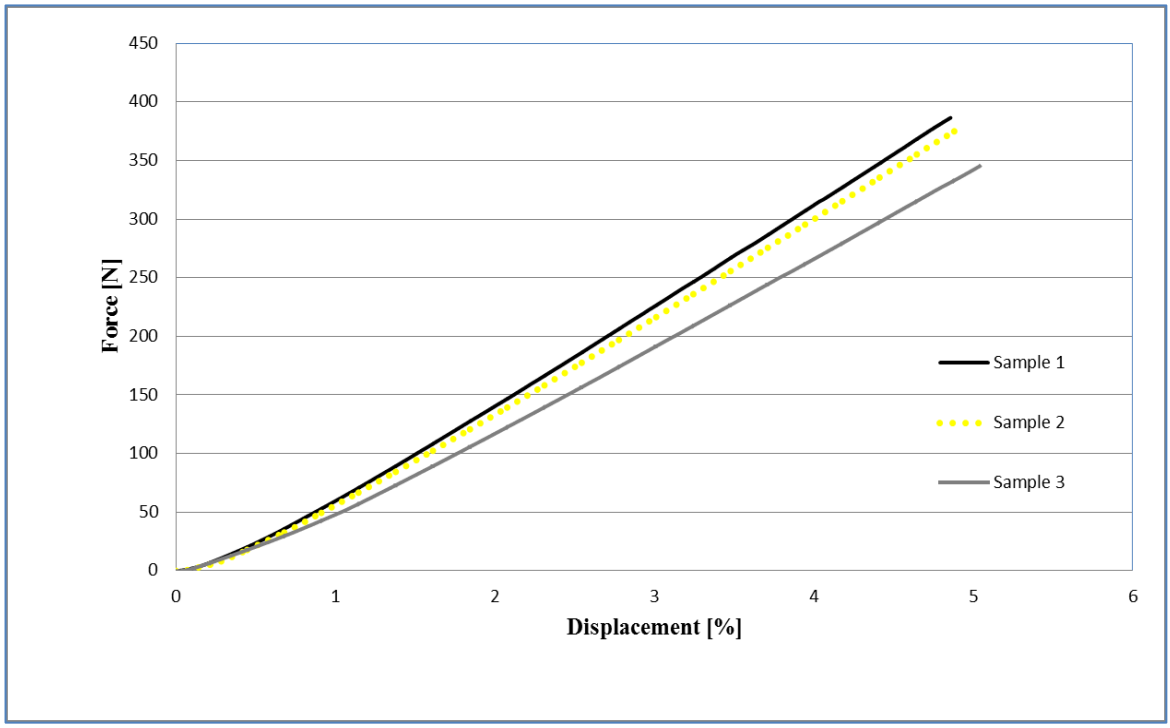

Figure 5.17. Force – displacement diagram for $[60_6]_s$ specimens.

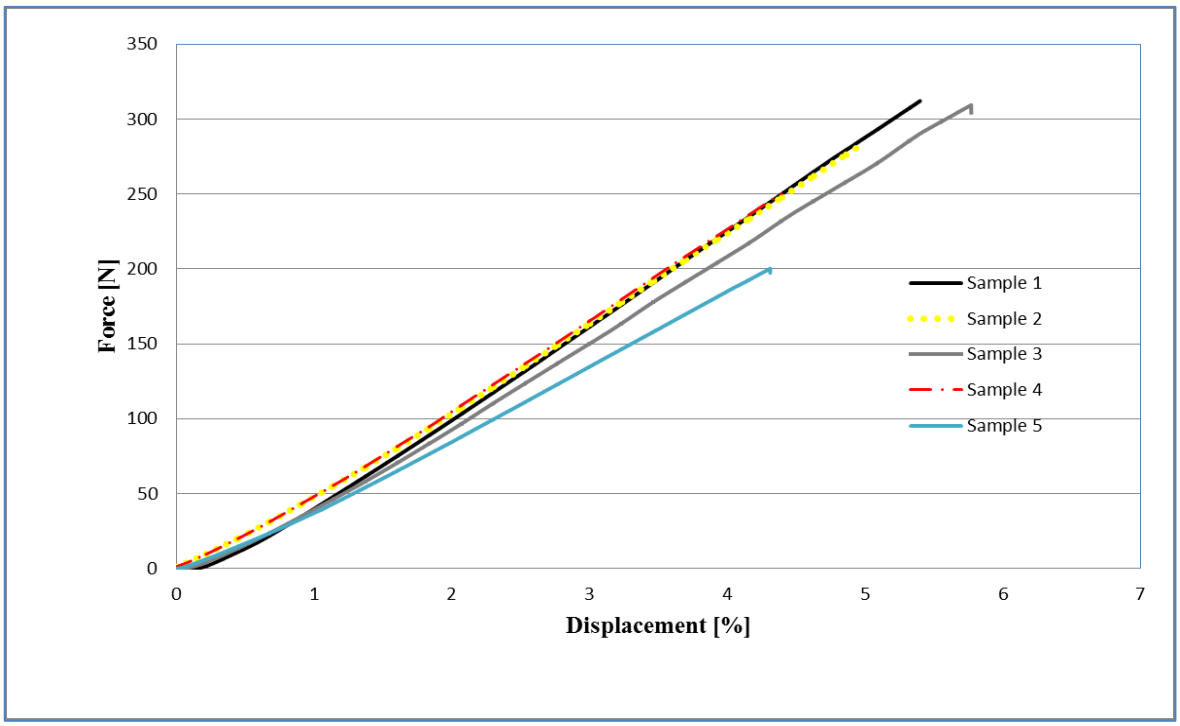

Figure 5.18. Force – displacement diagram for $[75_6]_s$ specimens

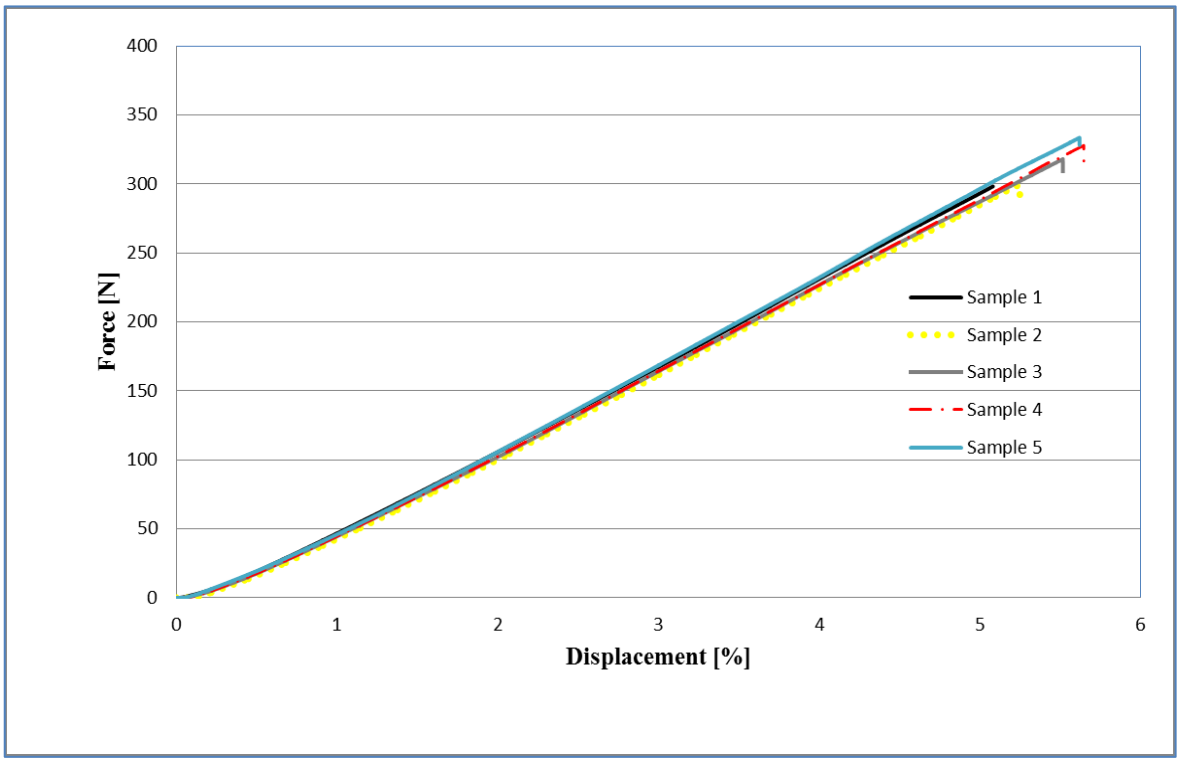

Figure 5.19. Force – displacement diagram for $[90_6]_s$ specimens.

Table 5.3. Experimental results of M_{max} for unidirectional off-axis $[\theta_6]_s$ specimens.

Fiber orientation angle	Allowable Force [N]	Mmax [Nm/m]
0	6945,32	1499,47
0	6542,03	1366,88
0	6973,91	1452,60
0	6983,66	1452,22
0	7157,67	1490,87
5	4143,50	887,54
5	3915,15	838,90
5	3388,43	725,44
5	3156,10	676,12
15	3819,01	793,29
15	3275,31	680,52
15	3034,31	650,30
15	2275,47	487,57
30	1133,18	243,67
30	1474,85	316,74
30	1608,91	344,89
30	1446,33	309,97
30	1462,09	314,52
45	541,64	117,25
45	683,94	147,28
45	653,05	140,05
45	574,39	123,43
45	714,56	153,33
45	566,99	121,57
60	386,41	83,75
60	379,70	82,35
60	345,09	74,47
75	283,99	60,86
75	309,31	66,47
75	250,24	53,78
75	200,18	42,99
75	312,08	65,07
90	298,24	60,89
90	299,72	62,31
90	318,02	66,13
90	327,93	68,17
90	333,55	69,55

5.2.2. Symmetric Balanced Laminates

In Figures 5.20 – 5.33, analytical and finite element M_{max} predictions obtained using the chosen failure criterion for symmetric balanced $[+\theta_6/-\theta_6]_s$ specimens are compared with experimental results. Experimental results of symmetric balanced laminates are given in Table 5.4.

Figure 5.20 shows that finite element and analytical predictions of Tsai-Wu criterion for symmetric balanced laminates change smoothly as the fiber orientation angle changes from 0° to 90° degrees. According to the figure, Tsai-Wu criterion underestimates the strength of the material if θ is less than 60°.

As a quadratic criterion, predictions of Tsai-Hill also changes smoothly. Figure 5.21 indicates that there is a large difference between finite element and analytical model predictions if θ is less than 30°. Analytical model prediction of Tsai-Hill underestimates M_{max} if θ is less than 60°. On the other hand, the finite element model correctly predicts M_{max} for 15°.

Predictions of Hoffman criterion, which are shown in Figure 5.22, are similar to that of Tsai-Hill criterion. Analytical and finite element predictions of Hoffman criterion differ below 50° and the gap between the predictions is larger as compared to Tsai-Hill criterion for θ less than 50°.

M_{max} predictions of quadric surfaces and modified quadric surfaces criteria are given in Figures 5.23 – 5.24, respectively. Analytical model predictions of the quadric surfaces and modified quadric surfaces do not smoothly change because of the inclusion of residual stresses. In both cases, analytical and finite element model predictions underestimate the strength of the material if θ is less than 60°.

According to Figure 5.25, Norris criterion predicts the failure trend of symmetric balanced laminates between 60° and 90° well with the finite element model; But it cannot predict the strengths of between 0° and 45°.

Similar to the UD laminates, failure prediction trend of physically based criteria are not smooth. Analytical model based predictions of maximum stress, maximum strain and Hashin criteria indicate that the strength increases as the fiber angle is varied from 0° to 2° – 4° degrees (Figures 5.26-29). Finite element model based predictions of maximum stress and Hashin criteria are close to the experimental results in the range of 30° – 90°. Maximum strain criterion's FE based predictions are close to the experimental results at 15°, 45°, 60°, 75° and 90°.

FE model based predictions in Figures 5.20 – 5.28 include the residual stresses. The effects of the inclusion of the residual stresses are shown in Figures 5.29 – 5.30 for quadratic (Norris) and physically based (maximum strain) criteria. As it can be seen, inclusion of residual stresses makes a difference in the predictions for angles between 10° and 75°. According to Figure 5.29, FE based predictions of Norris criterion correlate well with the experimental results between 30° and 45° when the residual stresses are excluded. However, when the residual stresses are included, FE based predictions underestimate the strength for these angles. Figure 5.30 demonstrates that FE based predictions of maximum strain criterion coincides are close to the experimental results at 15° and 60° when residual stresses are included; yet, the strength of the material is underestimated between 30° and 45°, in which of FE based predictions coincides with the experimental results if residual stresses are excluded. The analytical and numerical models generally underestimate the strength of the plates under bending. Inclusion of residual stresses always results in lower values for M_{max}. For this reason, inclusion of the residual stresses does not improve the results. However, development of residual stresses in a laminate during manufacturing is a factor affecting the strength. If all the other factors are accounted for correctly, inclusion of residual stresses is expected to improve the correlation.

M_{max} predictions of the chosen criteria for $[\theta_3/-\theta_3]_s$ configuration based on the analytical and finite element models are compared with the experimental results in Figures 5.31 – 5.33. The figures show that analytical model predictions underestimate the experimental results if θ is less than 60°. Figure 5.30 illustrates that finite element model based predictions of the failure criteria gives the most realistic results. Including residual stresses improves the accuracy of the predictions in case of analytical model.

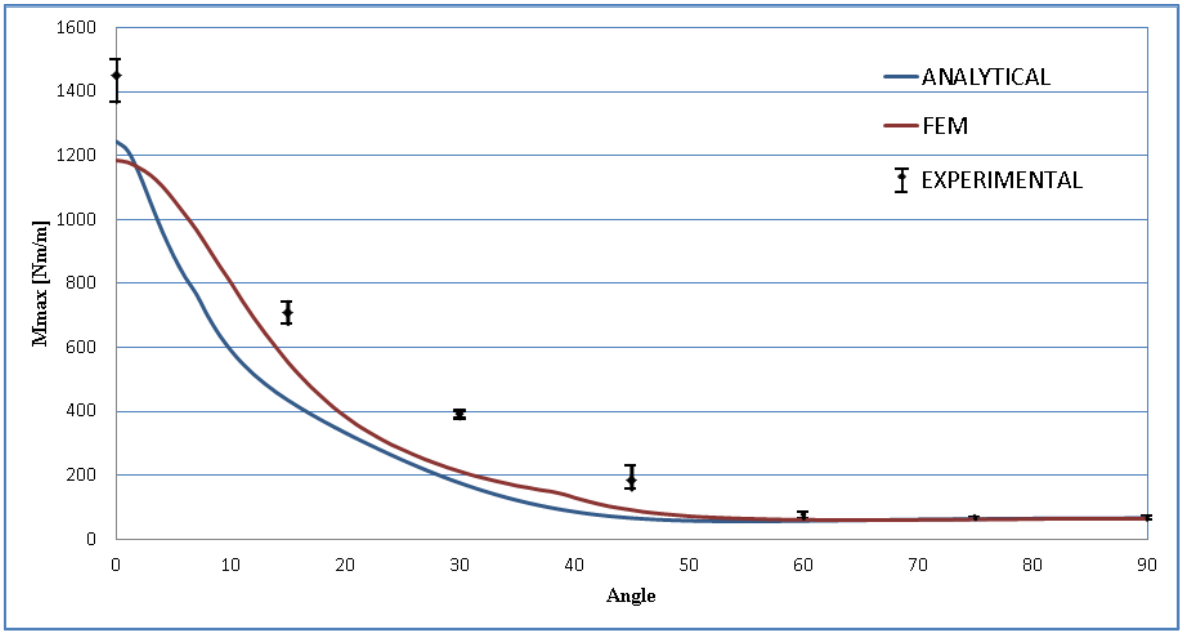

Figure 5.20. Comparison of the analytical and finite element M_{max} predictions obtained using Tsai-Wu criterion for multidirectional $[+\theta_3/-\theta_3]_s$ specimens with the experimental results.

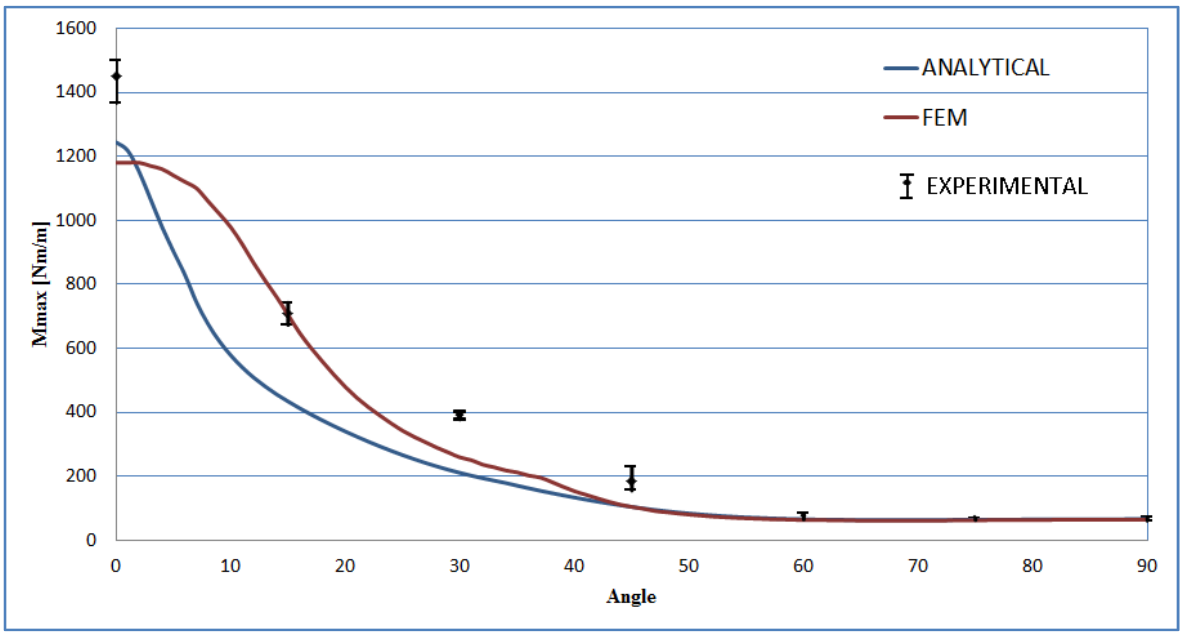

Figure 5.21. Comparison of the analytical and finite element M_{max} predictions obtained using Tsai-Hill criterion for multidirectional $[+\theta_3/-\theta_3]_s$ specimens with the experimental results.

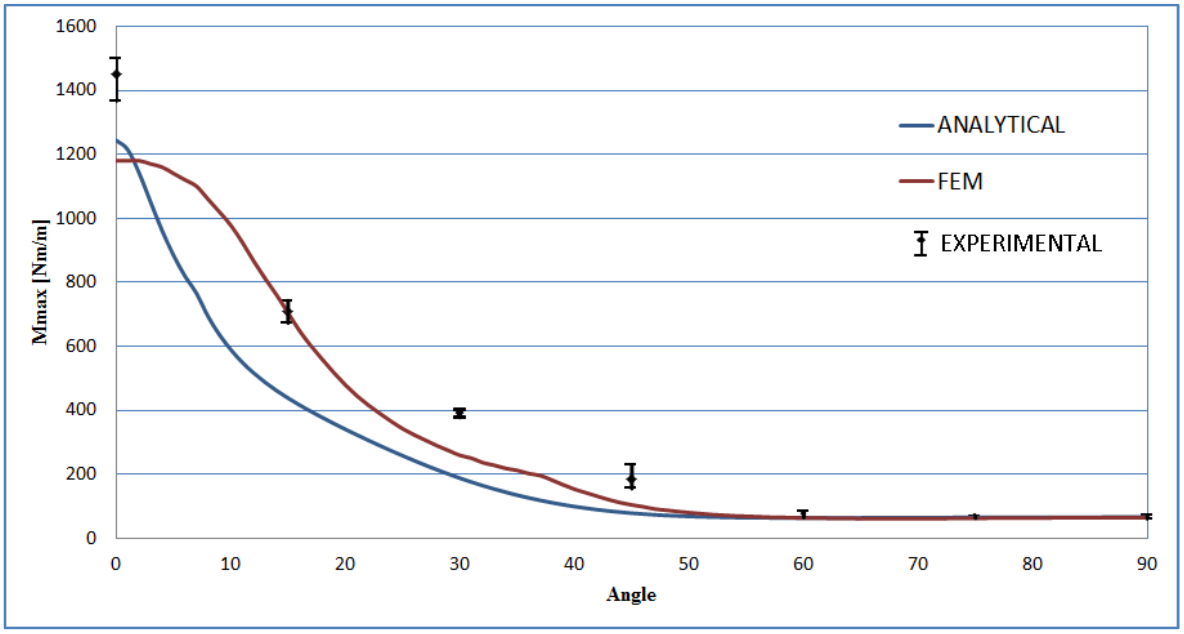

Figure 5.22. Comparison of the analytical and finite element M_{max} predictions obtained using Hoffman criterion for multidirectional $[+\theta_3/-\theta_3]_s$ specimens with the experimental results.

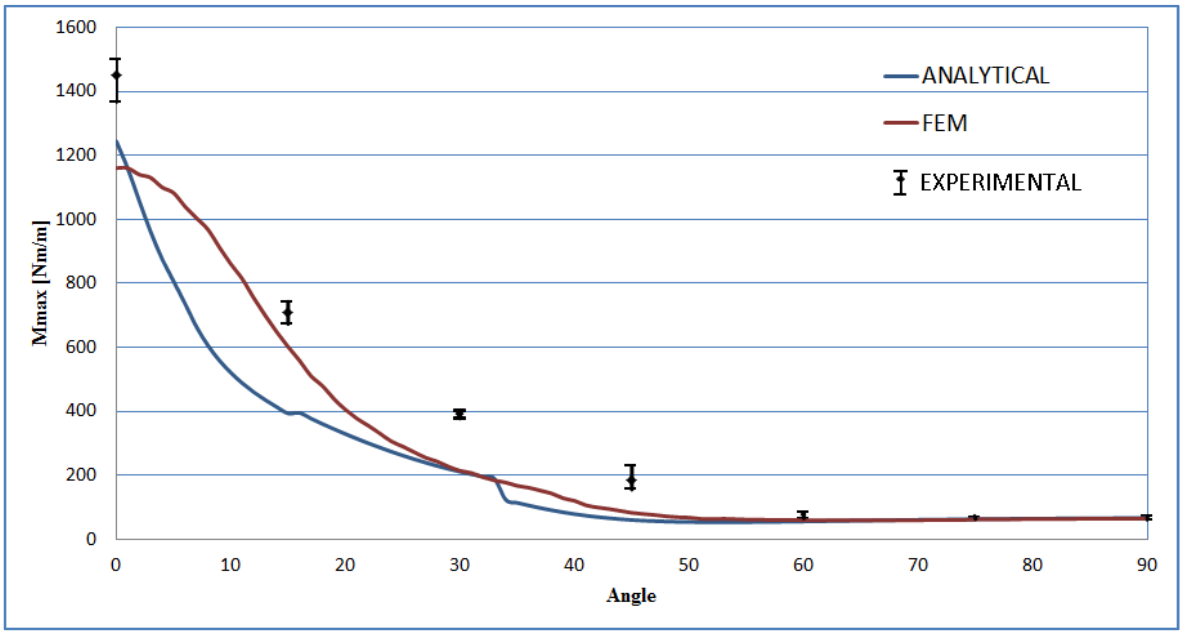

Figure 5.23. Comparison of the analytical and finite element M_{max} predictions obtained using quadric surfaces criterion for multidirectional $[+\theta_3/-\theta_3]_s$ specimens with the experimental results.

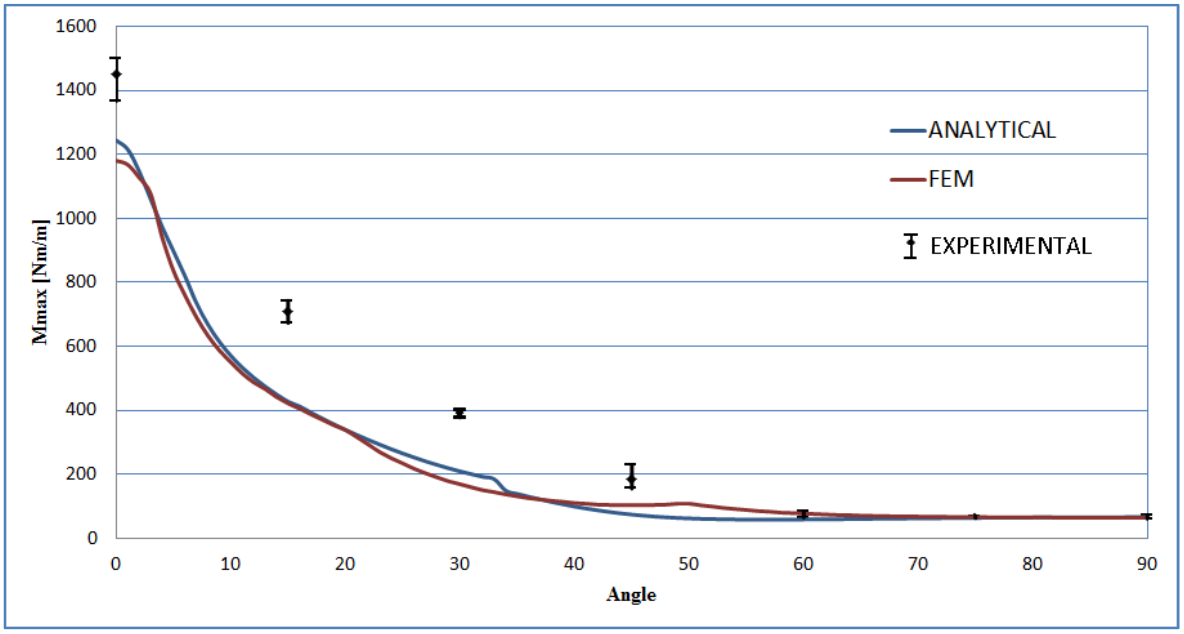

Figure 5.24. Comparison of the analytical and finite element M_{max} predictions obtained using modified quadric surfaces criterion for multidirectional $[+\theta_3/-\theta_3]_s$ specimens with the experimental results.

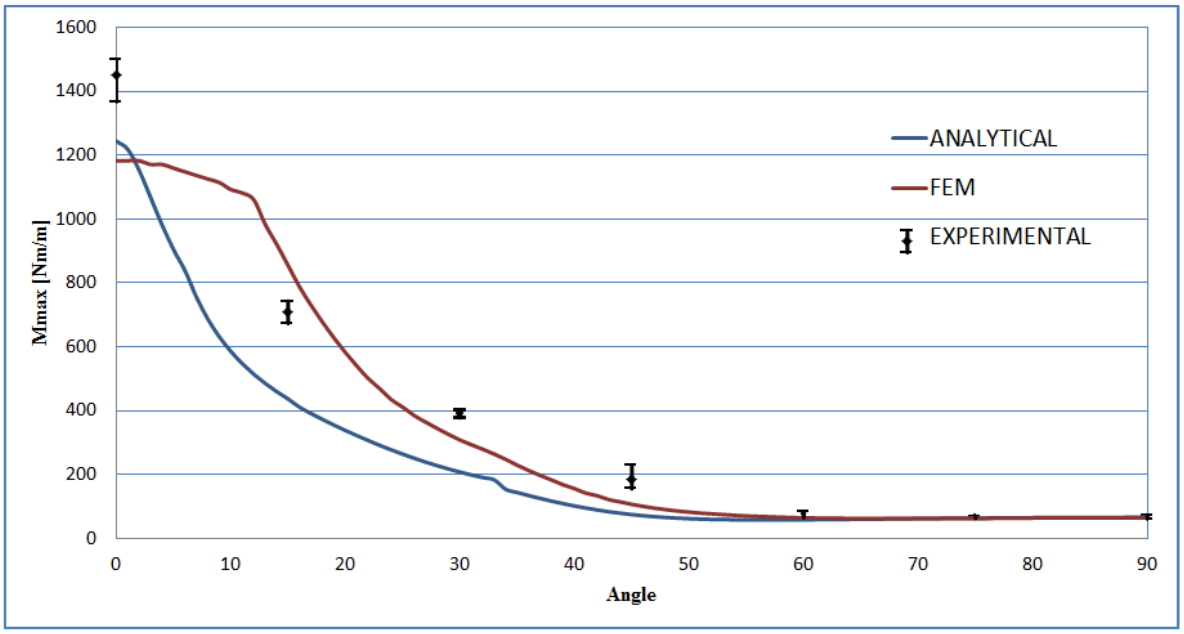

Figure 5.25. Comparison of the analytical and finite element M_{max} predictions obtained using Norris criterion for multidirectional $[+\theta_3/-\theta_3]_s$ specimens with the experimental results.

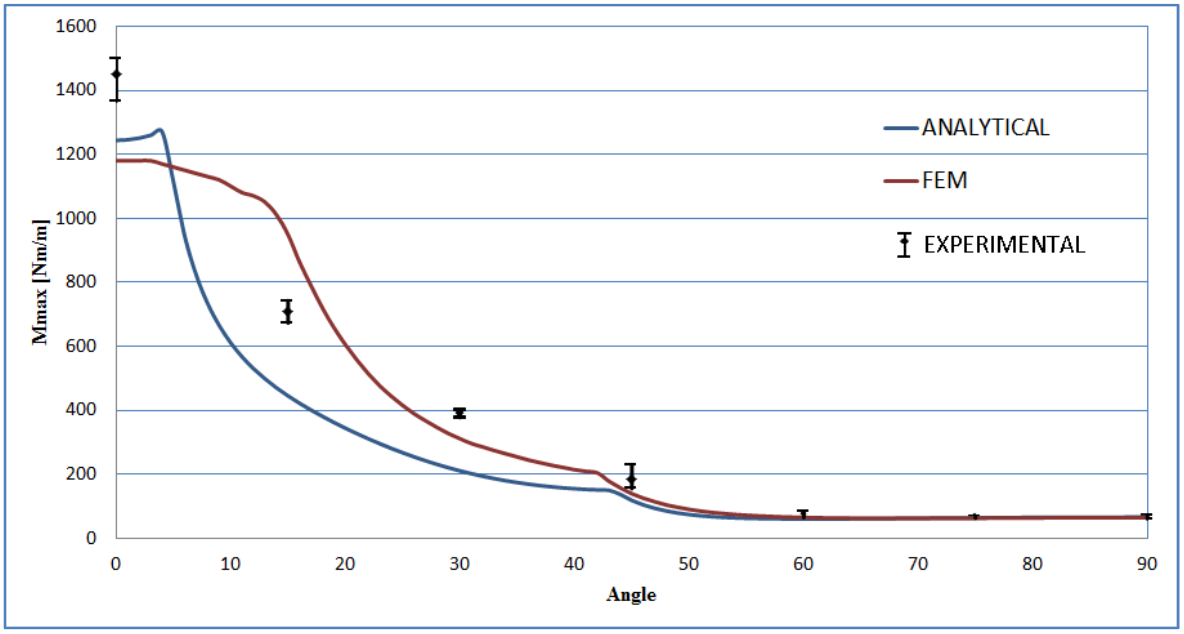

Figure 5.26. Comparison of the analytical and finite element M_{max} predictions obtained using the maximum stress criterion for multidirectional $[+\theta_3/-\theta_3]_s$ specimens with the experimental results.

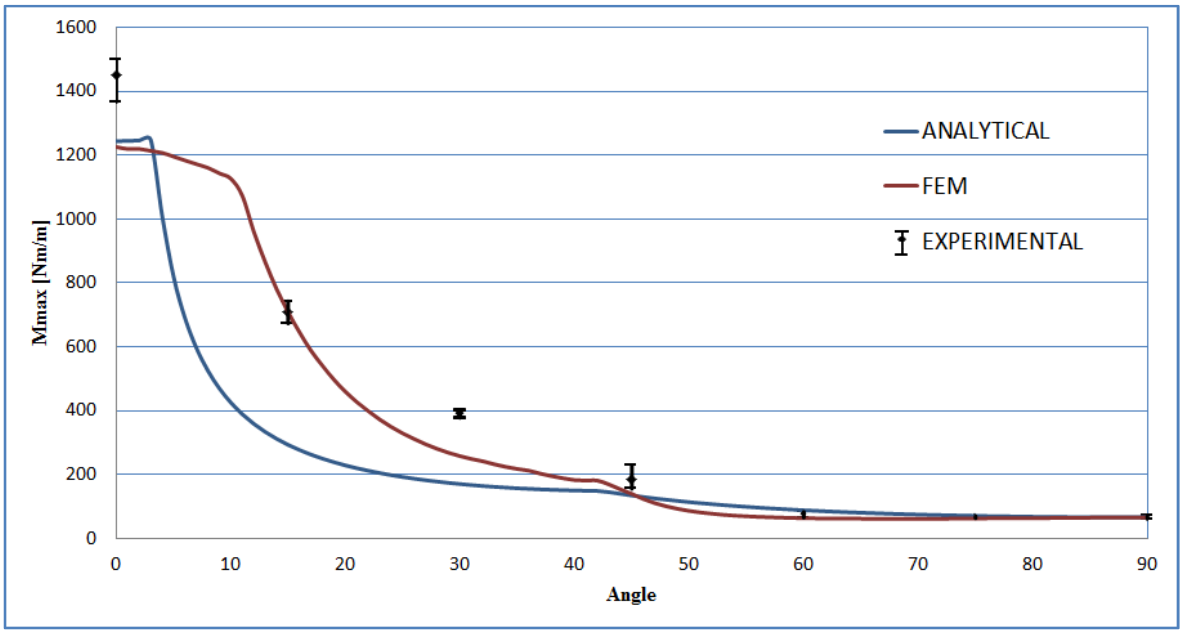

Figure 5.27. Comparison of the analytical and finite element M_{max} predictions obtained using the maximum strain criterion for multidirectional $[+\theta_3/-\theta_3]_s$ specimens with the experimental results.

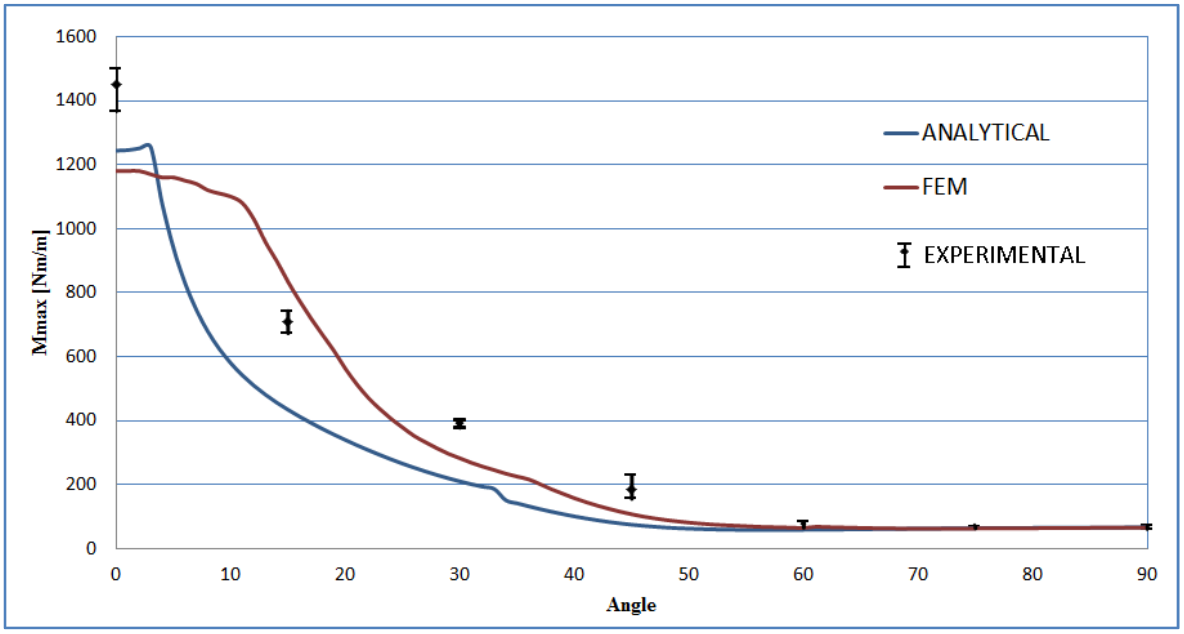

Figure 5.28. Comparison of the analytical and finite element M_{max} predictions obtained using Hashin criterion for multidirectional $[+\theta_3/-\theta_3]_s$ specimens with the experimental results.

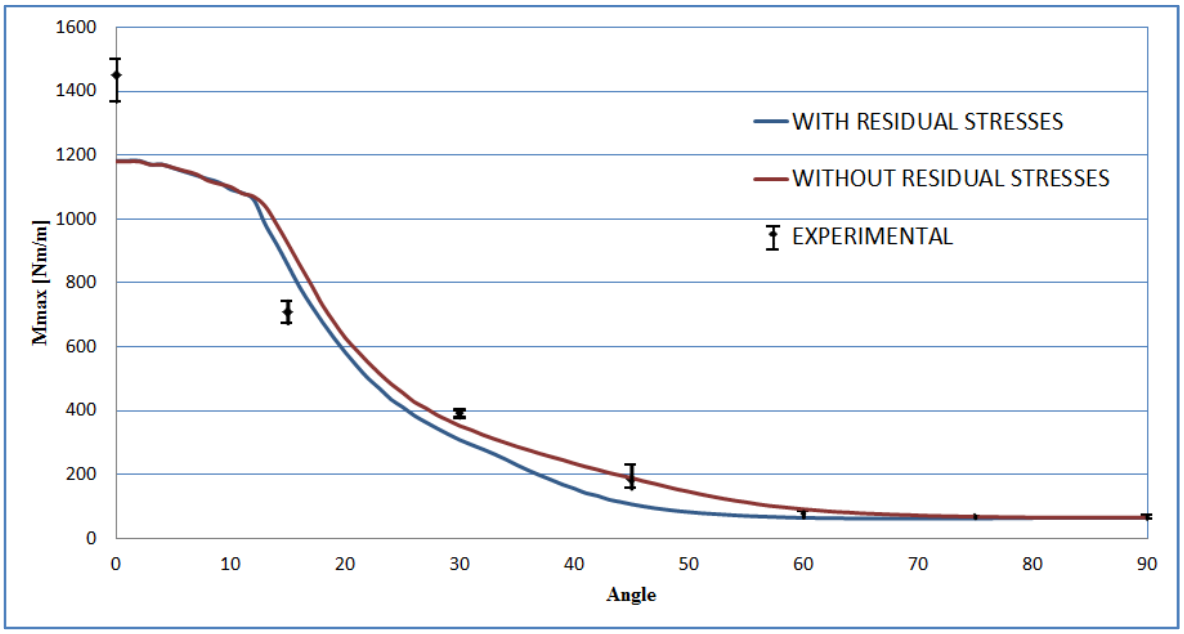

Figure 5.29. Comparison of the finite element M_{max} predictions obtained using Norris criterion for multidirectional $[+\theta_3/-\theta_3]_s$ specimens including and excluding residual stresses with the experimental results.

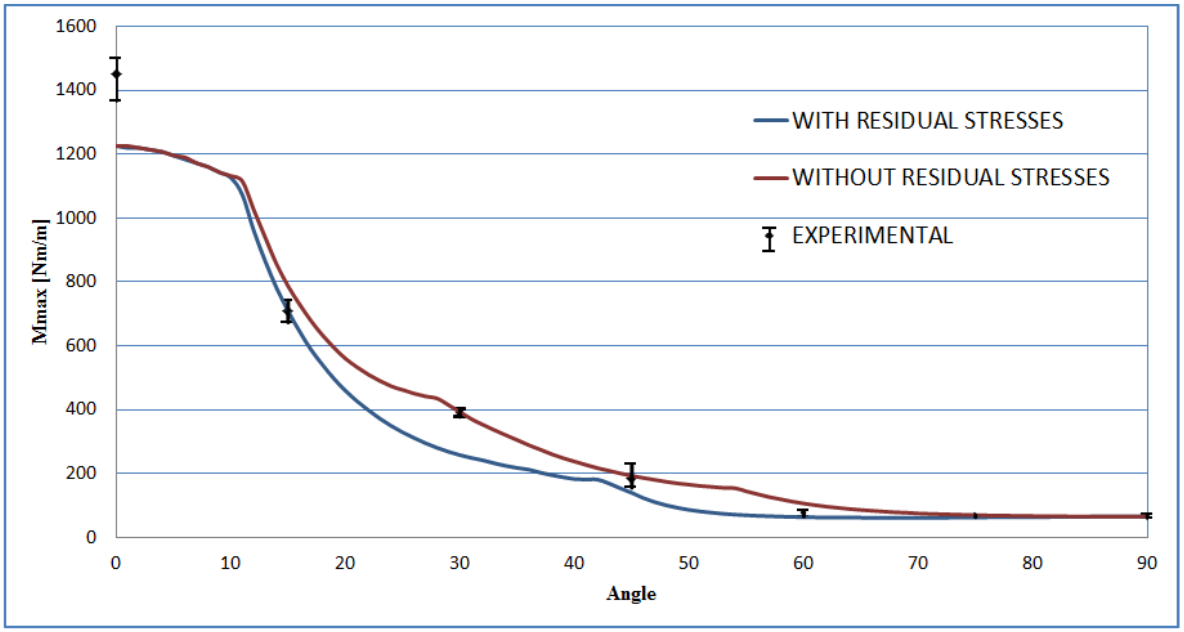

Figure 5.30. Comparison of the finite element M_{max} predictions obtained using maximum strain criterion for multidirectional $[+\theta_3/-\theta_3]_s$ specimens including and excluding residual stresses with the experimental results.

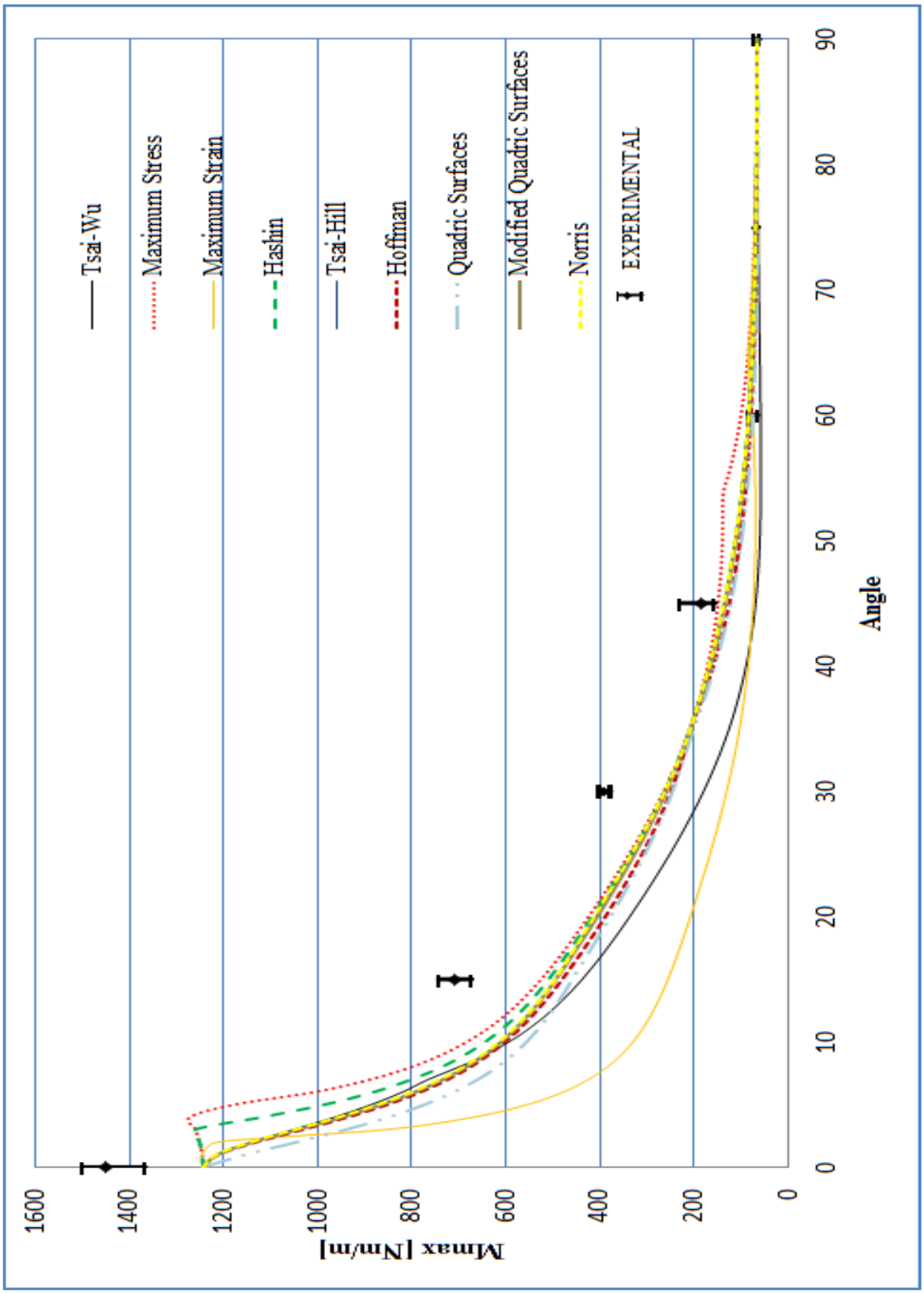

Figure 5.31: Comparison of M_{max} predictions for $[\theta_3/-\theta_3]_s$ configuration based on the analytical model excluding residual stresses.

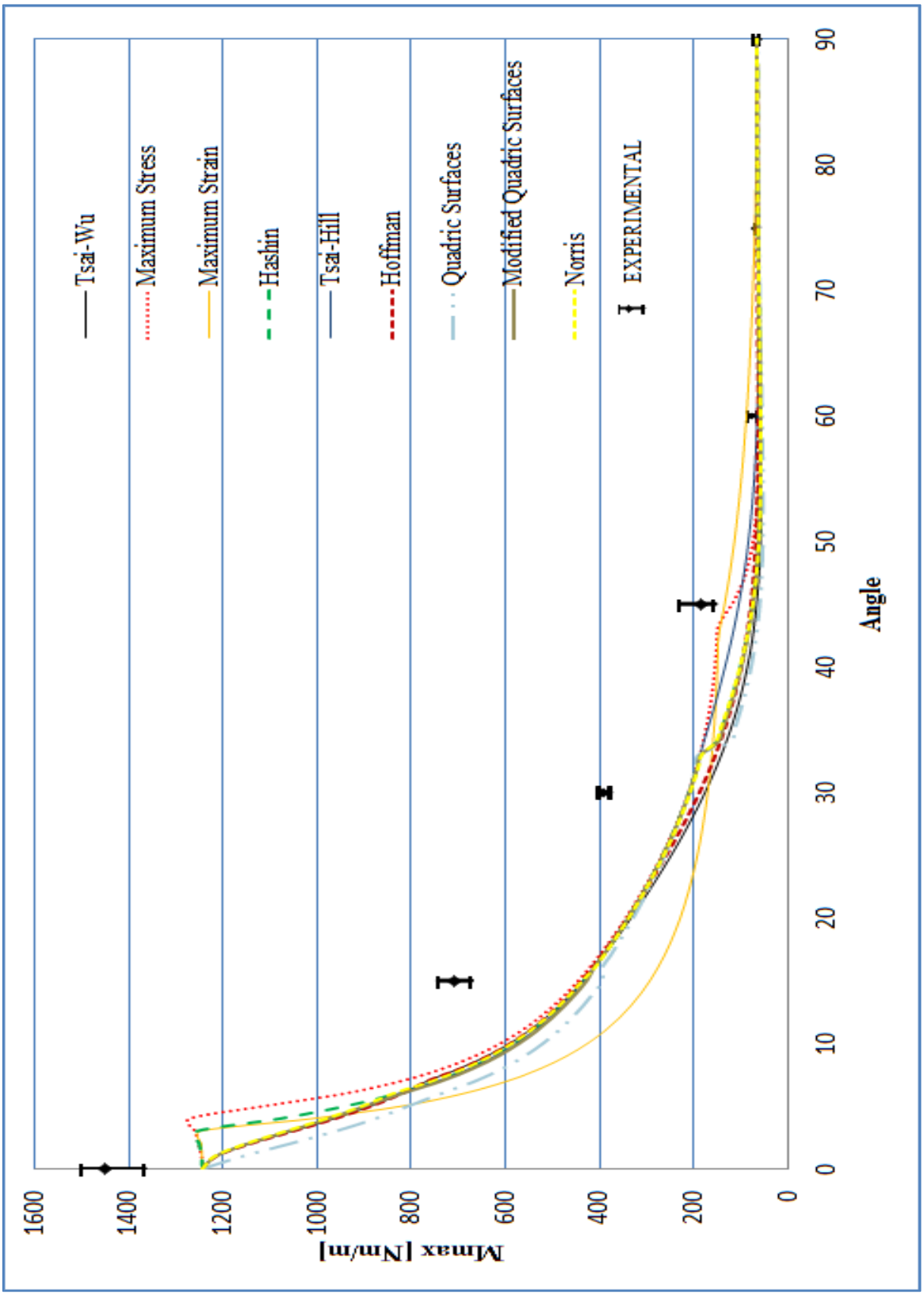

Figure 5.32: Comparison of M_{max} predictions for $[\theta_3/-\theta_3]_s$ configuration based on the analytical model.

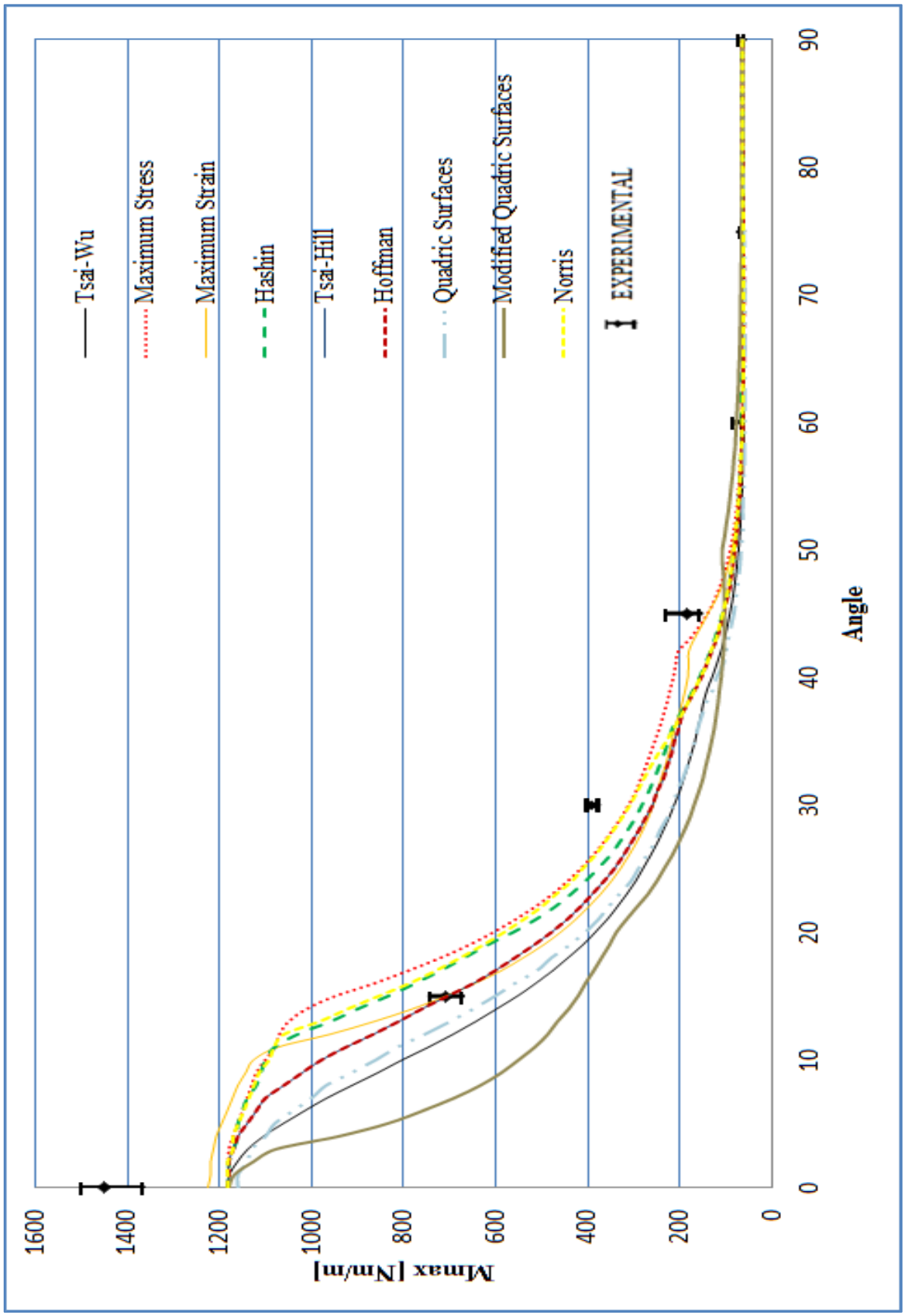

Figure 5.33: M_{max} predictions for $[\theta_3/-\theta_3]_s$ configuration based on the finite element model.

Figures 5.34 – 5.38 illustrate force – displacement diagrams of the experimental results. When fiber orientation angle, θ, is 0° and 90° symmetric balanced laminates become unidirectional; hence, force – displacement diagrams for these angles are not given in this section.

Force – displacement diagrams show that the failure behavior of symmetric balanced laminates is complex compared to UD laminates. Progressive failure occurs instead of a sudden failure. Similar to the unidirectional plates, moment resultant value at the first ply failure is taken as M_{max}.

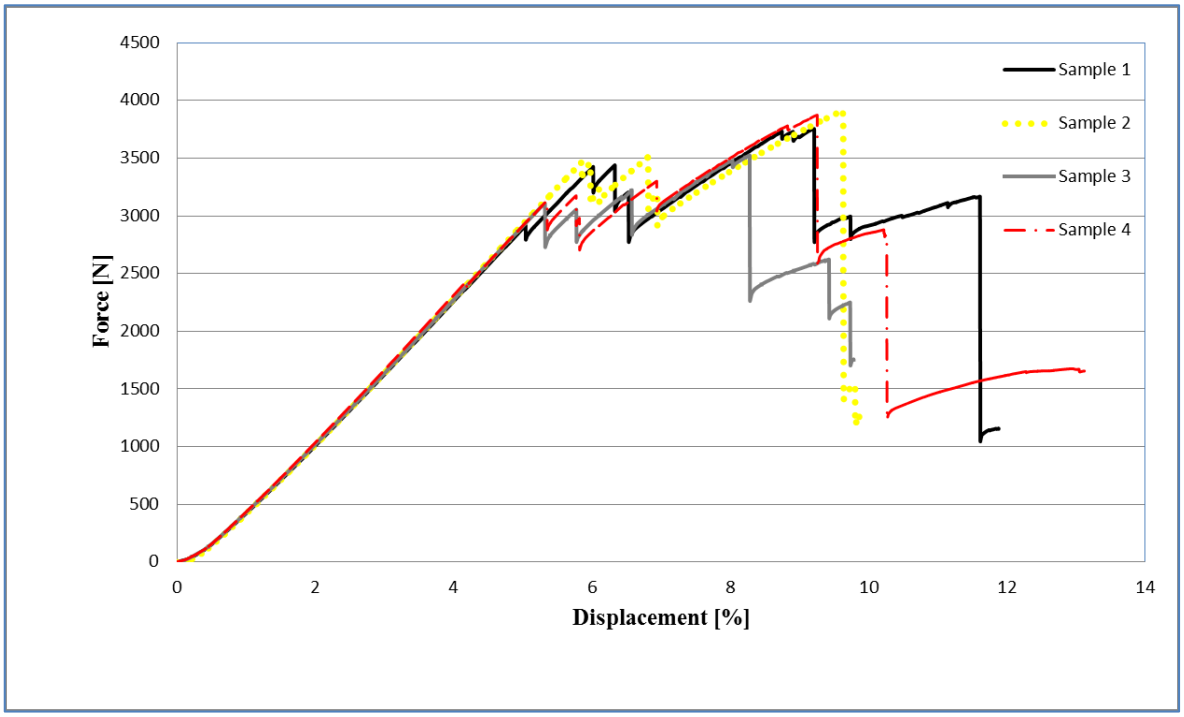

Figure 5.34. Force – displacement diagram of experimental results for $[15_3/-15_3]_s$ specimens.

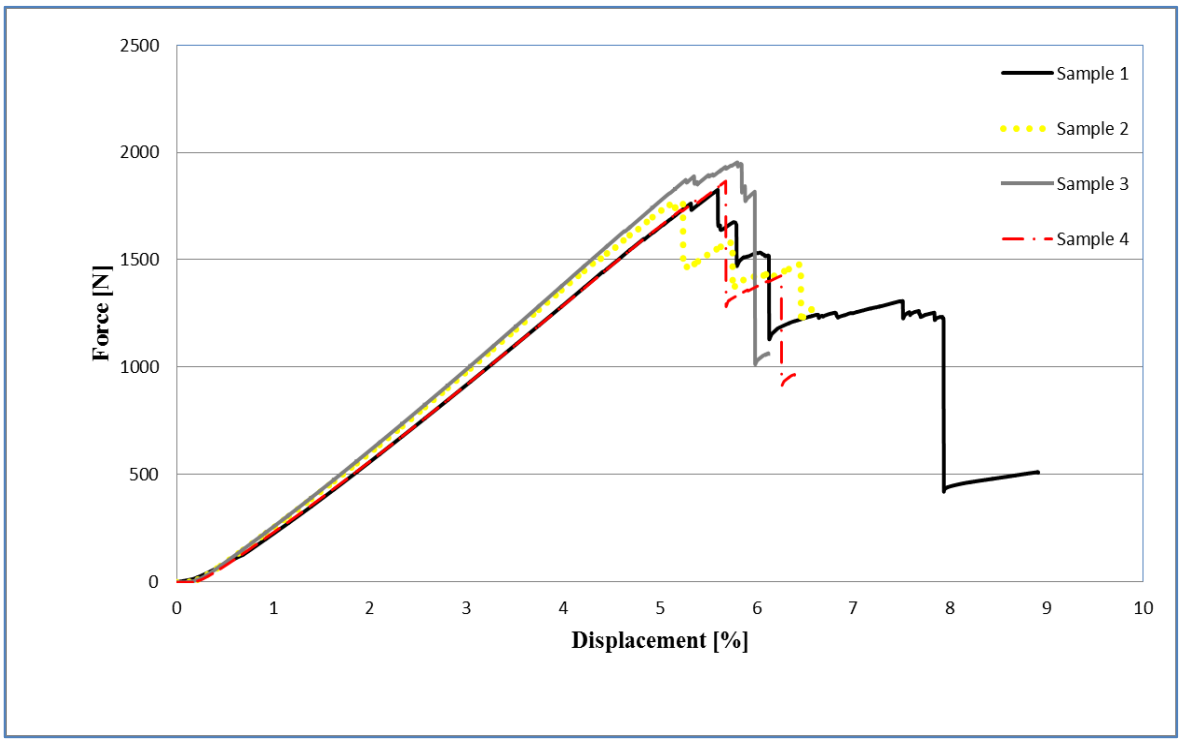

Figure 5.35. Force – displacement diagram of experimental results for $[30_3/-30_3]_s$ specimens.

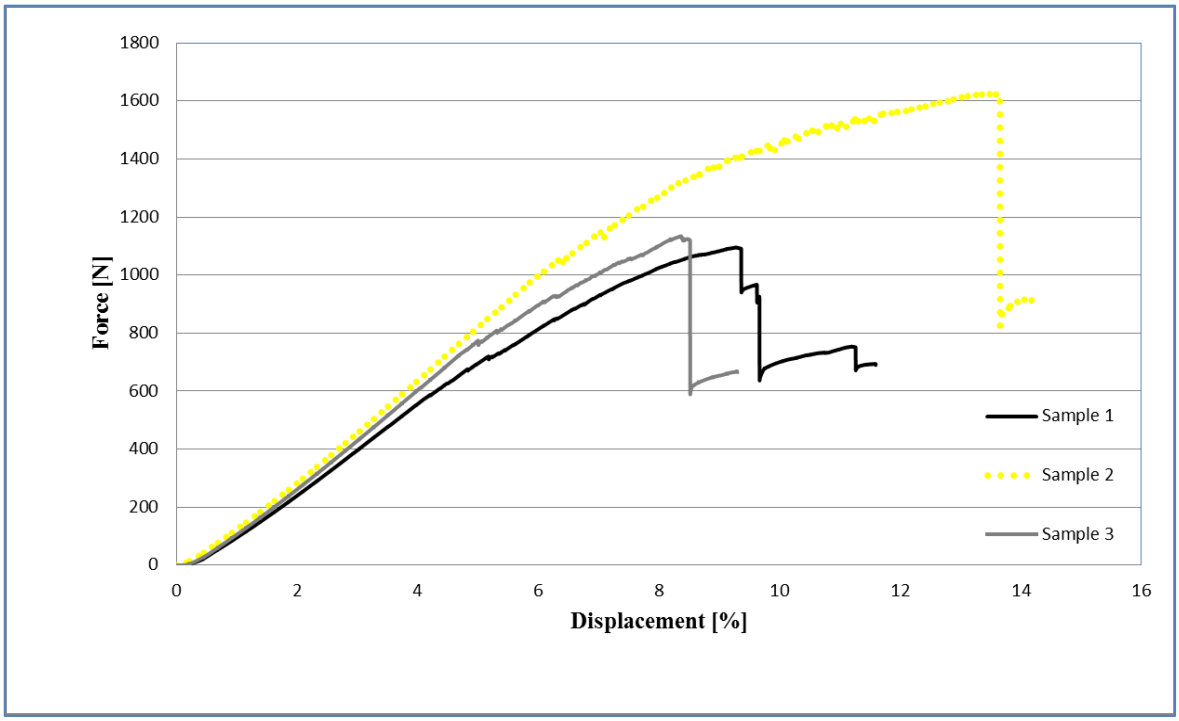

Figure 5.36. Force – displacement diagram of experimental results for $[45_3/-45_3]_s$ specimens.

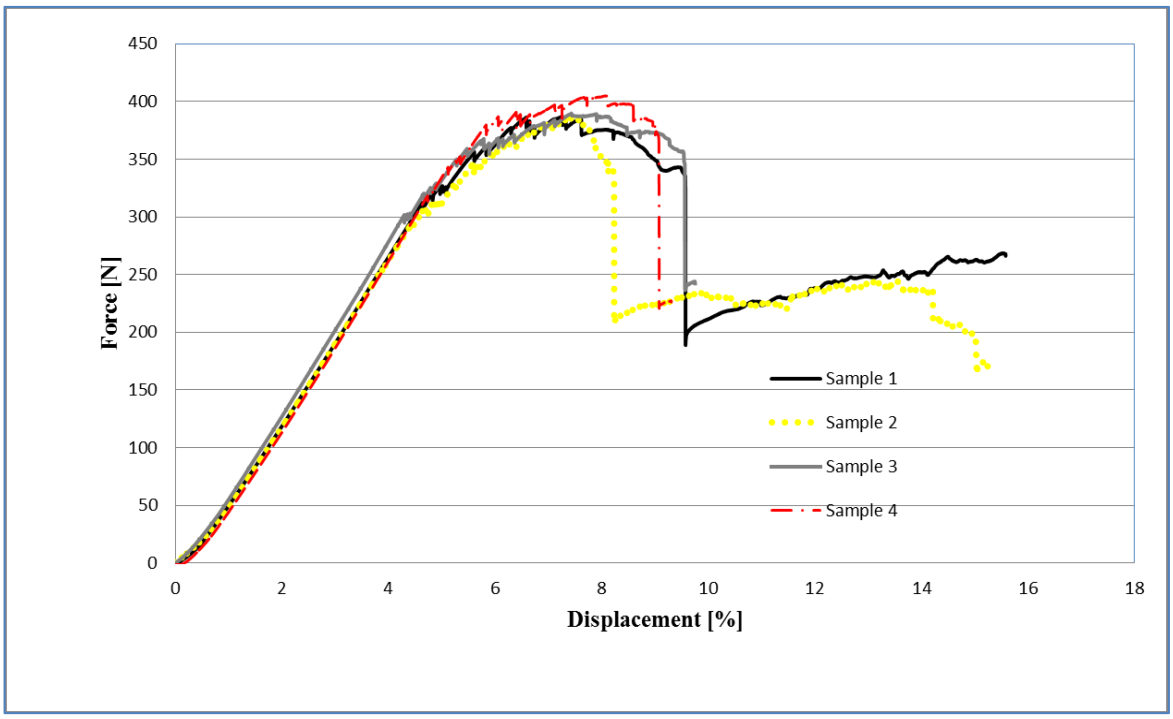

Figure 5.37. Force – displacement diagram of experimental results for $[60_3/-60_3]_s$ specimens.

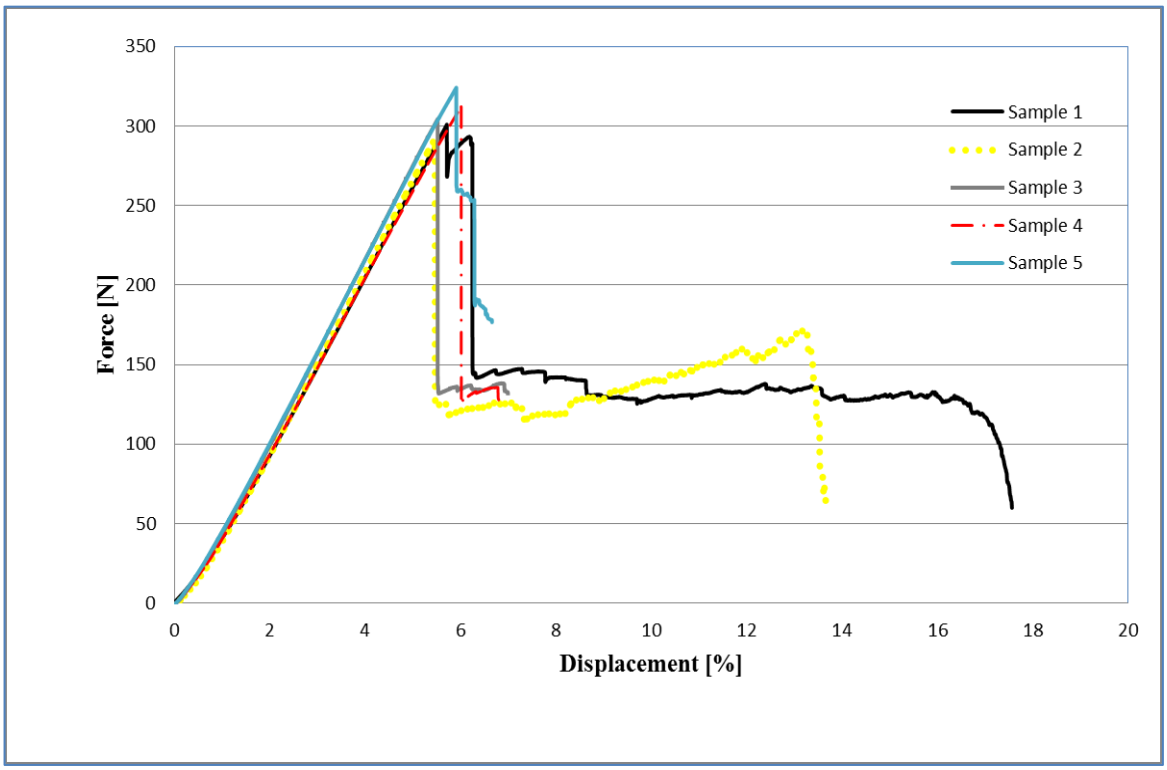

Figure 5.38. Force – displacement diagram of experimental results for $[60_3/-60_3]_s$ specimens.

Table 5.4. Experimental results of M_{max} for unidirectional off-axis $[+\theta_3/-\theta_3]_s$ specimens

Fiber orientation angle	Allowable Force [N]	M_{max} [Nm/m]
0	6945	1499
0	6542	1367
0	6974	1453
0	6984	1452
0	7158	1491
15	3439	739
15	3457	742
15	3107	673
15	3129	675
30	1826	392
30	1760	377
30	1872	402
30	1778	382
30	1842	396
45	720	155
45	1064	229
45	774	167
60	387	83
60	386	83
60	302	65
60	318	68
75	301	65
75	292	63
75	304	65
75	312	67
75	324	69
90	298	61
90	300	62
90	318	66
90	328	68
90	334	70

5.2.3. Microstructure of Specimens

Figures 5.39 – 5.44 show the microstructure of unidirectional specimens with 0^o and 15^o fiber orientation angles. It is observed in the figures that the amount of voids is relatively large around the midplane of the specimens. As it is seen from the figures that specimens are void free around the surfaces because gases escape from the surface of specimens during the manufacturing process. Figures 5.1 – 5.11 and 5.20 – 5.33 show that

the strength of the $[0_6]_s$ specimens is underestimated by all the criteria under out-of-plane loads. This arises from the difference between in-plane and out-of-plane loading. When specimens are subjected to simple tension or compression loading, uniform stresses develop in the cross-section of the specimens and failure starts at the weakest point. However, stresses are a function of the thickness when specimens are loaded under four-point bending. Maximum stresses develop on the top and bottom surfaces and symmetry plane is stress free. This means that the most critical parts of the laminates are the top and the bottom surfaces. One may assume that the void content of the surfaces is less than the middle regions because escape of gases is easier, which makes the outer regions stronger. This may explain why the models underestimate the strength of the laminates under out-of-plane loading.

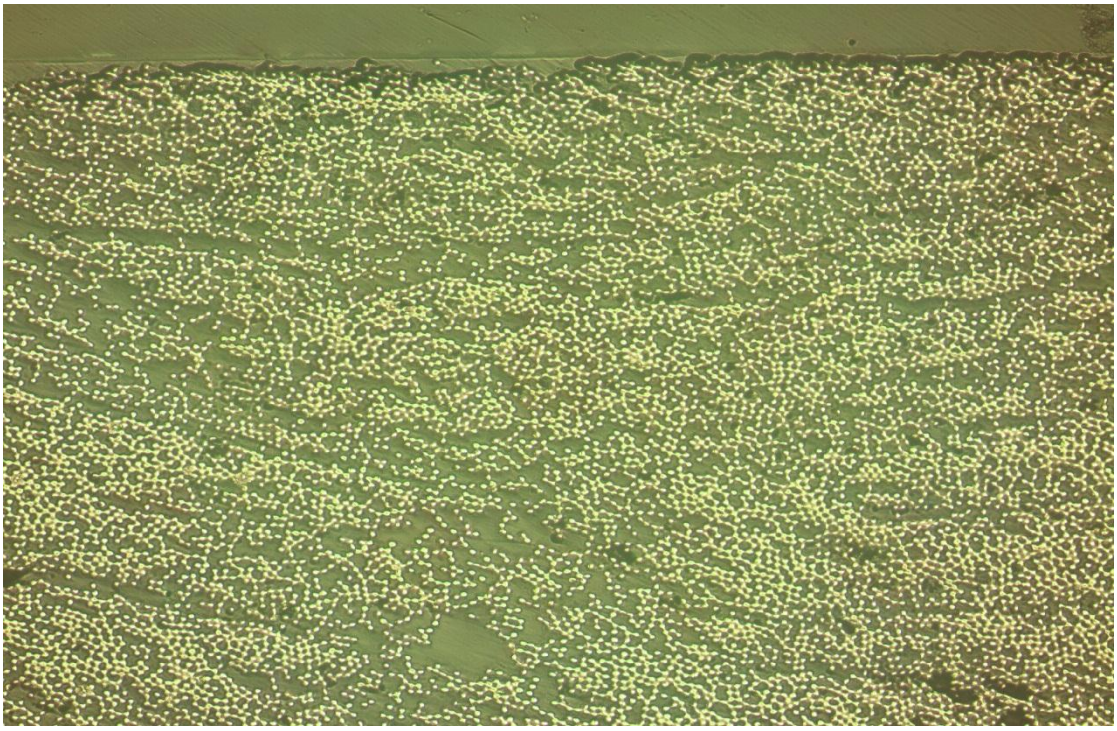

Figure 5.39. Microstructure of $[0_6]_s$ specimen (10x magnified).

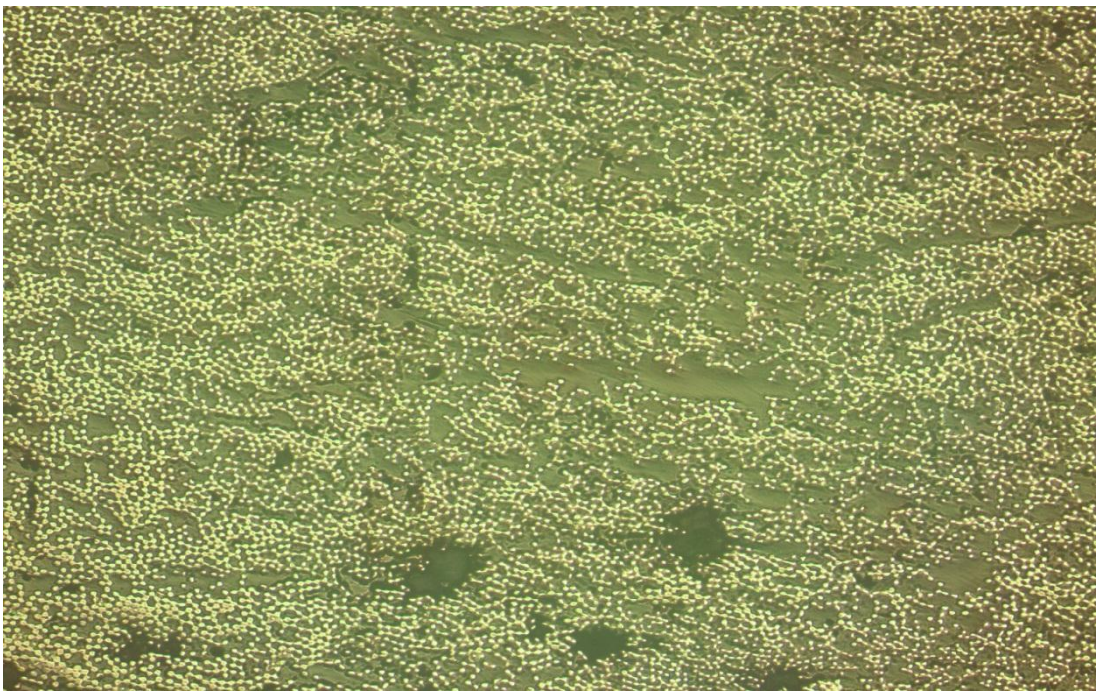

Figure 5.40. Microstructure of $[0_6]_s$ specimen (10x magnified).

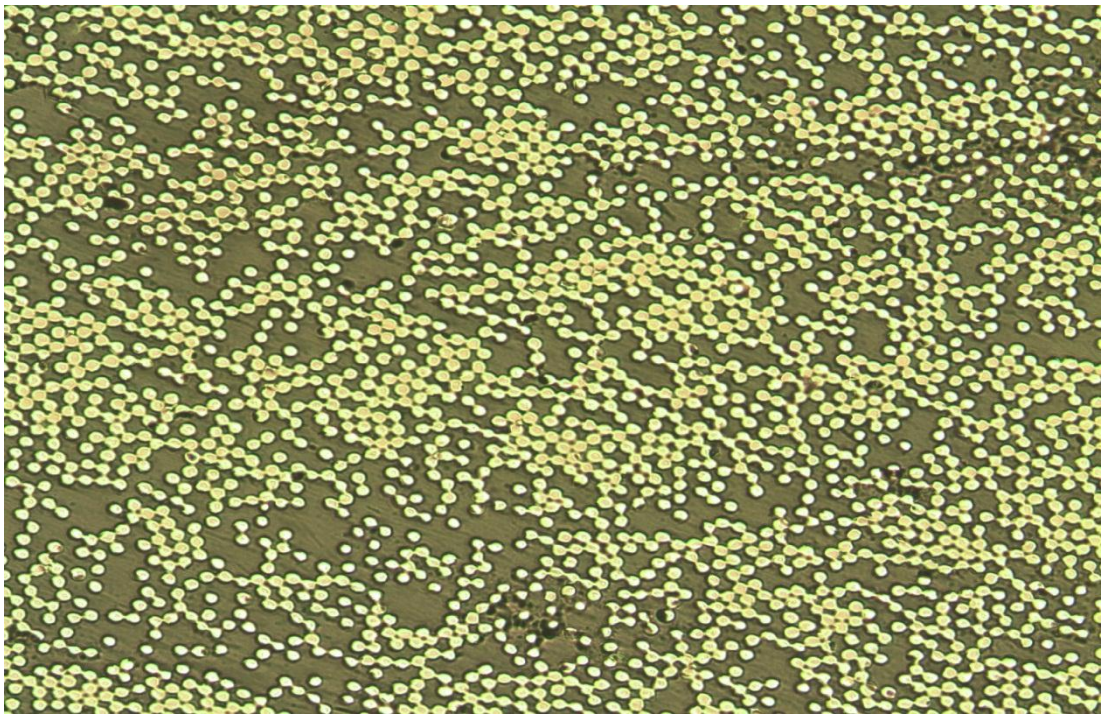

Figure 5.41. Microstructure of $[0_6]_s$ specimen (20x magnified).

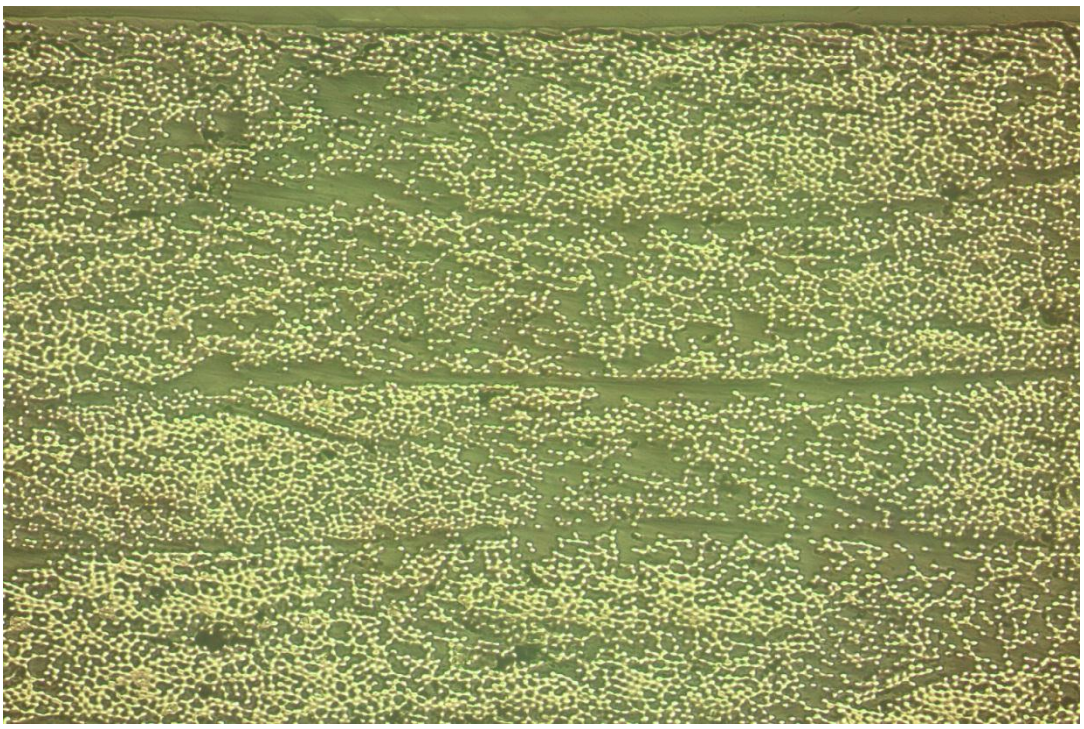

Figure 5.42. Microstructure of $[15_6]_s$ specimen (10x magnified).

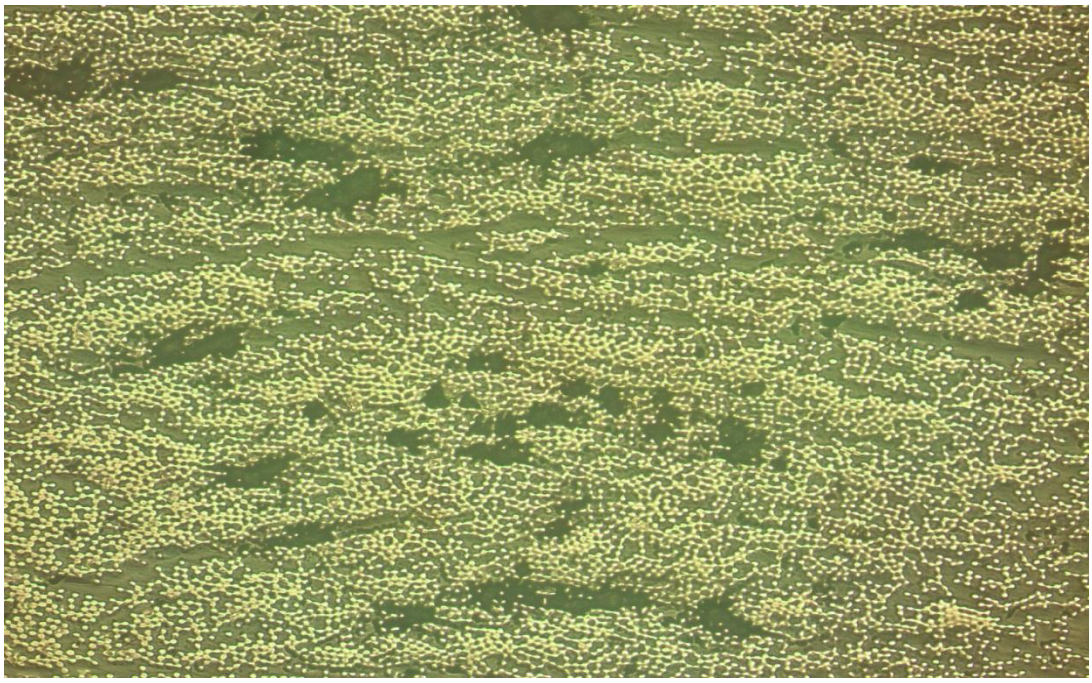

Figure 5.43. Microstructure of $[15_6]_s$ specimen (10x magnified).

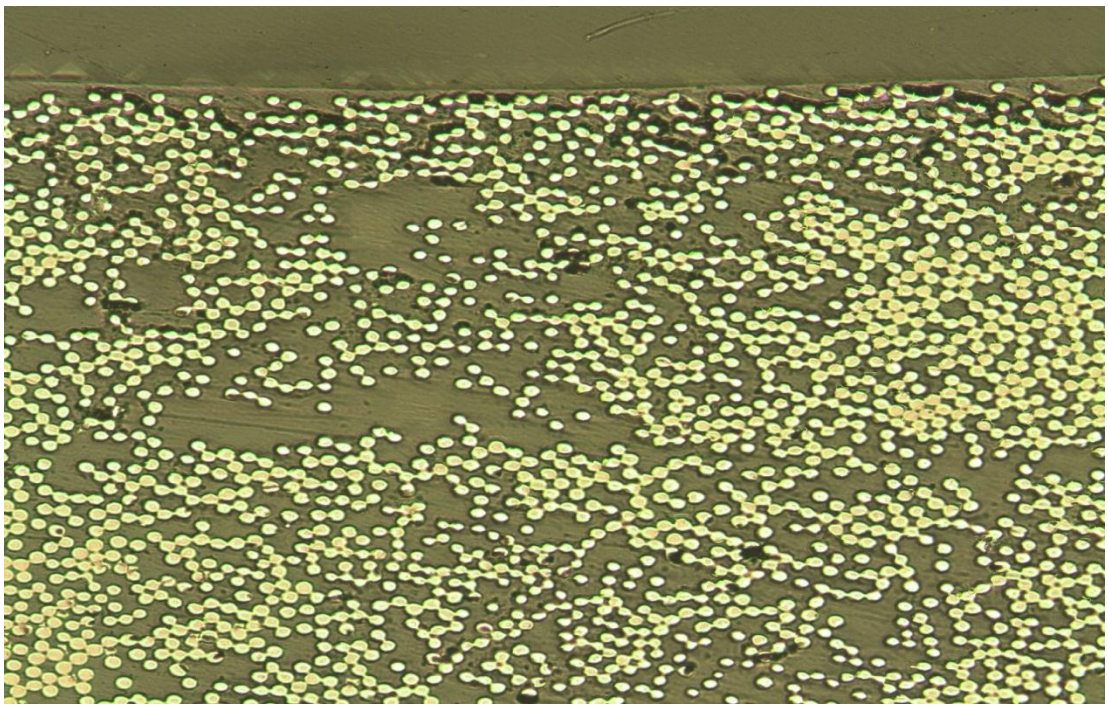

Figure 5.44. Microstructure of $[15_6]_s$ specimen (20x magnified).

5.2.4. Comparison of In-Plane and Out-of-Plane Failure Trend Predictions

There are published studies that investigated the failure trend of unidirectional composites for in-plane loads as a function of fiber orientation angle, θ, in the literature. Figures 5.45 – 5.46 show the failure trend predictions of the maximum stress and maximum strain criteria for glass epoxy composites. As it can be seen from the figures, the trend predictions of the both criteria are not smooth, which are similar to out-of-plane failure trend predictions shown in Figures 5.7 – 5.8. Similarly both of the criteria predict increase in strength as the fiber angle is varied from 0° to 2° – 4° degrees. Figure 5.47 demonstrates the Tsai-Hill criterion's failure trend prediction for unidirectional glass epoxy material. As a quadratic, failure mode independent criterion, Tsai-Hill's failure trend prediction is smooth. This is similar to the out-of-plane predictions of the same criterion given in Figure 5.2. The same correlation is observed between Tsai-Hill and Hoffman criteria under in-plane loads. Figure 5.48 shows the predictions of Hoffman criterion for unidirectional carbon - epoxy material. Lastly, Figure 5.41 illustrates the failure trend prediction of Tsai-Wu criterion for unidirectional boron-epoxy composite material. As it is expected, predictions of Tsai-Wu criterion are smooth. According to Figures 5.45 – 5.48,

the maximum stress, maximum strain and Tsai-Hill criteria predict increase in strength under compression as the fiber orientation angle is varied from 45^o – 70^o. Considering that specimens are subjected to both tension and compression under four-point bending, and tensile strength of the material in the matrix dominant region is higher than the compression strength, failure trend predictions of this study is similar to the predictions in Figures 5.37 – 5. 39 under tensile loading. There are differences as well between the failure trend predictions of the failure criteria under in-plane and out-of plane loads. For example, Figures 1.2 shows that Tsai-Wu criterion predicts increase in the strength of symmetric balanced laminates as the fiber orientation angle varies from 0^o to 90^o under in-plane loads. Yet, Figure 1.4 illustrates that no increase is predicted by Tsai-Wu criterion under out of plane loads for the same stacking sequence. In a similar fashion, maximum stress criterion's failure trend predictions do not coincide under in-plane and out-of-plane loads specifically for small fiber angles as shown in Figures 1.1 and 1.3.

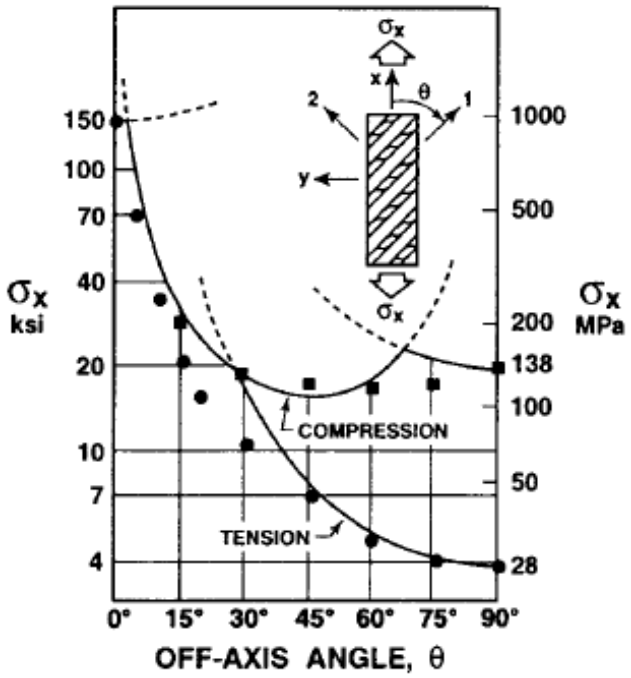

Figure 5.45. Strength predictions of maximum stress failure criterion for E-glass epoxy material as a function of fiber orientation angle, θ.

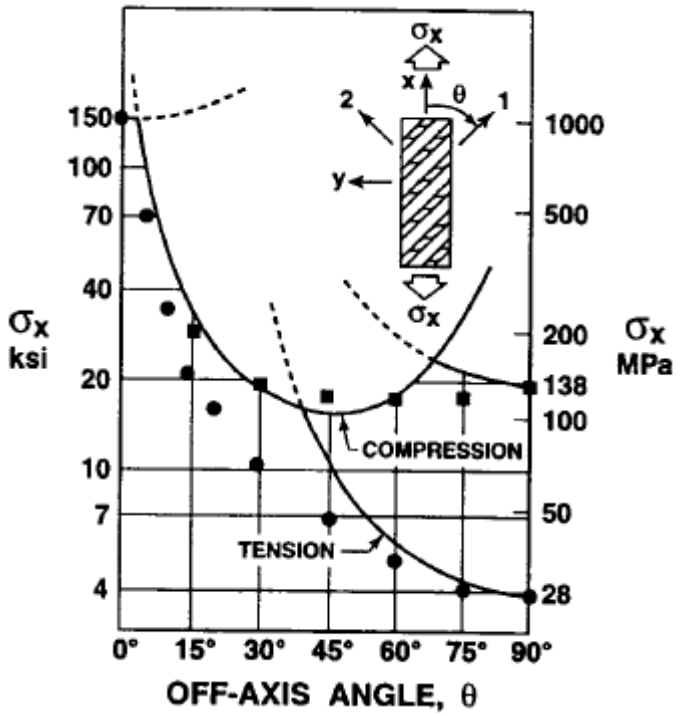

Figure 5.46. Strength predictions of maximum strain failure criterion for E-glass epoxy material as a function of fiber orientation angle, θ.

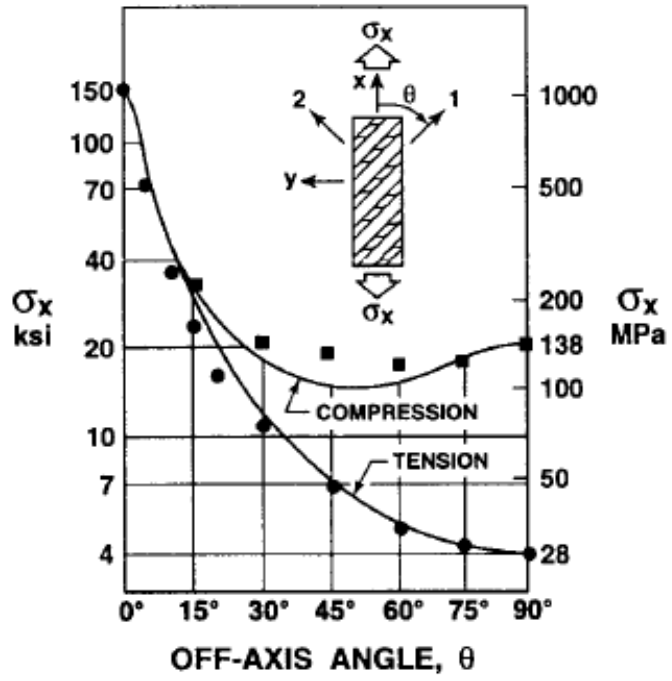

Figure 5.47. Strength predictions of Tsai-Hill failure criterion for E-glass epoxy material as a function of fiber orientation angle, θ.

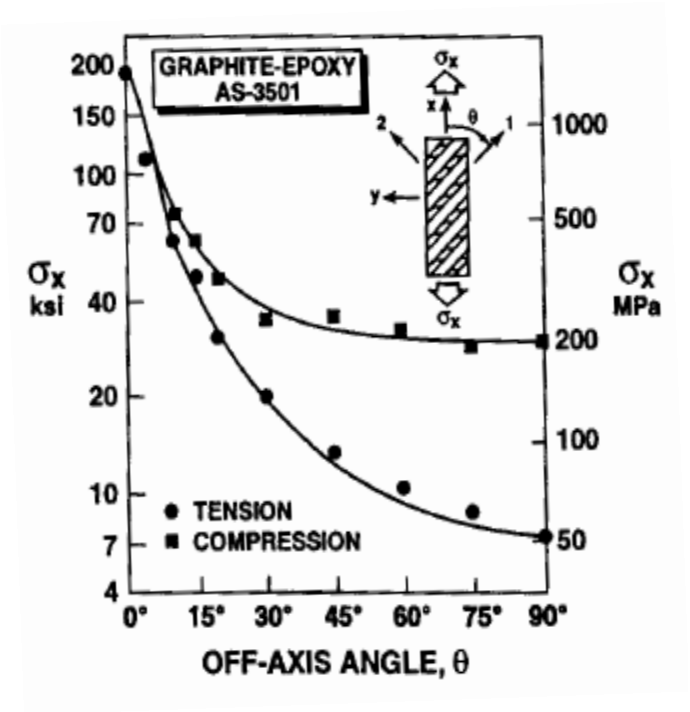

Figure 5.48. Strength predictions of Hoffman failure criterion for graphite epoxy material as a function of fiber orientation angle, θ

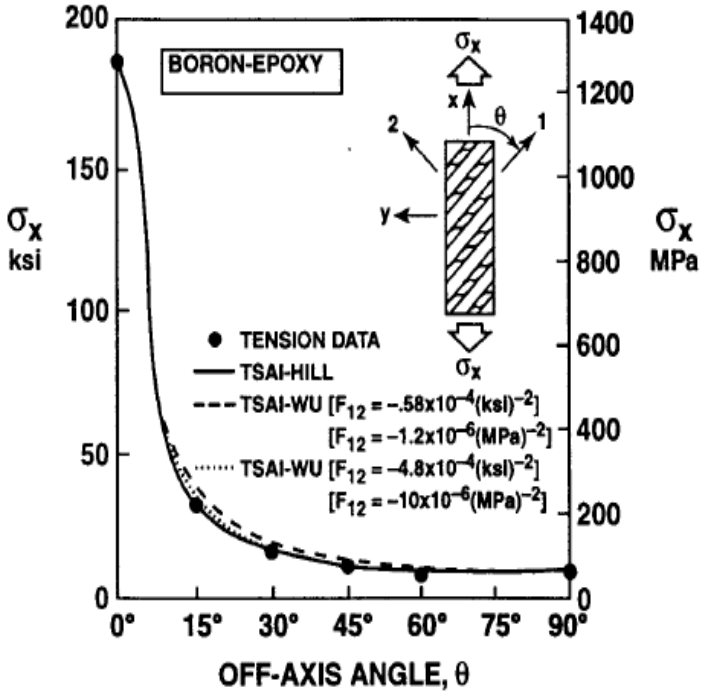

Figure 5.49. Strength predictions of Tsai-Wu failure criterion for boron epoxy material as a function of fiber orientation angle, θ.

6. CONCLUSIONS AND THE FUTURE WORK

In this thesis, the failure behavior of unidirectional off-axis and symmetric balanced laminates under four-point bending loading was investigated. A four-point bending test setup was designed and constructed such that the static failure modes would be the dominant failure mode rather than delamination. Experiments were conducted for $[\theta_6]_s$ and $[\theta_3/-\theta_3]_s$ layup sequences for fiber angles of 0°, 5°, 15°, 30°, 45°, 60°, 75°, and 90°. Both CLT and FEM were utilized to simulate the four - point bending tests. Maximum allowable moment resultant, M_{max}, predictions of nine different failure criteria were compared with the experimental results. The residual stresses developed during manufacturing were accounted for to increase the reliability of the predictions.

In this study, the predictions of the criteria based on the analytical and FE models are found to be quite similar in the case of unidirectional off-axis specimens. Failure trend predictions of the criteria with similar characteristics, e.g. quadratic or physically based, are quite coherent. While the analytical models of physically based failure criteria predict increase in strength as the fiber angle is changed from 0° to 3° - 4° , the quadratic criteria predict decrease.

Whether the analytical model or FE model is used, all of the criteria underestimate the strength of unidirectional laminates in the fiber dominant region, i.e. between 0° and 30°. The only exception is $[5_6]_s$ specimens. Microstructure of the specimens showed that there are voids around the midplane; however, these voids do not affect the first ply failure strength of the specimens remarkably. Before deciding on the success of the failure predictions of the criteria, it should be taken into account that specimens can carry higher stresses under out-of-plane loads owing to higher strength of the critical regions. In addition to this, force – displacement diagrams show that the failure behavior of composite plates in the fiber dominant region is complex. For example, Figure 5.12 show that the force – displacement diagram of $[0_6]_s$ specimens become non-linear above 6000 N load. Figure 5.13, on the other hand, states that $[15_6]_s$ specimens can carry loads after first ply failure. In some cases, specimens can even carry higher loads after first ply failure. Another point is that, specimens always fail below the symmetry plane wherein they are subjected to tensile loads. Considering that the tensile strength is greater than the

compression strength, this is unexpected. Advanced techniques such as acoustic emission might help to observe the cracking density inside the specimens. It is also observed that the finite element model based simulations of the chosen failure criteria predict the maximum allowable moment resultants for symmetric balanced laminates with better accuracy as compared to analytical model simulations. Between 30^o and 45^o, in which maximum residual stresses develop, inclusion of residual stresses decrease the predictive capability of FE model based predictions. This is a result of the fact that the strength of the composite plates are underestimated under out-of-plane loads in the fiber dominant region. Hence, including residual stresses may decreases the reliability between 30^o and 45^o. However, for relatively small and large fiber angles magnitude of residual stresses are small and may increase the predictive capability of the criteria. For example, according to Figure 5.30, FE model based predictions of maximum strain criterion for $[+15_3/-15_3]_s$ and $[+60_3/-60_3]_s$ correlate better when residual stresses are included. It seems that finite element based predictions of the maximum strain criterion are close to the experimental results. FE model based failure trend predictions of the other criteria should be found to decide about the effect of residual stresses on the success of the failure prediction.

In this thesis, the first ply failure approach was adopted. As a future work, progressive failure modes and ultimate strengths as a function of fiber orientation angle can be investigated. Also, different failure criteria, e.g. Puck, Christensen, modified Hashin, Fischer, etc., can be tested. Furthermore, different out-of-plane loading types like anti-clastic bending, which creates biaxial loading, can be utilized to test the failure criteria.

REFERENCES

1. Jenkins**,** C., F., *Report on Materials and Construction Used in Air-Craft and Air-Craft Engines*, H. M. Stationary Office, London, 1920.

2. Hill, R., "A Theory of Yielding and Plastic Flow of Anisotropic Metals", *Proceedings of the Royal Society Series A: Mathematical and Physical Sciences*, Vol. 193, No. 1033, 1948.

3. Hill, R., *The Mathematical Theory of Plasticity,* Oxford University Press, London, 1950.

4. Norris, C., B., *"*Strength of Orthotropic Materials Subjected to Combined Stress", *Forest Products Laboratory,* Report 1816, 1962.

5. Hoffman, O., "The Brittle Strength of Orthotropic Materials", *Journal of Composite Materials*, Vol.1, No. 2, pp. 200-206, 1967.

6. Fischer, L., "Optimization of Orthotropic Laminates", *Journal of Engineering for Industry*, 1967.

7. Chamis, C., C., "Failure Criteria for Filamentary Composites", Composite Materials: Testing and Design. ASTM STP 460, 1969.

8. Tsai, S., W. and WU, E., M., "A General Theory of Strength for Anisotropic Materials", *Journal of Composite Materials*, Vol.5, pp. 58-80, 1971.

9. Hashin, Z., "Failure Criteria for Unidirectional Fiber Composites", *Journal of Applied Mechanics,* Vol. 47, pp. 329-334, 1980.

10. Puck, A., "A Failure Criteria Shows the Direction", *Kunststoffe: German Plastics*, Vol. 82, pp. 29-32, 1992.

11. Trochu, F., and Echaabi, J., “Failure Mode Dependent Strength Criteria for Fiber Composites”, *International Journal of Solids and Structures*, Vol. 34, pp. 529-543, 1997.

12. Rotem, A., “Prediction of Laminate Failure with Rotem Failure Criterion”, *Composites Science and Technology*, Vol. 58, pp. 1083-1094, 1998.

13. Liu, K. -S., and, Tsai, S., W., “A Progressive Quadratic Failure Criterion for a Laminate”, *Composites Science and Technology*, Vol. 58, pp. 1023-1032, 1998.

14. Yeh, H. -L., “Quadric Surfaces Failure Criterion for Composite Materials”, *Journal of Reinforced Plastics and Composites*, Vol. 6., 2003.

15. Yeh, H. -L., and, Yeh, H. -Y., **“**Modified Quadric Surfaces Failure Criterion for Composite Materials”, *Journal of Reinforced Plastics and Composites*, Vol. 21, 2003.

16. Puck, and, Schurrman., “Failure Analysis of FRP Laminates by Means of Physically Based Phenomenological Models”, *Composites Science and Technology*, Vol. 58, pp. 1045-1067, 2002.

17. Christensen, R., M., “Stress Based Yields/Failure Criteria for Fiber Composites”, *International Journal of Solids and Structures*, Vol 34, pp. 529-543, 1997.

18. Christensen, R., M., *Failure Criteria for Anisotropic Fiber Composite Materials*, 2008, http://www.failurecriteria.com/Media/Failure_Criteria_for_Anisotropic_Fiber_Composite_Materials.pdf, accesed at July 2010.

19. Eckold, G., C., Failure Criteria for Use in the Design Environment, *Composites Science and Technology*, Vol. 58, p. 1095, 1998.

20. Sandhu, R., S., “A Survey of Failure Theories of Isotropic and Anisotropic Materials”, *Technical Report, Ohio : Air Force Flight Dynamics Laboratory Wright-Patterson AFB*, 1972.

21. Rowlands, R., E., **"**Strength (Failure) Theories and Their Experimental Correlation", *Failure Mechanics of Composites*, Vol.3, pp. 71-124, 1985.

22. Paris, F., A., "A Study of Failure Criteria of Fibrous Composite Materials", *NASA, CR-2001-210661,* 2001.

23. Davila, C., G., Camanho, P., P. and Rose, C., A., "Failure Criteria for FRP Laminates", *Composite Science and Technology*, Vol. 62, pp. 1725-1797, 2005.

24. Soni, S., R., "A Comparative Study of Failure Envelopes in Composite Laminates", *Journal of Reinforced Plastics and Composites*, Vol. 2, 1983.

25. Soden, P., D., and Hinton, M., J., "Predicting Failure in Composite Laminates: The Background to Exercise", *Composite Science and Technology*, Vol. 58, 1998.

26. Soden, P., D., Hinton, M., J., and Kaddour A., S., "A Comparison of the Predictive Capabilities of Current Failure Theories for Composite Laminates", *Composite Science and Technology*, Vol. 58, pp. 1225-1254, 1998.

27. Kaddour, A., S., Soden, P., D., and Hinton, M., J., **"**Biaxial Test Results for Strength and Deformation of a Range of E-Glass and Carbon Fiber Reinforced Composite Laminates: Failure Exercise Benchmark Data", *Composite Science and Technology***,** Vol. 62, pp. 1489-1514, 2002.

28. Hinton, M., J., Soden, P., D., and Kaddour, A., S., "A Comparison of the Predictive Capabilities of Current Failure Theories for Composite Laminates, Judged Aganist Experimental Evidence", *Composite Science and Technology*, Vol 62., pp. 1725-1797, 2002.

29. Grief, R., "Investigation of Successive Failure Modes in Graphite/Epoxy Laminated Composite Beams", *Journal of Reinforced Plastics and Composites*, Vol. 12, pp. 602-621, 1993.

30. Trochu, F., Echaabi, J, Pham, X., T., and Ouellet, M., **"**Theoretical and Experimental Investigation of Failure and Damage Progression of Graphite-Epoxy Composites in Flexural Bending", *Journal of Reinforced Plastics and Composites*, Vol. 15, 1996.

31. Echaabi, J., Trochu, F., Irhirane, El H., Aboussaleh, M., and Hattabi, M., "Matrix and Fibre Stiffness Degradation of a Quasi-Isotrope Graphite Epoxy Laminate Under Flexural Bending Test", *Journal of Reinforced Plastics and Composites*, Vol. 28, 2009.

32. Huang, Z., -M., "Modeling and Characterization of Bending Strength of Braided Fabric Reinforced Laminates", *Journal of Composite Materials*, Vol. 26, 2002.

33. Akbulut, M. and Sonmez, F., Ö., "Optimum Design of Composite Laminates for Minimum Thickness", *Computers & Structures*, Vol. 86, pp. 1974–1982, 2008.

34. Akbulut, M. and Sonmez, F., Ö., "Design Optimization of Laminated Composites Subject to in-Plane and out-of-Plane Loads", *Computers & Structures*, Vol.89, 2010.

35. Jones, R., M., *Mechanics of Composite Materials,* 2nd Edition, Taylor & Francis Inc., Philadelphia, 1999.

36. Hyer, M., W., *Stress Analysis of Fiber-Reinforced Composite Materials.* McGraw-Hill, Michigan, 1998.

37. *ANSYS Help System*, Version 13.0, 2010.

38. Vinson J., R. and Sierakowski, R., R., *The Behavior of Structures Composed of Composite Materials, 2nd Edition.* Kluver Academic Publishers, The Netherlands, 2004.

39. *ANSYS Help System Mechanical APDL Element Reference*, Version 13.0, 2010.

40. Ersoy, N., Garstka, T., Potter, K., Wisnom, M., R., Porter, D., Clegg, M., and Stringer, G., "Development of the Properties of a Carbon Fibre Reinforced Thermosetting

Composite Through Cure*", Composites Part A: Applied Science and Manufacturing*, Vol. 3, pp. 401-409, 2010.

41. Ersoy, N. and Vardar, O., Measurement of Residual Stresses in Layered Composites by Compliance Method, *Journal of Composite Materials*, Vol. 34, pp. 575-598, 2000.

42. Tserpes, K., I., Papanikos, P., and Kermanidis, Th., "A Three Dimensional Progressive Damage Model For Bolted Joints in Composite Laminates Subjected to Tensile Loading", *Fatigue Fract. Engng. Mater. Struct*, Vol. 24, pp. 663-675, 2001.

43. Unluhisarcikli, O., *Control and Optimization of Cure Cycle for Thick-Sectioned Thermoset Composites Manufacturing*, M.S. Thesis, Bogazici University, 2008.

44. Zwick-Roell, *Zwick-Roell Tensile Test Machine Catalogue*, www.zwick.com, 2012, accessed at July 2012

45. Clarkson, E., "Hexcel 8552 AS4 Unidirectional Prepreg Qualification Statistical Report", *NATIONAL INSTITUTE FOR AVIATION RESEARCH*, Wichita State University

46. Hou, M., Ye, L., Lee, H., J., and Mai, Y., W., "Manufacture of A Carbon-Fabric-Reinforced Polyetherimide (CF/PEI) Composite Material", *Composite Sciences and Technology*, Vol. 58, pp. 181-190, 1998.

47. Hou M., Ye L., Lee H. J., Mai Y. W., "Manufacturing Process and Mechanical Properties of Thermoplastic Composite Components", *Journal of Materials Processing Technology*, Vol. 63, pp. 334-338, 1997.

48. Sudarisman, I. J. D., "The Effect of Processing Parameters on the Flexural Properties of Unidirectional Carbon-Fibre-Reinforced Polymer (CFRP) Composites", *Journal of Materials Science and Engineering A*, 2008.

49. Hull, D. and Clyne, T., W., *An Introduction to Composite Materials*, Cambridge University Press, Cambridge, 1996.

50. Hexcel Composites, *HexPly 8552 Epoxy Matrix*, 2008, http://www.hexcel.com/Resources/DataSheets/Prepreg-Data-Sheets/8552_us.pdf, accessed at July 2010.

51. Muzzy, J., D., "Thermoplastics-Properties", *Comprehensive Composite Materials*, Vol. 2, pp. 57-76, 2000.

52. Varma, K., Gupta, V., B**.,** "Thermosetting Resin-Properties", *Comprehensive Composite Materials*, Vol. 2, pp. 1-56, 2000.

53. Choo, V., K., S., *Fundamentals of Composite Materials,* Knowen Academic Press Inc., Delaware, 1990.

54. Love, A., E., H., *A treatise on the Mathematical Theory of Elasticity*, Cambridge University Press, Cambridge, 1927.

APPENDIX A: COMPOSITES

Composites are combination of two or more materials to obtain a useful third one in macroscopic scale. The word “macroscopic” demonstrates the difference between composites and alloys. Composites are nonhomogeneous materials with two distinct phases: reinforcing material and matrix. As reinforcing material bears load, matrix material bonds reinforcing material together and transmits load. Classification of composite materials in the academic literature is based on the phases. For example, Vinson and Sierakowski [38] classified composites as fiber composites, particulate composites, flake composites, filled composites and laminar composites depending on the reinforcing material. Hull [49], on the other hand, classified composites with respect to matrix material as metallic matrix composites (MMC), ceramic matrix composites (CMC) and polymeric matrix composites (PMC). Each type of composites has their own pros and cons. However, glass and carbon fiber reinforced composites with polymer matrix are most widely used among others.

A material is usually stronger in fiber form as compared to the same material in bulk form because of the decreased amount of imperfections such as dislocations. Diameter of fibers of composites is tiny (8 μm for AS4/8552 prepregs [50]) to increase strength and stiffness. Matrix materials are needed to bind long and narrow fibers. Fibers are homogeneously distributed in matrix during the manufacturing process.

Matrix is typically lighter, softer and weaker than fibers. There are two types of polymeric matrix: thermoplastics and thermosetting. Thermoplastics are high weight molecular polymers with linear chains which turn into liquid when heated and solid when cooled properly. The polymer becomes a viscoelastic fluid at about 100 °C above its T_g (glass transition temperature) and can be processed as a melt. Thermoplastics can be recycled and remelted under high processing pressures; however, expensive product tooling and high energy input are required during process as a result of high pressure [49]. Thermosets, on the contrary, are usually low molecular weight monomers or oligomers. During the curing process, thermoset molecules form three-dimensional cross-linked solid network structure. Thermosets are not recyclable and they do not melt when heated. It is easier to process and produce as compared to thermoplastics owing to relatively low

processing pressure and energy input [49, 51-52]. Attention is paid on Hexcel®'s AS4/8552 carbon fiber reinforced thermoset polymer (CFRP) composites in this study.

Mechanics of composites may be considered in micro and macro level. Composites are nonhomogeneous in microscale because of its constituents. In micromechanics, mechanical behavior of both fiber and matrix and interactions between them are taken into account. However, utilizing micromechanical approach for analysis of large scale materials is a tedious task and macromechanical approached should be used instead during analyses. If fibers are homogeneously distributed in matrix, a composite becomes homogeneous in macroscale. Macromechanical approach neglects individual failure behavior of fibers and matrix in microscale and considers the overall stress-strain relations of the structure.

Mechanical properties of composite laminates are a function of stacking sequence. In this thesis, two types of stacking sequence was studied: unidirectional $[\theta_6]_s$ and symmetric balanced $[+\theta_3/-\theta_3]_s$. In this representation, θ refers to the principal material directions, ie. orientation angles of the laminae. Numbers, which are shown in subscript, refer to the number of lamina in the θ direction and subscript s refers to the word "symmetric. Namely, a composite laminate, in this study, is composed of twelve plies.

A lamina is assumed to be an orthotropic, linear, elastic continuum. Considering these assumptions, normal and shear components of stress tensor $\sigma_1, \sigma_2, \sigma_3, \sigma_{12}, \sigma_{13}, \sigma_{23}$ on a small volume element are shown in Figure A.1.

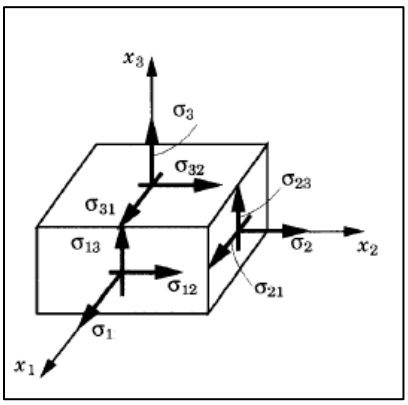

Figure A.1. Stress state on a small volume element [35].

Stress-strain relations are stated below in indicial notations by means of Generalized Hooke's law:

$$\varepsilon_{ij} = S_{ijkl}\sigma_{kl} \tag{A.1}$$

$$\sigma_{ij} = C_{ijkl}\varepsilon_{kl} \tag{A.2}$$

where C_{ijkl} and S_{ijkl} are fourth order stiffness and compliance tensors, respectively. The relationship between C and S is given in Equation A.3.

$$C_{ijkl} = S_{ijkl}^{-1} \tag{A.3}$$

Components of strain tensor are functions of displacements. Relationship between the components of strain tensor and displacement is given in Equation A.4 and expanded in Equations A.5 – 10.

$$\varepsilon_{ij} = \frac{1}{2}\left(\frac{\partial u_i}{\partial x_j} + \frac{\partial u_j}{\partial x_i}\right) \tag{A.4}$$

where

$$\varepsilon_1 = \frac{\partial u}{\partial x} \tag{A.5}$$

$$\varepsilon_2 = \frac{\partial v}{\partial y} \tag{A.6}$$

$$\varepsilon_3 = \frac{\partial w}{\partial z} \tag{A.7}$$

$$\varepsilon_{12} = \frac{1}{2}\left(\frac{\partial u}{\partial y} + \frac{\partial v}{\partial x}\right) \tag{A.8}$$

$$\varepsilon_{13} = \frac{1}{2}\left(\frac{\partial u}{\partial z} + \frac{\partial v}{\partial x}\right) \tag{A.9}$$

$$\varepsilon_{23} = \frac{1}{2}\left(\frac{\partial v}{\partial z} + \frac{\partial w}{\partial y}\right) \tag{A.10}$$

where u, v, and w are displacements in x_1, x_2 and x_3 directions, respectively. In some cases, it is more convenient to use engineering shear strains γ_{12}, γ_{13}, γ_{23} instead of tensor shear strains ε_{12}, ε_{13}, ε_{23}.

$$\varepsilon_{12} = \frac{1}{2}\gamma_{12} \qquad \varepsilon_{13} = \frac{1}{2}\gamma_{13} \qquad \varepsilon_{23} = \frac{1}{2}\gamma_{23} \tag{A.11}$$

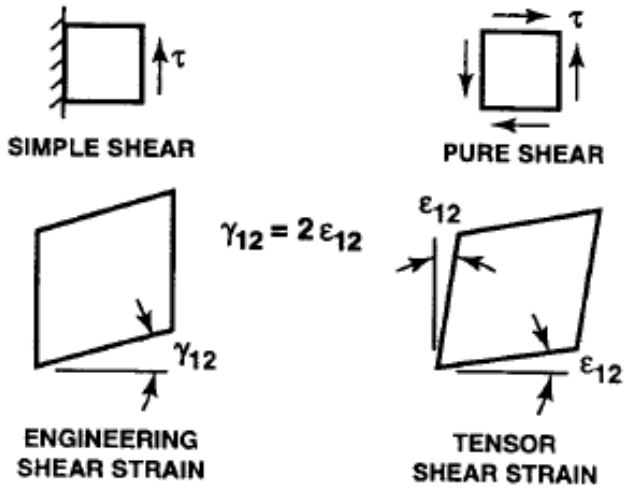

FigureA.2. Engineering shear strain versus tensor shear strain [35].

Stress-strain relations are illustrated in matrix form with the help of so called compliance and stiffness matrices in Equations A.12 – 13.

$$\begin{bmatrix} \varepsilon_1 \\ \varepsilon_2 \\ \varepsilon_3 \\ \varepsilon_{23} \\ \varepsilon_{13} \\ \varepsilon_{12} \end{bmatrix} = \begin{bmatrix} S_{11} & S_{12} & S_{13} & S_{14} & S_{15} & S_{16} \\ S_{12} & S_{22} & S_{23} & S_{24} & S_{25} & S_{26} \\ S_{13} & S_{23} & S_{33} & S_{34} & S_{35} & S_{36} \\ S_{14} & S_{24} & S_{34} & S_{44} & S_{45} & S_{46} \\ S_{15} & S_{25} & S_{35} & S_{45} & S_{55} & S_{56} \\ S_{16} & S_{26} & S_{36} & S_{46} & S_{56} & S_{66} \end{bmatrix} \begin{bmatrix} \sigma_1 \\ \sigma_2 \\ \sigma_3 \\ \sigma_{23} \\ \sigma_{13} \\ \sigma_{12} \end{bmatrix} \tag{A.12}$$

$$\begin{bmatrix} \sigma_1 \\ \sigma_2 \\ \sigma_3 \\ \sigma_{23} \\ \sigma_{13} \\ \sigma_{12} \end{bmatrix} = \begin{bmatrix} C_{11} & C_{12} & C_{13} & C_{14} & C_{15} & C_{16} \\ C_{12} & C_{22} & C_{23} & C_{24} & C_{25} & C_{26} \\ C_{13} & C_{23} & C_{33} & C_{34} & C_{35} & C_{36} \\ C_{14} & C_{24} & C_{34} & C_{44} & C_{45} & C_{46} \\ C_{15} & C_{25} & C_{35} & C_{45} & C_{55} & C_{56} \\ C_{16} & C_{26} & C_{36} & C_{46} & C_{56} & C_{66} \end{bmatrix} \begin{bmatrix} \varepsilon_1 \\ \varepsilon_2 \\ \varepsilon_3 \\ \varepsilon_{23} \\ \varepsilon_{13} \\ \varepsilon_{12} \end{bmatrix} \tag{A.13}$$

Composite laminates are orthotropic materials and have three planes of symmetry. An important consequence of this is that the number of independent terms of compliance matrix reduces considerably as it is stated in Equations A.14 – 15.

$$\begin{bmatrix} \varepsilon_1 \\ \varepsilon_2 \\ \varepsilon_3 \\ \varepsilon_{23} \\ \varepsilon_{13} \\ \varepsilon_{12} \end{bmatrix} = \begin{bmatrix} S_{11} & S_{12} & S_{13} & 0 & 0 & 0 \\ S_{12} & S_{22} & S_{23} & 0 & 0 & 0 \\ S_{13} & S_{23} & S_{33} & 0 & 0 & 0 \\ 0 & 0 & 0 & S_{44} & 0 & 0 \\ 0 & 0 & 0 & 0 & S_{55} & 0 \\ 0 & 0 & 0 & 0 & 0 & S_{66} \end{bmatrix} \begin{bmatrix} \sigma_1 \\ \sigma_2 \\ \sigma_3 \\ \sigma_{23} \\ \sigma_{13} \\ \sigma_{12} \end{bmatrix} \tag{A.14}$$

$$\begin{bmatrix} \sigma_1 \\ \sigma_2 \\ \sigma_3 \\ \sigma_{23} \\ \sigma_{13} \\ \sigma_{12} \end{bmatrix} = \begin{bmatrix} C_{11} & C_{12} & C_{13} & 0 & 0 & 0 \\ C_{12} & C_{22} & C_{23} & 0 & 0 & 0 \\ C_{13} & C_{23} & C_{33} & 0 & 0 & 0 \\ 0 & 0 & 0 & C_{44} & 0 & 0 \\ 0 & 0 & 0 & 0 & C_{55} & 0 \\ 0 & 0 & 0 & 0 & 0 & C_{66} \end{bmatrix} \begin{bmatrix} \varepsilon_1 \\ \varepsilon_2 \\ \varepsilon_3 \\ \varepsilon_{23} \\ \varepsilon_{13} \\ \varepsilon_{12} \end{bmatrix} \tag{A.15}$$

Relationships between stiffness and compliance matrix elements are given in Equations A.16 – 24.

$$C_{11} = \frac{S_{22}S_{33} - S_{23}^2}{S} \tag{A.16}$$

$$C_{12} = \frac{S_{13}S_{23} - S_{12}S_{33}}{S} \tag{A.17}$$

$$C_{13} = \frac{S_{12}S_{23} - S_{13}S_{22}}{S} \tag{A.18}$$

$$C_{22} = \frac{S_{33}S_{11} - S_{13}^2}{S} \tag{A.19}$$

$$C_{23} = \frac{S_{12}S_{13} - S_{23}S_{11}}{S} \tag{A.20}$$

$$C_{33} = \frac{S_{11}S_{22} - S_{12}^2}{S} \tag{A.21}$$

$$C_{44} = \frac{1}{S_{44}} \tag{A.22}$$

$$C_{55} = \frac{1}{S_{55}} \tag{A.23}$$

$$C_{66} = \frac{1}{S_{66}} \tag{A.24}$$

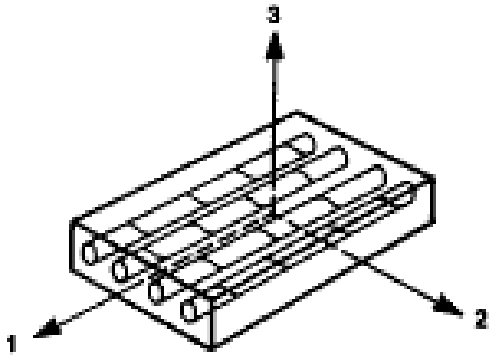

Figure A.3. Native coordinates of single lamina [35].

Compliance matrix S_{ij} may be stated as a function of engineering constants elastic moduli, shear moduli and Poisson's ratios.

Poisson's ratio can be stated in terms of strains as follows:

$$\nu_{ij} = -\frac{\varepsilon_j}{\varepsilon_i} \tag{A.25}$$

where

$$\nu_{12} = -\frac{\varepsilon_2}{\varepsilon_1} \tag{A.26}$$

$$\nu_{13} = -\frac{\varepsilon_3}{\varepsilon_1} \tag{A.27}$$

$$\nu_{23} = -\frac{\varepsilon_3}{\varepsilon_2} \tag{A.28}$$

Only ν_{12}, ν_{13}, ν_{23} are needed to state stiffness and compliance matrices in terms of engineering constants because ν_{21}, ν_{31}, ν_{32} can be expressed in terms of the first group by means of the equation given below:

$$\frac{\nu_{ij}}{E_i} = \frac{\nu_{ji}}{E_j} \tag{A.29}$$

For laminates made of unidirectional prepregs with fiber and matrix symmetry, number of independent engineering constants reduces to five. Such laminates are called transversely isotropic. The independent constants are E_1, E_2, G_{12}, ν_{12} and ν_{23}.

$$E_2 = E_3;\ G_{12} = G_{13};\ \frac{\nu_{21}}{E_2} = \frac{\nu_{12}}{E_1} \tag{A.30}$$

$$G_{23} = \frac{E_2}{(1 + \nu_{23})} \tag{A.31}$$

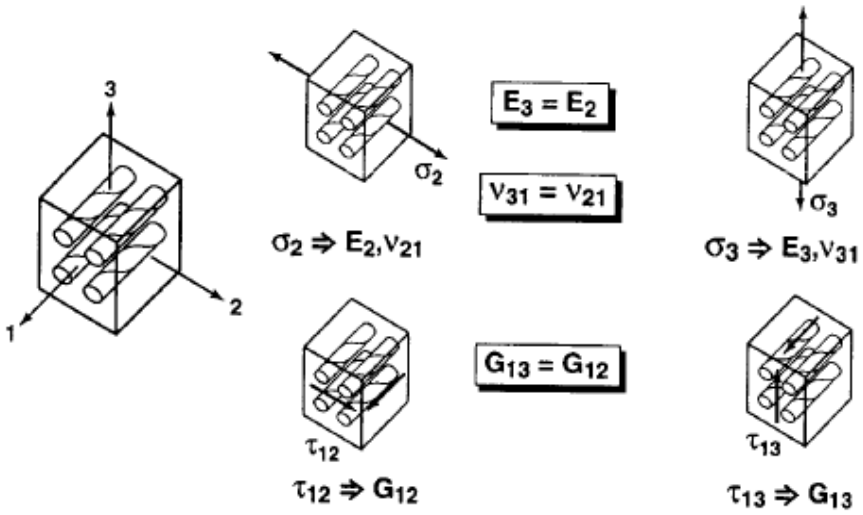

Figure A.4. Physical symmetry of a unidirectionally reinforced lamina [35].

Compliance matrix S_{ij} of a transversely isotropic lamina, in terms of engineering constants, is given in Equation A.32.

$$S_{ij} = \begin{bmatrix} \frac{1}{E_1} & -\frac{\nu_{21}}{E_2} & -\frac{\nu_{21}}{E_2} & 0 & 0 & 0 \\ -\frac{\nu_{21}}{E_2} & \frac{1}{E_2} & -\frac{\nu_{23}}{E_2} & 0 & 0 & 0 \\ -\frac{\nu_{21}}{E_2} & -\frac{\nu_{23}}{E_2} & \frac{1}{E_2} & 0 & 0 & 0 \\ 0 & 0 & 0 & \frac{1}{G_{12}} & 0 & 0 \\ 0 & 0 & 0 & 0 & \frac{1}{G_{12}} & 0 \\ 0 & 0 & 0 & 0 & 0 & \frac{1}{G_{23}} \end{bmatrix} \quad \text{(A.32)}$$

Stiffness matrix C_{ij} can be stated as function of engineering constants as well, using Equations A.16-A.24.